

Integration of Battery-Based Energy Storage Element in the CERTS Microgrid

Prepared For:
US Department of Energy

Robert Lasseter
Micah Erickson

Prepared By:
University of Wisconsin-Madison

CERTS
CONSORTIUM FOR ELECTRIC RELIABILITY TECHNOLOGY SOLUTIONS



Final Report Task 4.
Value and Technology Assessment to Enhance
the Business Case for the CERTS Microgrid

October 27, 2009
DE-FC02-06CH11350

Acknowledgments

The authors are grateful for the support of Merrill Smith, U S Department of Energy, Office of Electricity Reliability and Energy Delivery and Steve Waslo, U S Department of Energy, Chicago Program Office. This research was funded by the U S Department of Energy under contract DE-FC02-06CH11350

This work has resulted in a U.S. Patent Application No.: 11 / 681017

Filing Date: 3/1/2007

Title: Control of Combined Storage and Generation in Dynamic Distribution Systems

Executive Summary

Battery energy storage units provide an added degree of freedom to a microgrid that allows time-shifting between the generation and use of energy. Microgrid energy storage elements are very similar to any other inverter-based source with the exception of bi-directional power flow capabilities. Having the ability to generate and accept power means that the demand and the supply can be disparate by as far as the power capabilities of the energy storage unit allow. This enables combined heat power systems to support a heat load demand independent of local electric power demand. Having an energy storage element on standby also allows for a certain amount of immediately available power to reduce the need for idling or lightly loaded rotating generators under the n-1 stability criterion. The relative speed of any inverter based source allows a sub-cycle change in power output to ensure that dynamic loads will be supplied regardless of the slow reaction of larger rotating sources that require seconds of response time to transients. Thirdly, they can act as a UPS system during grid faults, providing backup power for some time even for non-essential loads while the microgrid is islanded. Lastly, the energy storage element can provide an economic and/or logistical advantage by regulating the power drawn by and supplied to the grid interface. This not only permits capitalizing on fluctuating power prices, but even regulating a line loading by making better use of off-peak hours to supply the daily energy needs.

For transients in the presence of a fixed-power source with a slow time constant like a fuel cell, the storage unit may have to absorb extra energy generated as the fuel cell slowly decreases its output power for the system to remain online. In this case, the energy storage unit may also be required to provide a reference voltage for the power injected by the fuel cell. In the case of an islanding event when no other sources were

online, the energy storage element then becomes the solitary source of fast power transients. Energy storage unit can help also decoupled loads and renewable fluctuation within a microgrid from the grid. The net effect is a significant reduction in peak power levels drawn from the grid reducing the peak power cost incurred by the utility.

Despite the obvious advantages of energy storage elements in a microgrid environment, it is still debated whether energy storage should exist at each source or whether a centralized energy storage element should bear the sole duty of energy storage. From an energy accounting perspective, the amount of energy absorbed and transmitted is a function only of the size of the unit, which is typically directly proportional to the cost. The power systems industry has used the economies of scale as reasoning for larger and larger power generation facilities, but since both battery and inverter costs scale at a linear rate there seems to be little economic advantage to a consolidated energy storage element. Reliability also supports the distributed model for storage by removing the storage as a single unit failure mode that could disable islanding of a microgrid.

Stand-alone energy storage becomes more dominant as the system scales. For the AEP microgrid it is cost effective to use inverters with traditional small generation allowing effective combined storage/generation. For microgrid systems at the distribution level, megawatt level inverter based generation is much less feasible. In the presence of generators with slow dynamic responses, an energy storage unit offers the ability to provide supplemental temporary power to compensate for the initial deficit of slower sources.

Identical with other CERTS DER units, CERTS storage regulates the voltage at its connection point and uses a power vs. frequency droop. Storage differs from other DER units since it has bi-directional power flow capabilities resulting in a negative minimum power limit and state-of-charge, (SOC), issues. One of the most important

components to the operation of an energy storage element in a Microgrid using the CERTS concept is the on-board management of state of charge. As the CERTS concept employs autonomous operation of individual distributed energy resources maintaining controlling the SOC is a task appointed to the on-board controller.

Assuming bi-directional power flow, the upper and lower SOC limits can be defined. Secondly, by defining the amount of reserve energy required for backup purposes in the event of islanding, the nominal operating space is limited further by an amount proportional to the duration and power rating of the specified backup requirement, defined as the energy reserve limit. Another point above the energy reserve limit, named the lower marginal limit is specified marginally greater than the energy reserve limit. The marginal limit defines a hysteretic point where the control of the energy storage element will return to nominal operation, as opposed to the at-limit control strategy. Key control of the SOC is through control of the power limits. For example if SOC is below the energy reserve limit the maximum output power limit is set to zero. The same concept applies for the minimum power level or charge rate as the storage reached its maximum SOC.

This work focuses on the SOC-limit operation of the energy storage element through load transients and SOC paths across specified limits. This is achieved through simulation and hardware studies on the UW microgrid. The basic systems studied are storage only, storage and inverter based source and storage and a CERTS diesel genset.

Tests include the step-changes of load, islanding and events that occur when SOC limits are encountered. Their response is dictated by the natural response of the system, in whatever mode it happens to be in, limited or nominal operation. The events that occur when SOC limits are encountered are intentionally slower in response than the load-changing transients to avoid imparting resonant dynamics on the system. The time

constant of each system is between two and four seconds, which is intentionally gauged against the time constant of a slow-reacting source such as a diesel genset. This ensures that even though the SOC limit controller will dictate the power output of the energy storage element in steady state, the transient power-sharing characteristic will still exist for conditions when slow-reacting sources suffer an output capability deficit during load transients. The accumulated SOC error during these transients is not significant in this case as it is assumed that the capacity of the energy storage element is much greater than that of the temporary accumulated error. Secondly, although the exact time-based characteristic of the charge current limitations is not known, the average recommended charge current may be exceeded in transient conditions but should not pose any significant battery damage. This conclusion comes from the relatively small response time to system transients on the order of seconds compared to the battery handling recommendations from the battery manufacturers that were reported to be on the order of fractional minutes.

Table of Contents

<i>Executive Summary</i>	2
<i>Table of Contents</i>	6
1. Introduction	8
1.1 Microgrid concept	8
1.2 The CERTS concept.....	9
1.3 Objective of this work.....	12
1.4 Basic types of energy storage.....	12
1.5 Current grid-tied energy storage elements (State of the art)	13
2. Theoretical capabilities of energy storage elements connected to a microgrid	17
2.1 Unit Placement	18
2.2 Spinning Reserve	19
2.3 Load-leveling from grid.....	19
2.4 Source-leveling for intermittent sources.....	20
2.5 Peak-shaving/Gap-filling.....	20
2.6 Stability buffer for slow-reacting sources (Frequency regulation)	21
3. Inverter Model Development	22
4. Battery Handling Requirements	25
4.1 Max power available	25
4.2 Lifetime effects.....	26
4.3 Charge and Discharge rates.....	26
5. Battery Modeling	28
5.1 Characterization	28
5.2 Model development	33
5.3 EMTP implementation	42
5.4 Microcontroller implementation.....	44
5.5 Battery conclusion	47
6. State-Of-Charge management	48
6.1 Automatic SOC limit algorithm.....	48
6.2 Automated SOC limit controller.....	53
7. System test results	56
7.1 Power mode stability under load changing & islanding	57
7.2 Flow mode stability under load changing & islanding.....	91
8. Conclusions	99

8.1 Summary of contributions:.....	99
8.2 Future Work	102
<i>References</i>	<i>103</i>
<i>Appendix A: Control System Block Diagrams</i>	<i>109</i>
A.1 Power vs. Frequency droop gain selection	110
A.2 Power limit controller explanation and gain selection	111
A.3 SOC limit controller explanation and gain selection	112
A.4 Battery observer estimation accuracy and conductance gain selection.....	118
A.5 Voltage magnitude controller explanation and gain selection	120
<i>Appendix B: Power Modifier SOC Limit Control Code</i>	<i>121</i>
<i>Appendix C: Hardware configuration diagram</i>	<i>125</i>
<i>Appendix D: Harmonic Oscillator Code</i>	<i>126</i>
<i>Appendix E: Battery Specification Sheet</i>	<i>127</i>

1. Introduction

Distributed generation is a proposed solution to curb price peaks during times of high demand. By placing generation near loads, the net effect is less utilization of the already stressed power distribution system which increases operational margin. In some cases, strategic placement of distributed generation can re-distribute power flows to also decrease loading on choke-points to a greater degree than that of the supplementary generation [32]. However, distributed generation is typically too small to participate in the power markets [11] and significantly increase the type of analysis required by a regional balancing authority to ensure stability of the grid.

1.1 Microgrid concept

A microgrid is essentially a solution to some of the major issues in implementing distributed generation. Currently, generation of electrical power is accomplished primarily by large coal plants which are not only slow to react to changes in demand by the system, but run off a non-renewable resource. Small sources such as natural gas turbines, diesel generators, wind turbines, hydrogen fuel cells, and photo-voltaic panels offer a variety of benefits depending on application, but can prove to be cheaper, more ecologically friendly, and can change their power output faster than large coal plants. Microgrids offer a solution to implementing these sources at or near the point of load that not only decreases the stress on the electrical transmission system but offers a significant increase in power system reliability with the ability to generate all of the necessary power required locally. By organizing a group of distributed generators in a facility with a severable grid connection, power system reliability becomes more of a local issue rather than a region-wide issue. The regional system operators can consider microgrids as a

limited-risk entity through the proper implementation of safety equipment at the connection point which allows more individual freedom to generate power on-site from a variety of sources. Secondly, with the increased capacity of installed intermittent renewable energy sources such as wind and solar, microgrids offer a solution that enables unlimited utilization of power from intermittent sources while still maintaining power system stability and reliability.

1.2 The CERTS concept

There are two main components to the CERTS concept which were originally outlined in [29]: the smart switch and the plug-and-play source. The plug-and-play source concept incorporates a 3-phase AC voltage supply that can vary its frequency and magnitude in coordination with a pre-programmed active and reactive power characteristic. The smart switch that connects the microgrid to the grid and will have programmed logic that will abide by the regulations described in IEEE-1547, the “Standard for Interconnecting Distributed Resources with Electric Power Systems”. The smart switch shoulders all of the compliance duties, leaving the plug-and-play sources free of regulations, lowering the total system cost for the microgrid.

The sources use operating frequency as the main form of communication which indicates the relative loading of the individual sources. The frequency of each source will increase if it generates less power than the programmed power set-point. This increase in frequency develops an increased difference angle between the resultant voltage at the source and the rest of the microgrid. Equation 1.1 indicates that there is a locally linear relationship between the difference angle and power exchange between sources.

$$P_{12} = \frac{V_1 V_2}{X} \sin(\delta) \quad (1.1)$$

where:

P_{12} = the power transferred from source 1 to source 2

V_1 = the magnitude of the voltage at source 1

V_2 = the magnitude of the voltage at source 2

X = the reactance between source 1 and source 2

This shifts the loading of each source toward a point of equality at a rate determined by the relative difference in frequency between two sources. The resulting response is first order natural decay due to the linear characteristic of pre-programmed power-frequency characteristic.

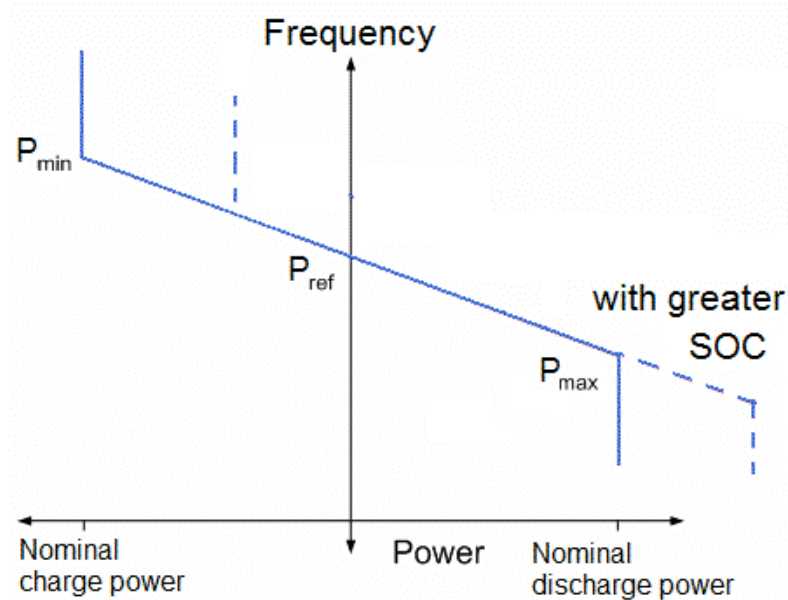


Figure 1.2.1 – Power vs. frequency characteristic as a function of State of Charge

The reactive power control via output voltage magnitude is less complex in its effect. By using the equation describing the flow of reactive power between sources, it is easy to see that there is a direct relation between the difference in magnitudes of output voltages and output of reactive power.

$$Q_{12} = \frac{V_1}{X} (V_1 - V_2) \cos(\delta) \quad (1.2)$$

Due to the unknown magnitude of reactive power loads, some reactive power must be supplied to support these loads, so this number can not be forced to zero for all sources. Therefore, using a linear relationship between voltage magnitude variation and reactive power output, the reactive power load is shared between the sources while limiting the circulating reactive power via the linear characteristic in figure 1.2.2.

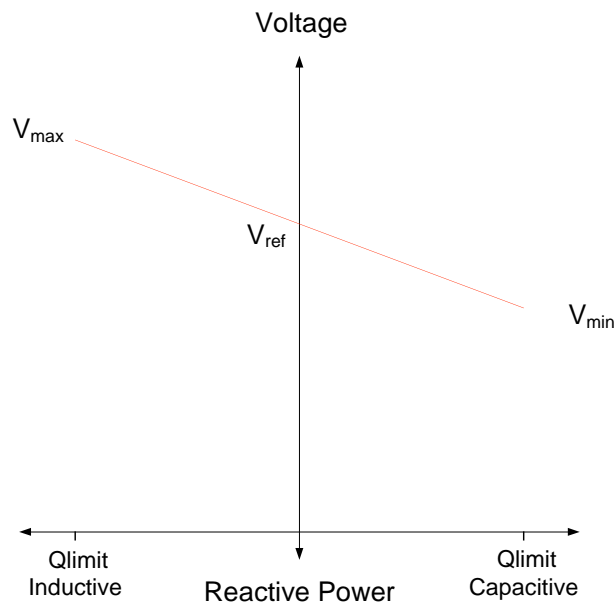


Figure 1.2.2 – Output voltage characteristic as a function of reactive output power

It is then clear that there are no external communications necessary to make this system operational and new sources can be added without reconfiguring the sources already on the network. Inverter-based sources are best suited to this control topology, but virtually any source can be adapted to operate with these characteristics including various types of rotating machines.

1.3 Objective of this work

Microgrids are a distinctively robust distributed generation solution that enables a reconfigurable and stable system assuming the power output of the system can be adjusted quickly enough to match the load demand. In cases where fixed power sources, slow reacting sources, and large load transients exist, supplementary fast-reacting power transmission and adsorption can effectively ensure or restore microgrid stability. A battery based energy storage unit is ideally suited to this requirement, because of the reasonable amount of energy storage that can be managed at a significantly slower rate than the natural time constants that exist in a power system as opposed to a solution implementing a flywheel or super-capacitors. By enacting energy-level management with slow enough response time, the interaction with natural power system resonant frequencies can be mitigated by reasonable spectral separation. Lastly, a controller will be developed to demonstrate that the battery state of charge can be maintained by a charge-state controller, regardless of user power settings, in a manner that does not adversely affect the stability and power quality of the microgrid.

1.4 Basic types of energy storage

Energy can be stored kinetically or potentially. Typical applications include physical, electrical, and electrochemical mediums [10]. However, the most energy-dense bi-directional energy storage medium is a mechanical flywheel at 120Wh/kg[9]. Chemical batteries come in second at 25Wh/kg but do not suffer significant standby losses that flywheels do in terms of wind resistance which is approximately 10% of capacity per hour [8]. Other sources include low-temperature superconducting coils (SMES), pumped hydraulic water storage, and super-capacitors.

1.5 Current grid-tied energy storage elements (State of the art)

Grid-tied energy storage systems are appearing quickly lately, as flywheel, battery, and magnetic energy storage technologies become more application-ready. Also, there are the few hydraulic storage systems in use, but they require a geography that enables such systems.

Flywheel systems have inspired many applications including automotive, but one of the most recent flywheel energy systems comes from Pentadyne Energy Corporation who has a scalable flywheel energy system that features a carbon fiber composite flywheel in a vacuum-sealed package.

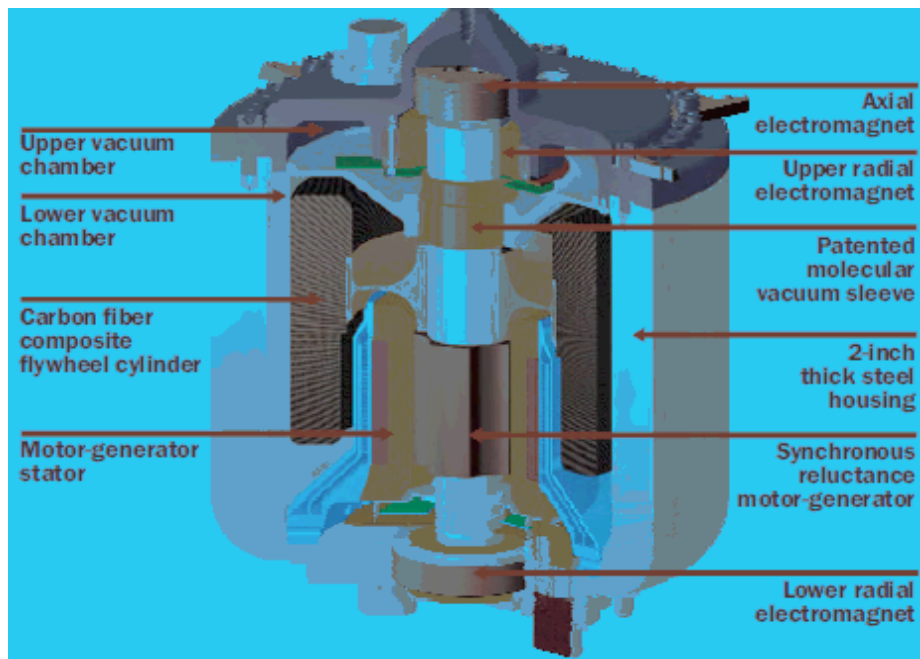


Figure 1.5.1 – Flywheel energy storage system diagram from Pentadyne Energy Corporation

The main drawback from these systems is the energy storage size. For example, a single flywheel can be configured to output 112.5kW for 18 seconds, for a total of 2MJ. To put this into perspective, a 540V battery pack (comparable to the flywheel DC bus voltage) would have an equivalent capacity of 1Ah. On the other hand, the power density

of the flywheel system is approximately 100 times that of a battery-based system of similar energy storage capabilities, assuming a 2C discharge rating.

Another popular power-centric energy storage medium is the Dynamic Superconducting Magnetic Energy Storage unit from American Superconductor which uses a cryogenically maintained low-temperature superconductor coil to store energy. The coil current is maintained at approximately 3000A which is effectively lossless except for the voltage drop across the lossy thyristor element which closes the circuit. Though the details of this product are still held quiet through the development phase, it is known that the field of the unit is well above the saturation limit of iron, which is why an air-core is used.

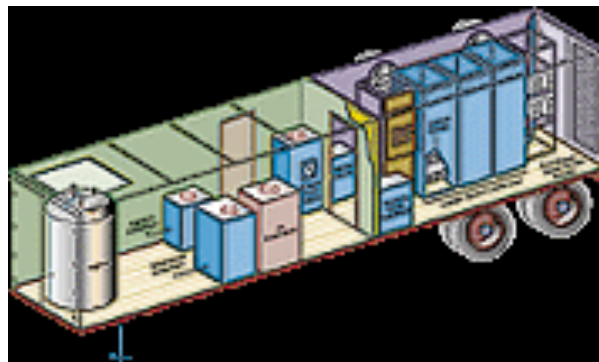


Figure 1.5.2 – D-SMES installation in a transportable container

This unit is advertised as a frequency regulator that maintains voltage magnitude on transmission lines after lightning strikes [7]. From figure 1.5.2, it can be seen that the cryostat, on the left side of the image, is kept at a distance from the remainder of the equipment, presumably to avoid the strong magnetic field and EMI when in use during transient events.

Pumped hydraulic storage is a remarkably niche market which is, unfortunately, critically utilized, leaving little room for growth. However, it is important to mention this technology as it is the foremost application of grid-tied energy storage. Pumped

hydraulic storage relies on the difference in potential energy stored in water while stored in one reservoir versus another immediately adjacent. A conduit connecting these reservoirs is fitted with turbines, much like a hydroelectric dam, except for the fact that pumped hydraulic energy storage implies bidirectional water flow. The largest of these facilities is in Bath County in Virginia. This facility has two reservoirs that have a 1260' differential in height, generating up to 2,100 MW at maximum discharge flow of 14.5 MGPM [6]. Obviously this is an interesting application but is logistically prohibitive for locations without such advantageous geography.

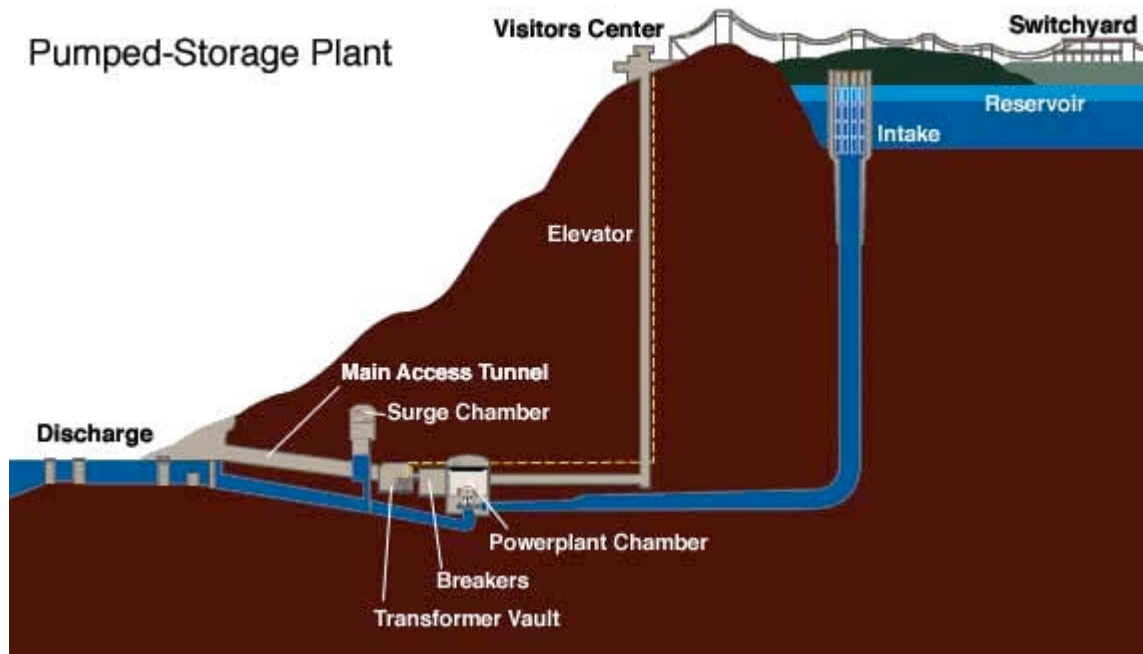


Figure 1.5.3 – Pumped hydraulic system-level configuration diagram

Neglecting pumped hydro, there are a variety of solutions to support energy storage needs, battery systems are the least expensive per kWh, at approximately \$1,200-\$1,500, reported in a 1997 report. As was stated in the same report, lead-acid batteries and power converters are mature technologies which can not be expected to reduce in cost by more than 10-15%. However, because approximately half the cost of the energy

storage systems comes from the supporting logistics (facilities, design/integration, and transportation), the total system price will fall with as a function of the cost of the supporting services [5].

2. Theoretical capabilities of energy storage elements connected to a microgrid

Battery energy storage units provide an added degree of freedom to a microgrid that allows time-shifting between the generation and use of energy. Grid-tied energy storage elements are very similar to any other inverter-based source with the exception of bi-directional power flow capabilities. Having the ability to generate and accept power means that the demand and the supply can be disparate by as far as the power capabilities of the energy storage unit allow. This enables combined heat power systems to support a heat load demand independent of local electric power demand. Having an energy storage element on standby also allows for a certain amount of immediately available power to reduce the need for idling or lightly loaded rotating generators under the n-1 stability criterion. The relative speed of any inverter based source allows a sub-cycle change in power output to ensure that dynamic loads will be supplied regardless of the slow reaction of larger rotating sources that require seconds of response time to transients. Thirdly, they can act as a grown-up UPS system during grid faults, providing backup power for some time even for non-essential loads while the microgrid is islanded. Lastly, the energy storage element can provide an economic and/or logistical advantage by regulating the power drawn by and supplied to the grid interface. This not only permits capitalizing on fluctuating power prices, but even regulating a line loading by making better use of off-peak hours to supply the daily energy needs.

The other defining characteristic of a battery energy storage unit is that although the amount of energy that can be stored and used is finite, its size provides for a relatively long time constant on the system. For a given discharge rate within the capability of the system, the time required for the greater capacity of the battery to be used provides

relatively slow dynamics. This allows for a long time period between when a lower limit on state of charge is reached and when supplemental generation is required. The relatively slow (minutes or hours) time period between preferred supplemental generation and the absolute need for it allows for communication between the energy storage elements and supplemental generators to be notably slow by the standards of the communication industry.

2.1 Unit Placement

Despite the obvious advantages of energy storage elements in a microgrid environment, it is still debated whether energy storage should exist at each source or whether a centralized energy storage element should bear the sole duty of energy storage. From an energy accounting perspective, the amount of energy absorbed and transmitted is a function only of the size of the unit which is typically directly proportional to the cost. The power systems industry has used the economies of scale as reasoning for larger and larger power generation facilities, but since both battery and inverter costs scale at a linear rate [21] there seems to be little economic advantage to a consolidated energy storage element.

In the case of storage placed on the unit itself, inter-source communication is largely unnecessary as the variations of any intermittent source can be buffered locally by a state of charge management algorithm. In the case of the stand-alone energy storage unit, a similar compensation for intermittent power generation can be accomplished by regulating the flow of power at the connection point of the connection to the microgrid when grid connected. In the event of islanded operation, the state of charge results from the integral of the difference between on-site generation and load. As a closed system the

battery absorbs any imbalance between the supply of power intermittently from nature to renewable sources, backup generation, and the load characteristics. All of these can be forecasted, but never guaranteed.

2.2 Spinning Reserve

Spinning reserve refers to available unused generation. The battery energy storage unit is well suited for this purpose considering the speed of the power electronic interface. It is capable of providing power under fault conditions such as islanding, where the power necessary to supply the load is required from the energy storage unit until a secondary unit can come online. This time can vary from source to source, but is typically less than a minute and well within the energy capacity of the battery even under maximum power output.

Conversely, for transients in the presence of a fixed-power source with a slow time constant like a fuel cell, the storage unit may have to absorb extra energy generated as the fuel cell slowly decreases its output power for the system to remain online. In this case, the energy storage unit may also be required to provide a reference voltage for the power injected by the fuel cell. Many grid-tied inverter systems lack the ability to generate a voltage on their own and rely on tracking of the local voltage to inject current at unity power factor [4]. In the case of an islanding event when no other sources were online, the energy storage element then becomes the solitary source of microgrid voltage.

2.3 Load-leveling from grid

As previously mentioned, if the energy storage unit is placed along the feeder for a local load, the variation in the loads can be decoupled from the input power from the

grid by measuring and regulating the grid flow. The net effect is a significant reduction in peak power levels drawn from the grid which reduces the peak power cost charged by the utility. The utility charges this fee to ensure enough spinning reserve is standing by to supply the peak power demand which indicates that the spinning reserve capability is provided by the energy storage unit with direct financial benefit.

2.4 Source-leveling for intermittent sources

One of the primary issues with intermittent renewable sources like wind and solar is their relatively unpredictable and variable power output. In theory, by predicting the average daily output of a given source, the energy storage unit could be placed within a wind or solar generation installment, effectively converting it to a constant power source. However, due to the limitations in capacity of energy storage units, conversion efficiency, and lifetime-use concerns, energy storage units are currently not well suited for this application [32]. However, this assertion breaks down in the cases where the perceived benefit of reliable power output outweighs the cost of energy storage of adequate size.

2.5 Peak-shaving/Gap-filling

Peak-shaving and gap-filling is very similar to load-leveling, except instead of constant power draw from the grid to supply the daily average load, less power is drawn from the grid during peak demand times. Consequently more power needs to be drawn at low demand time to replace the expended stored energy during peak times.

The net effect is similar to feeder-flow regulation except that some of the external load is supplied by the microgrid, further leveling the output of the generators on the grid. However, to accommodate this function, more storage capacity will be required as change in energy through the daily peak/gap cycle on top of local load profiles. Daily

local load profiles can be assumed to be similar to the rest of the power system which means that the work of the energy storage unit is compounded. Since there is no local benefit for this service aside from drawing even less power at peak-time price, it is likely that additional subsidies will be needed to make this an economically driven decision from the microgrid side.

2.6 Stability buffer for slow-reacting sources (Frequency regulation)

In the presence of generators with rotating machines and other generators with slow dynamic responses, an energy storage unit offers the ability to provide supplemental temporary power to compensate for the initial deficit of slower sources. One of the greatest benefits that energy storage elements have as a byproduct of utilizing a DC or variable frequency source is the requirement for a power electronic front end. These systems are limited by the frequency of modulated voltage output and the impedance of the power filter elements, which are typically tuned to a frequency between the modulation frequency and the fundamental power frequency, resulting in sub-cycle transient response.

3. Inverter Model Development

The inverter model represents the characteristics of the hardware setup in the simulation program EMTP. It incorporates all of the sensing and control algorithms required to operate the units in the Plug-and-Play mode discussed in chapter 2. The EMTP inverter model was developed based primarily from the model presented in [35]. As such, the details of the unchanged portion of the inverter model will be omitted; however, the portion altered to operate from a variable DC bus voltage will be discussed below. As can be seen in figure 3.1.1, the inverter voltage definition comes as a function of the DC bus voltage multiplied by a modulation index in F_{m1} . Although the PI controller will reduce the output error of the applied voltage, it has requires a finite settling time to achieve this. During a transient response to a step change in input voltage, a similar variation of output voltage would result, causing a large variation in reactive power. One point to consider is that though the DC bus voltage will vary significantly, the primary portion of voltage drop on the lead acid battery pack utilized for this research occurs with a natural response time constant of 4 seconds or greater. The remainder, however, is approximated to occur as a series resistance which results in a non-causal function that is directly proportional to the output current from the battery. This will be discussed further in chapter 5. This means that during step-changes in system loading and consequently inverter current, that the battery terminal voltage will drop in part due to a non-causal function of current, causing possible large variations in reactive power as discussed previously. However, the DC bus capacitors will maintain the DC bus voltage to be represented as a continuous function which will be to some benefit of the PI controller attempting to track the error.

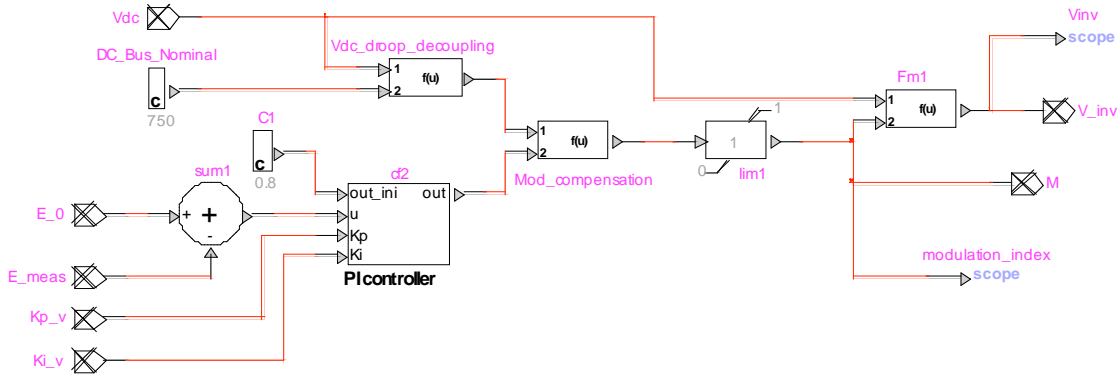


Figure 3.1.1 – EMTP inverter voltage block

To compensate for the droop or surge on the output voltage from large changes in DC bus voltage, a DC-bus voltage decoupling block has been implemented which begins by developing a ratio of the preferred or nominal DC bus voltage to the voltage present on the bus:

$$V_{\text{compensate_pu}} = \frac{V_{\text{dc_nominal}}}{V_{\text{dc_measured}}} \quad (3.1)$$

This voltage ratio is then used to modify the modulation index developed by the PI controller block:

$$M_{\text{mod}} = V_{\text{compensate_pu}} * M = \frac{V_{\text{dc_nominal}}}{V_{\text{dc_measured}}} * M \quad (3.2)$$

Finally, the voltage applied to the inverter is as a result of the modified modulation index multiplied by the DC bus voltage, effectively removing the variation of DC bus voltage on the inverter output voltage:

$$V_{\text{inverter}} = V_{\text{dc}} * M_{\text{mod}} = V_{\text{dc}} * \frac{V_{\text{dc_nominal}}}{V_{\text{dc_measured}}} * M \approx V_{\text{dc_nominal}} * M \quad (3.3)$$

This scheme drastically improves the performance of the inverter unit, theoretically removing all voltage variations from the output of the inverter. However, this scheme requires an accurate measurement of the DC bus voltage and any noise present in the measurement will be amplified by the ratio of the nominal DC bus voltage

to the actual DC bus voltage, as described in equation 3.1, making this system more noise-sensitive when this ratio becomes higher at lower battery voltages. It is also important to note that this scheme will only work in a region where the modified modulation index $M_{\text{mod}} \leq 1$ due to the inability of the inverter to generate a line-to-line voltage differential greater than that of the DC bus for a single-level inverter.

The actual output voltages fed to the system are generated by an average-model approximation that describes the output voltage not as a train of bi-level pulses, but as the average value based on the pulse width. The source v_{bc} represents a line-to-line voltage that is referenced to ground for simulation purposes. This ground reference is lost on the microgrid side as the output is sent through an isolation Y- Δ transformer.

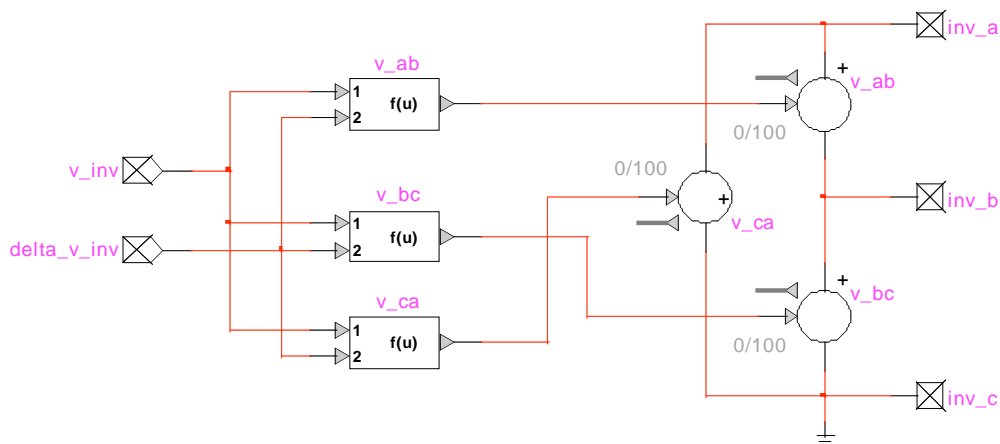


Figure 3.1.2 – EMTP average-model inverter output block

This linear assumption is an approximation, but doing so reduces the voltage harmonics imparted to the system and decreases the complexity of the simulation. The approximation itself is arguably of minor importance, given that the dual-stage (L-C-L) output filter on the hardware setup significantly reduces the output harmonics as well.

4. Battery Handling Requirements

Secondary chemical batteries are energy dense petroleum-alternatives and rechargeable which explains their use in hybrid-electric like in the Toyota Prius and full electric vehicles like the Tesla Roadster. However, because their performance characteristics change as a function of state of charge (SOC), temperature, age, and relative loading just prior to use, batteries are complex nonlinear systems. Battery handling specifications typically outline recommended output current limit, charge current, operating temperature, storage temperature

4.1 Max power available

The maximum power available from a battery is determined by both the necessary terminal voltage at which the power is required and the duration of the required power. Using a 2nd order Randle model, it is clear that the equivalent series resistance is time variant, and depends largely on the previous direction, magnitude, and duration of battery current.

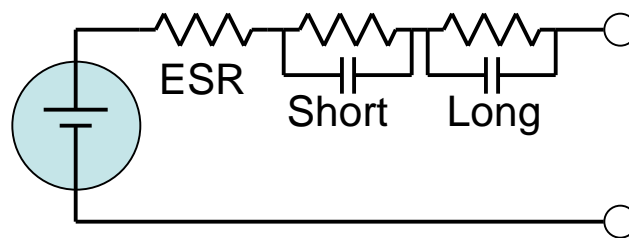


Figure 4.1 – 2nd Order Randle battery equivalent circuit model

As a general characteristic, the maximum power available from the battery could be determined from using only the sum of the series resistances and the internal voltage as a function of the state of charge. However, in this case, it is required that the DC-bus voltage needs be above a minimum voltage to maintain control of the terminal voltage

from the inverter. As an example, the internal resistance of the pack at full charge has an internal resistance of 0.864Ω ($27\text{m}\Omega/\text{cell}$), corresponding to a battery pack voltage of 874V . Assuming the minimum voltage necessary to approximate the 480vrms output from the inverter is 679V , the purely resistive drop would equate to 225A of output current. It is important to note that this value exceeds the 150A maximum output current recommendation of the battery pack, the 100A limit of the power electronic module and the 60A limit on the battery pack fuses. Since this is the theoretical absolute maximum output of the battery under severe operating conditions, it is safe to say that the battery is capable of providing the output power capabilities necessary under reasonable states of charge.

4.2 Lifetime effects

The three main factors that effect Valve-Regulated Lead Acid (VRLA) batteries are positive grid corrosion, water loss [3], and sulfate deposits [33]. Positive grid corrosion occurs when the lead on the positive terminal combines with water molecules and creates PbO_2 , along with hydrogen ions and electrons. This reaction consumes water which is in limited supply in the absorbed glass mat (AGM) construction of a VRLA. Water also is lost through electrolysis and inefficient oxygen recombination. Lastly, the lead dioxide created from the positive grid corrosion can combine with the sulfuric acid to create lead sulfate. The lead sulfate can be returned to the positive plate through charge/discharge cycling, but the net loss of water from the process is permanent.

4.3 Charge and Discharge rates

VRLA batteries achieve rated capacity at a 20-hour discharge rate. Any increase in discharge rate yields progressively decreased capacity, which indicates a trend of increasing efficiency with higher discharge rate [2]. The same trend is also true for the

charging condition, except that the hydrogen and oxygen recombination rate restricts the maximum continuous charge current allowable without running a risk of venting the disassociated gaseous hydrogen and oxygen [1].

5. Battery Modeling

To establish a good sense of state of charge (SOC), an accurate battery model must be employed to track SOC through the varying power trends demanded from the energy storage unit by the loads. Battery datasheets provide voltage characteristics for a battery undergoing a constant-current discharge but will be shown irrelevant for a non-uniform current profile. Therefore, a battery observer was developed from the battery model which can be utilized to modify an open loop coulomb-counting SOC algorithm. The effective modification will compare the actual terminal voltage to the model terminal voltage and add a modification current to change the battery's state of charge over time in an effort to converge the initial SOC estimation on the actual SOC of the battery over time.

5.1 Characterization

For this paper, a second order Randle model will be employed, a model previously presented in [16] amongst others. This model was chosen because from preliminary testing of transient response of terminal voltage to currents could not be accurately modeled with a first-order system. Further experimentation revealed a strong correlation between the second-order model form and measured data.

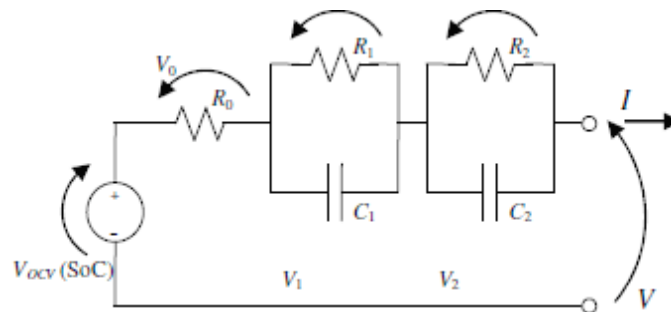


Figure 5.1.1 – 2nd order Randle model [16]

The model itself assumes an internal EMF with an output impedance of a series resistance in cascade with two RC branches. It is also assumed that the time constant of each RC branch is significantly different than the other, prohibiting the combination and simplification of the model into a single order system. Secondly, though each element is initially assumed linear, they will vary with both SOC and relative battery loading, which essentially supersedes the assumption of linear elements. It will be seen in particular that end-effects, or effects that become pronounced near the limits of both SOC and battery current, will be responsible for the large majority of the non-linear characteristics.

The characterization began with measuring the terminal voltage and current of one of the BP5-12 12V cells undergoing the same stair-step current profile utilized in [16] but it was discovered that due to the limitations of the data rate and voltage measurement accuracy, a modified stair current profile elucidated more of the second-order characteristics.

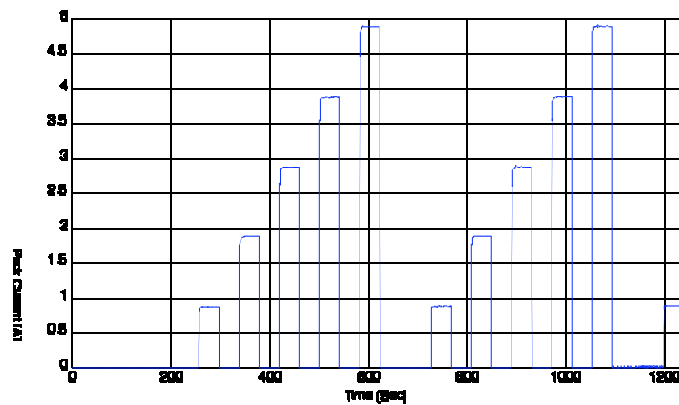


Figure 5.1.2 – Modified-Stair discharge current characteristic for impedance analysis

From figure 5.1.2 it can be seen that there are five discrete steps for each repeated cycle. For the data set used for characterization of the battery, each current step was commanded for a forty second duration followed by a forty second relaxation or recovery

period. At the end of each cycle, the battery was allowed to relax for 100 seconds. This characteristic allowed for the battery voltage to exhibit a large enough transient response to characterize while the period of relaxation in between each current pulse allowed the terminal voltage to approach the open circuit voltage which is helpful for the back-EMF calculation.

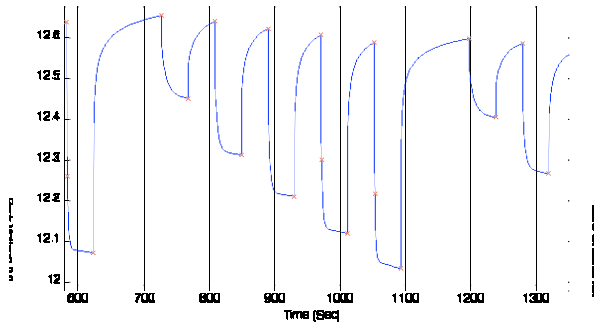


Figure 5.1.3a Terminal voltage characteristic during modified stair discharge with transition markers

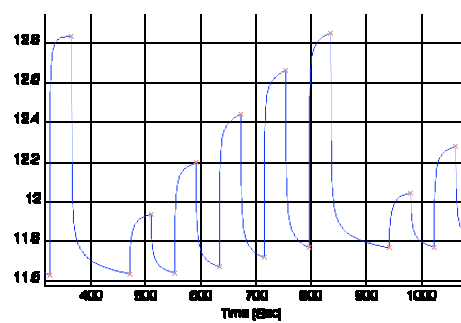


Figure 5.1.3b Terminal voltage characteristic during modified stair charge with transition markers

The transition markers indicated on figures 5.1.3a&b were extracted from the data by noting changes in discharge current, called ‘jumps’, indicating the beginning and end of the transient response characteristic to model. The terminal voltage transient response form of equation 1 is assumed to model the parameters assuming a first order response.

$$V(t) = ae^{-t/\tau} + c \quad (5.1)$$

The magnitude constant ‘a’ is positive for discharges and charging relaxation and negative for charges and discharge relaxations. This magnitude constant represents the magnitude of voltage change that the system undergoes for a given current difference. Therefore, this value, scaled by the magnitude of the current transition was used to estimate the resistance value for the equivalent circuit. The constant ‘c’ is the dc offset which can represent the internal EMF during relaxations. The difference in dc offset

when discharging or charging will be used to represent the sum of the series resistances in the equivalent circuit.

To estimate the ‘a’, ‘c’, and ‘τ’ constants, the DC offset was removed by taking the derivative of equation 5.1, presented in equation 5.2.

$$\frac{dV(t)}{dt} = (-a/\tau)e^{-t/\tau} \quad (5.2)$$

Finally the expression was reduced to a simple linear model in equation 5.3 by taking the natural log of equation 5.2.

$$\ln\left(\frac{dV(t)}{dt}\right) = \ln(-a/\tau) + (-1/\tau)t = b + mt \quad (5.3)$$

This allowed a simple linear regression to determine the constants for a given transient response. Although the value of ‘c’, the DC offset, was lost by taking the derivative of equation 5.1, it was back-calculated by taking the average difference between the measured data and the response with no DC offset.

As previously mentioned, it was determined that a 2nd order model was necessary to appropriately model the response characteristic. Figures 5.1.4a&b illustrate the relative cohesiveness of the model to the measured data.

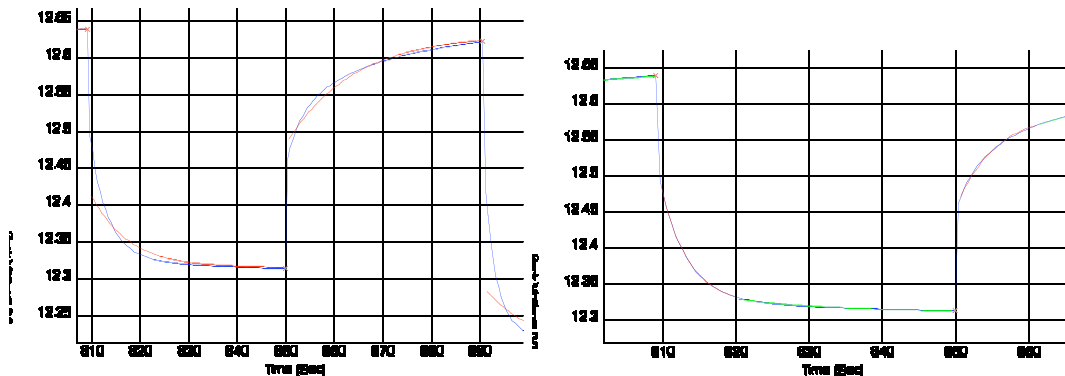


Figure 5.1.4a Single-stage exponential curve-fit of discharge voltage response characteristic

Figure 5.1.4b Two-stage exponential curve-fit of discharge voltage response characteristic

It can be seen from the first-order model that the model is a poor fit all around. In the beginning of the transient, the model describes a rate that is much too slow, indicating the presence of an unmodled faster time-constant and allowing for notable divergences between the measured and modeled response. The two-stage approach appears to have little to no discrepancies. The break-point between the two stages was chosen manually at 11 seconds, which appeared to allow each decay model to exhibit the best coherence to the measured data.

An important point to note was the addition of a compensation for the effects on the terminal voltage due to discharge or charge of the battery over time. The net result is a change in the SOC of the battery and the EMF of the battery as a function of SOC. Equation 1 was re-expressed to include this effect in equation 5.4.

$$V(t) = ae^{-t/\tau} + \frac{1}{C_{batt}} \int i_{batt} + c \quad (5.4)$$

Equation 5 shows that if this effect can be considered constant for the linear region of the EMF(SOC), then the derivative of the measured data is biased by a factor proportional to the charge or discharge current. Therefore, the derivative was modified by a similar value, decoupling the effect of the change on the EMF in order to isolate the first-order response characteristic.

$$\frac{dV(t)_{mod}}{dt} = (-a/\tau)e^{-t/\tau} + \frac{i_{batt}}{C_{batt}} - \frac{i_{batt}}{C_{batt}} \quad (5.5)$$

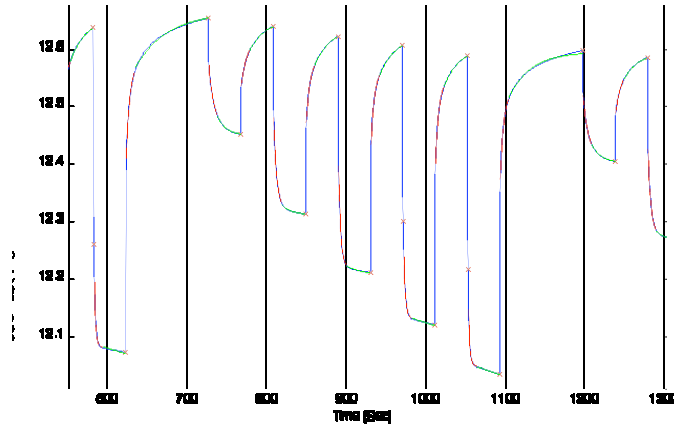


Figure 5.1.5 – Two-stage exponential curve-fit of discharge voltage response characteristic for one modified-stair cycle

With the same method applied to the entire discharge characteristic, the parameters of the equivalent circuit model can be expressed as a function of SOC and of output current. The effects of temperature, for this analysis, have been neglected.

5.2 Model development

From an initial inspection of the time constants gathered from the regression analysis of the transient response, it appeared that there was a time constant of approximately four seconds for the first branch and twenty seconds for the second. As this represents a spectral separation of the time constants by a factor of 5, superposition will be used to develop the model, assuming that the effects are relatively independent of each other.

To assist in the model generation, each parameter was extracted from the compiled data as a function of SOC and current. The characteristics for charge and discharge were different enough to model them separately and incorporate them into the

model using a conditional check of the battery current to determine which parameters will be used.

The first parameter extracted was R_0 , which was simply calculated from the change in terminal voltage one time sample, 0.5 seconds, after a change in the battery current. Under the assumptions of the model, there should be an immediate response and though the 0.5 second sample period is relatively long, faster data was not available to verify how fast the initial response was and how much of the response of the faster RC branch was taken into account by the time between samples. With this disclaimer stated, the parameter data displayed here was only used as a guideline for tuning the model later by hand. For more accurate parameter estimation, a faster sample-rate is necessary.

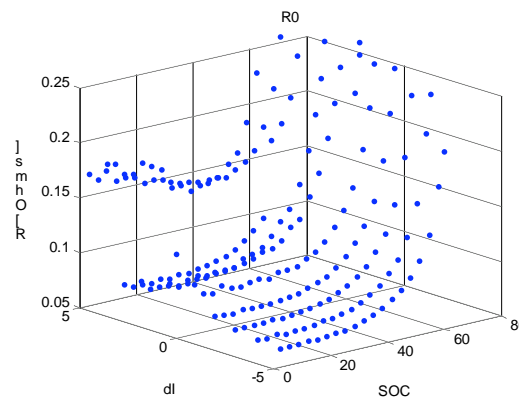


Figure 5.2.1 – Parameter extraction of the 0th stage equivalent series resistance (ESR) as a function of state of charge and step-change in current

The 0th stage ESR (R_0) is plotted for the various discharge currents and relaxations. For the positive current out of the battery, the battery is discharging. For the negative currents described in the figure, this is the response or relaxation at zero current from a previous discharge current of the same magnitude. One interesting characteristic to note is the high series resistance for the full range of SOC at 4A and above. This is

likely due to the mass transport limitation mentioned in [20], but could equally be attributed to the sample-time delay effects from the 0.5second sample time. The increase in ESR in towards the lower end of SOC is a characteristic end-effect where the electrolyte concentration diminishes.

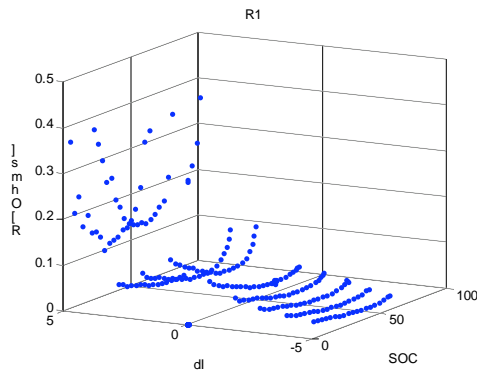


Figure 5.2.2a

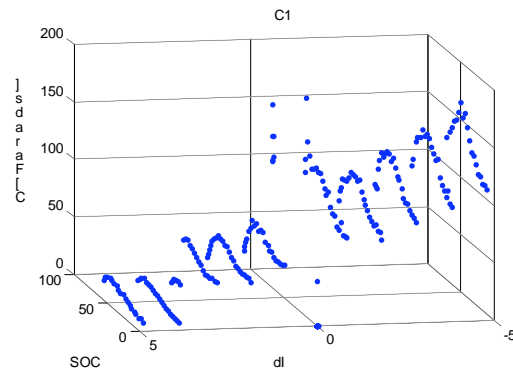


Figure 5.2.2b

Parameter extraction of the 1st stage equivalent series resistance (a) and capacitance (b) as a function of stat of charge and step-change in current

The extracted parameters for the first RC time constant, the one modeled after the initial 11 seconds of the transient are presented in figures 5.2.2a&b. It is interesting to note that the effective resistance is lower as current increases and there is a noted increase in resistance towards the 4-5A region during discharge. This increase in resistance could be attributed to mass transport limitations, but upon inspection of the associated capacitance, it appears that the time constant does not change significantly. It is only the ratio of the resistance to capacitance that changes, indicating that there is more change in voltage for the transient response during the first 11 seconds.

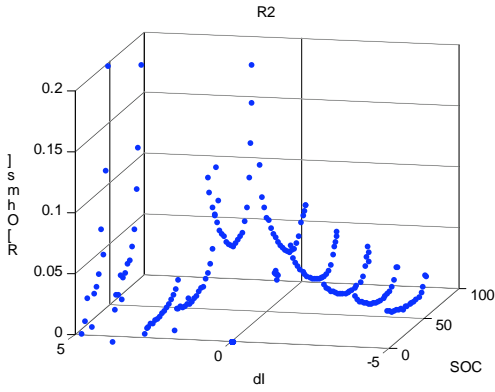


Figure 5.2.3a

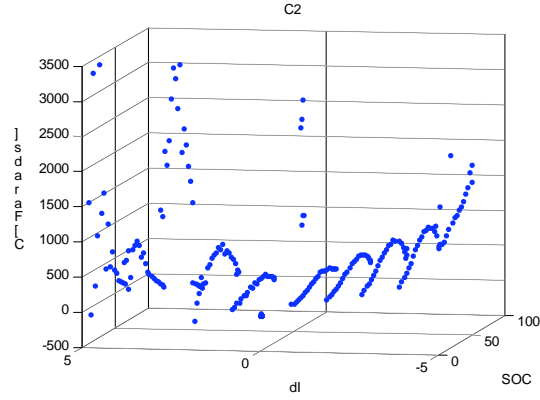


Figure 5.2.3b

Parameter extraction of the 2nd stage equivalent series resistance (a) and capacitance (b) as a function of stat of charge and step-change in current

For the second stage of the transient, the resistance trends higher at lower currents than compared to higher currents. It is interesting to note the similarity in trends between the extracted values for R1 and R2. This indicates a common phenomenon connecting the parameter estimates of both stages of RC networks. The capacitance in the second stage shows a mild trend towards the mid one hundreds. For the purposes of modeling the response, the value will be assumed constant.

After manual alteration, the equation for R0 as a function of SOC and output current is presented in equation 6. It includes the addition resistance that occurs at low charge states while discharging and high charge states while charging. These effects are polar, which justifies the multiple forms of the equation.

$$\begin{aligned}
 R_0 &= R_{00} + R_{0end} * e^{-SOC/\tau_{SOC0}} && \text{for } I_{batt} \geq 0 \\
 &R_{00} + R_{0end} * e^{(SOC-1)/\tau} && \text{for } I_{batt} < 0
 \end{aligned}
 \tag{5.6}$$

The equation for R_1 is similar to that of R_0 except it includes a scale factor that is altered by the output current. This was implemented to account for the decreased settling time observed at high currents.

$$R_1 = \begin{cases} (R_{10} + R_{1end} * e^{(SOC-1)/\tau_{1end}}) * e^{(1-I_{batt})/\tau_{1I}} & \text{for } I_{batt} \geq 0 \\ (R_{10} + R_{1end} * e^{(SOC-1)/\tau_{1end}}) * e^{(I_{batt}+1)/\tau_{1I}} & \text{for } I_{batt} < 0 \end{cases} \quad (5.7)$$

The equation for R_2 is relatively simple and as it resulted in a fairly small value with a relatively long time constant due to the large associated capacitance, increases in resistance due to end were only modeled into the discharge polarity.

$$R_2 = \begin{cases} (R_{20} * e^{(-I_{batt})/\tau_{2I}} + R_{2end} * e^{-SOC/\tau_{2end}}) & \text{for } I_{batt} \geq 0 \\ (R_{20} * e^{(I_{batt}+1)/\tau_{2I}}) & \text{for } I_{batt} < 0 \end{cases} \quad (5.8)$$

Parameter	Discharge value ($I_{batt} \geq 0$) (per 12V pack)	Charge value ($I_{batt} < 0$) (per 12V pack)
R_{00}	0.085 [Ω]	0.095 [Ω]
R_{0end}	0.34 [Ω]	0.20 [Ω]
τ_{SOC0}	1/15 [Cycles]	1/6 [Cycles]
R_{10}	0.055 [Ω]	0.07 [Ω]
R_{1end}	0.13 [Ω]	0.20 [Ω]
τ_{1end}	1/10 [Cycles]	1/3 [Cycles]
τ_{1I}	1.8 [A]	1.2 [A]
R_{20}	0.075 [Ω]	0.07 [Ω]

R_{2end}	0.15 [Ω]	-
τ_{2end}	1/14 [Cycles]	-
τ_{21}	1/0.3 [A]	1/0.8 [A]

Table 5.2.1 – Battery model parameter constants

To test the model, a battery observer was constructed which utilized the previously established model which used the measured battery current as feedforward. The SOC was modified by a proportional controller operating off the error between the model and measured terminal voltage which will be addressed in more detail in this section.

The model terminal voltage was defined as described in equation 5.9, as a function of the internal EMF, modified by the voltage drop of the effective impedance model.

$$V_{model}(k) = E(k) - V_0(k) - V_1(k) - V_2(k) \quad (5.9)$$

The components to equation 5.9 are described below in equations 5.10-15 where V_0 is the voltage across the resistor R_0 and V_1 and V_2 are the voltages across the first and second RC branches respectively. The index value k indicates the most current value based off of the most recent current and voltage samples. The $k-1$ index implies a reference to the most recent previous value calculated for the respective parameter; the $k+1$ indicates a prediction that will be used as a current value in the next cycle of calculation.

$$V_0(k) = R_0(k) * I_{batt}(k) \quad (5.10)$$

$$V_1(k) = V_1(k-1) * e^{-T/(R_1(k) * C_1(k))} + I_{batt}(k) * R_1(k) * (1 - e^{-T/(R_1(k) * C_1(k))}) \quad (5.11)$$

$$V_2(k) = V_2(k-1) * e^{-T/(R_2(k) * C_2(k))} + I_{batt}(k) * R_2(k) * (1 - e^{-T/(R_2(k) * C_2(k))}) \quad (5.12)$$

Equations 5.11 and 5.12 describe the voltage across the RC network after a time of T with an initial voltage of V(k-1). They include a portion of the equation that accounts for the natural response that includes the initial condition and a separate part that can be considered the forcing function which utilizes the battery current. The equations are of the form consistent with the physical process driven from a constant battery current, which is a necessary assumption in discrete time systems and are valid for any sample time T.

$$V_1(k) = V_1(k-1) * (1 - \Delta t / (R_1(k) * C_1(k))) + I_{batt}(k) * \Delta t / C_1(k) \quad (5.13)$$

$$V_2(k) = V_2(k-1) * (1 - \Delta t / (R_2(k) * C_2(k))) + I_{batt}(k) * \Delta t / C_2(k) \quad (5.14)$$

Equations 13 and 14 represent the discrete-time calculations for RC-network voltage under the assumption $T \ll 1/(R * C)$ so that there exists local linearity between each sample instant. This assumption is valid for simulations with low sample time, but invalid for comparison with the measured data which has a sample time of $T \approx 0.5$ seconds.

$$E(k) = E_{min} + E_{linear} * SOC(k) - E_{end} * e^{-SOC * \tau_{v-soc}} \quad (5.15)$$

Equation 5.15 describes the internal voltage of the battery, or internal EMF. It was found to be largely a linear characteristic as a function of SOC with a significant decay at lower charge states.

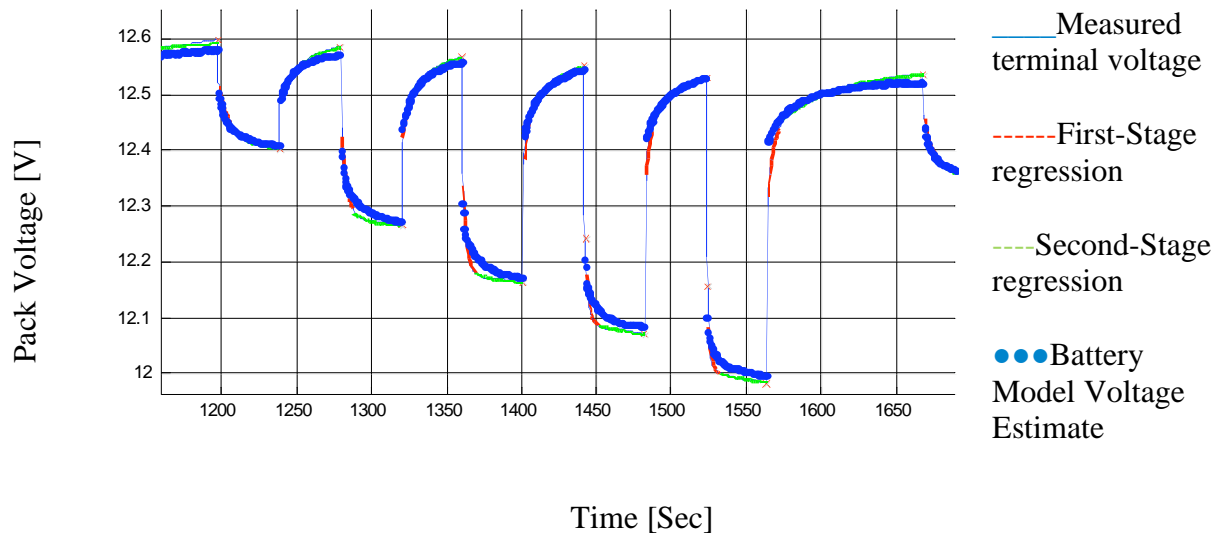


Figure 5.2.4 – Closed-loop battery observer superimposed on measured terminal voltage

Figure 5.2.4 shows the tracking of the battery observer to the terminal characteristics. It can be seen that the relaxation/recoil characteristic that occurs from a zero output current has much less error than that of the initial seconds following a discharge transient. The error increases with higher current transients. The positive point is that the integrated error is small because the model does eventually converge with the transient characteristic. The integrated error is an important factor involved in the closed-loop SOC tracking which will be discussed further below.

It is also important to note that this work employed a black-box approach to transient modeling which inherently did not take into account all modes of operation and simply fails to model some components of the transient response.

The closed-loop effect comes from equation 5.16 where the measured battery current is summed with an artificial current that is proportional to the error between measured and observed battery voltage. Due to the relative linearity of the internal EMF of the battery as a function of SOC, the voltage mismatch will be reduced by modifying the model internal EMF over time as a function of the integrated voltage error.

$$\text{SOC}(k+1) = \text{SOC}(k) - (I_{\text{batt}} + V_{\text{err}}/R_{\text{aSOC}})*\Delta t/Q_{\text{capacity}} \text{ [PU]} \quad (5.16)$$

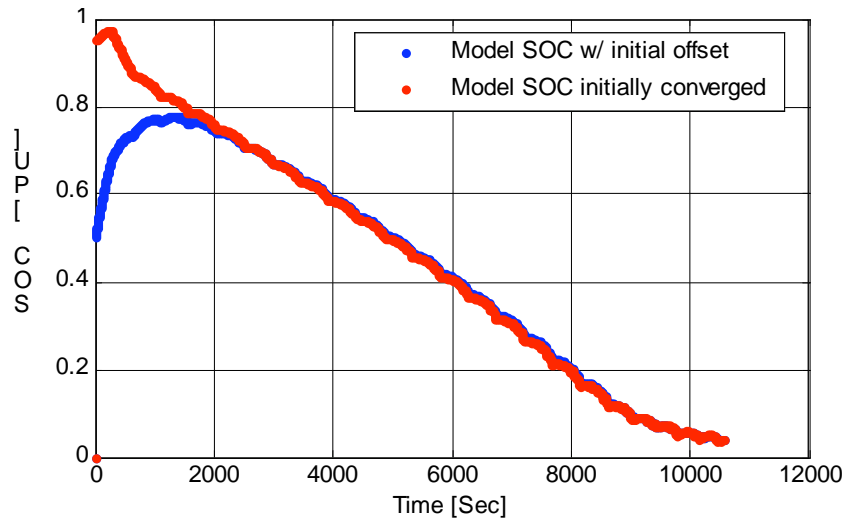


Figure 5.2.5 – Closed-loop battery observer SOC estimates

Figure 5.2.5 shows the convergence of an initial offset in the SOC to a SOC estimate that initially had no offset. The ripple effect comes from the modified stair discharge characteristic which makes a ripple not only acceptable, but expected. Since actual SOC is relatively elusive in real time, comparison of the estimated SOC to actual SOC is difficult and omitted for the purposes of the work contained herein. However, the initially converged SOC trace has relatively small integrated error and is a reasonable representation for SOC as a sole function of integrated current. Nevertheless, the

convergence algorithm indicates a stable and well-damped response that is on the order of 600 seconds. Previous tests were conducted with a higher $1/R_{aSOC}$ gain that showed convergence in much less time but was reduced here for the purposes of illustrating the transition.

5.3 EMTP implementation

With the development of the model complete, implementation in EMTP, the main simulation platform employed for this research, is a simple matter of scaling the impedance into the configuration of the full-scale test stand. For the battery configuration used, there are two parallel strings of 64 series 12V batteries. Essentially, all resistances are scaled by 32 and the capacitances are scaled by the inverse of the same factor which maintains the previously established RC time constants.

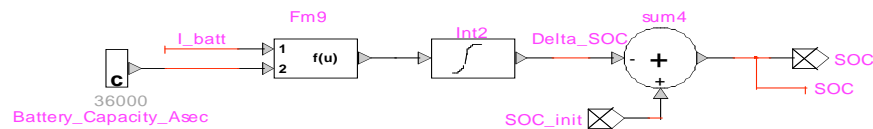


Figure 5.3.1 – State of Charge tracking sub-circuit within battery model

The state of charge is determined by a coulomb integrator which has been noted to provide a reasonably accurate charge estimate [16]. However, a simple integrator requires both the initial state of charge and an accurate current measurement to avoid SOC drift as a function of current measurement error over time. Though a closed-loop system with terminal voltage feedback will be employed in the actual test setup, the relative time scales of the simulations to be run in EMTP make a closed-loop approach unnecessary. Any accumulated error from rounding would not be present for a long

enough time to cause any significant errors in the system for the transient operation simulations which usually are run for less than one minute.

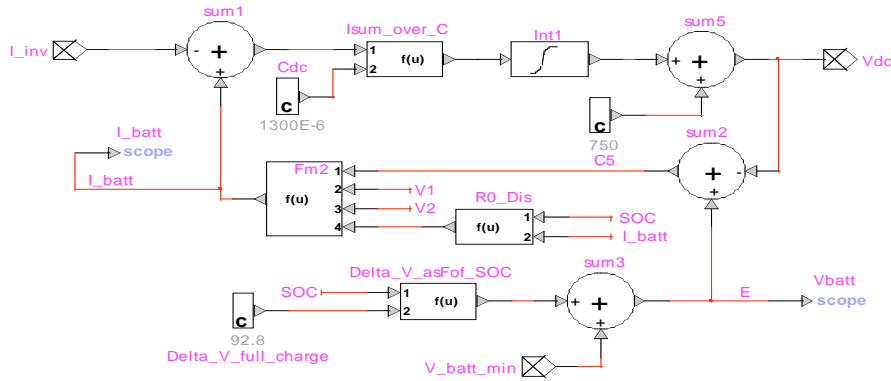


Figure 5.3.2 – Terminal voltage sub-circuit within battery model

The terminal voltage is defined as the voltage on the capacitors connected to the battery’s output terminals. The voltage differential between the internal EMF of the battery and the capacitor bank is then a deterministic quantity assigned to the sum of voltages across the output impedance of the battery model. From the Fm2 block in figure 5.3.2, it can be seen that the output current is defined as a function of the difference in battery EMF and the capacitor voltage (V_{dc}), the voltage in the first and second stages of the Randle model, and finally the linear ESR, R_0 . Since the voltage on the DC bus can change during transients in the system much faster than the Randle model RC branches, the output current is initially characterized by R_0 . After a transient occurs, V_1 and V_2 will change over time which will eventually change the terminal voltage further.

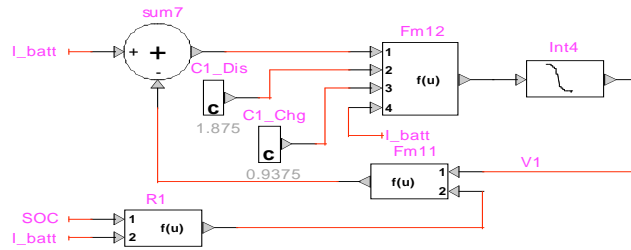


Figure 5.3.3 – First-stage RC voltage sub-circuit within battery model

The first of the RC branches is depicted in figure 5.3.3, which is identical in structure to the second RC branch. It is essentially an integrator with a negative feedback proportional to the voltage across the capacitance (V_1) multiplied by the feedback resistance (R_1). The circuit itself utilizes a separate parameter set for positive currents versus negative currents, which explains why two of the blocks utilizing the circuit parameters require inputs of the battery current. The Fm12 block has a polarity trigger to decide which C1 value to use, C1_Dis or C1_Chg for discharging and charging respectively. The R1 block has a similar trigger, but also includes the effects of current magnitude and SOC end-effects, employing the resulting parameter equations found in section 5.2.

5.4 Microcontroller implementation

To implement the battery model in the microcontroller, a greatly simplified version was employed compared to that used in MATLAB and EMTP due to the need for a low computational time. Although the loop was executed in the main loop which is interruptible by the primary control loop, but causes a delay in the limit-checking safety features which run in the main loop as well. The algorithm was modified primarily to

omit the exponential decays which amount to a significant approximation but tracks within 5% of the SOC developed by the more complex model.

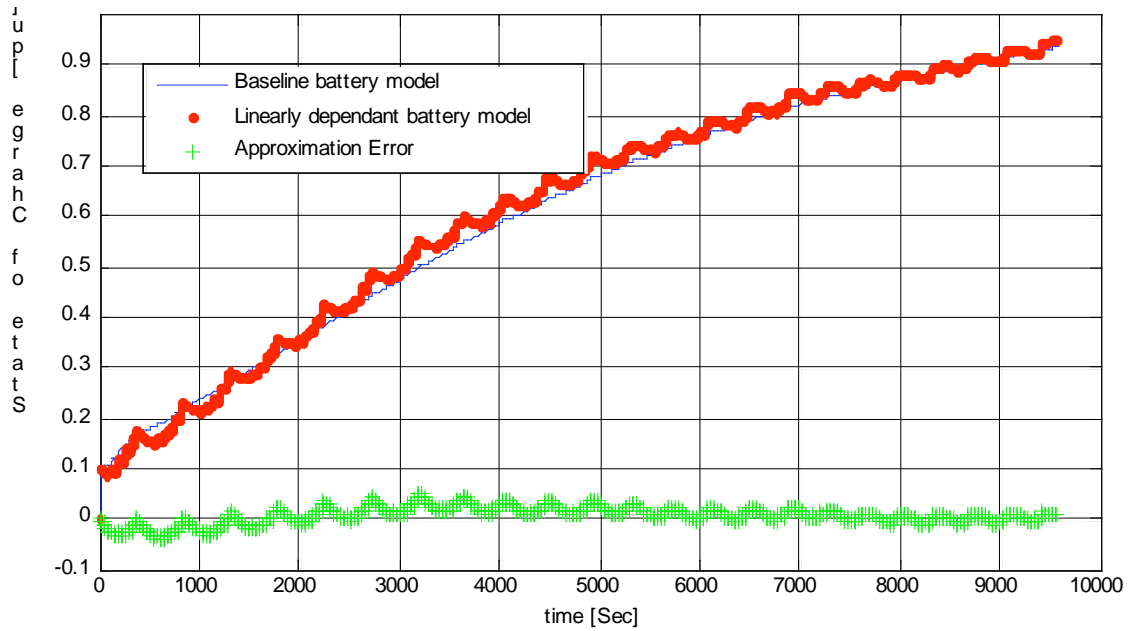


Figure 5.4.1 - SOC estimation error by linearly dependant parameter approximation during a modified-stair charge cycle

The equations to describe the simplified model are presented in equations 5.17-20. These depict a constant as well as an inverse relationship to the current which essentially decreases the effective resistance for higher current levels, resulting in a shorter settling time of the transient characteristics. These effects are very similar to what was observed in the original modeling process.

$$R_0 = R_{00} + \frac{R_{0I}}{I_{batt}} \quad (5.17)$$

$$R_1 = R_{10} + \frac{R_{1I}}{I_{batt}} \quad (5.18)$$

$$R_2 = R_{20} \quad (5.19)$$

$$E = E_{\min} + E_{\text{linear}} \text{SOC} \quad (5.20)$$

Parameter	Discharge value ($I_{\text{batt}} \geq 0.5\text{A}$) (per 12V pack)	Low-Current value ($-0.5 < I_{\text{batt}} < 0.5$) (per 12V pack)	Charge value ($I_{\text{batt}} < -0.5\text{A}$) (per 12V pack)
R_{00}	0.083 [Ω]	0.108 [Ω]	0.149 [Ω]
R_{0I}	0.025 [Ω]	0.0 [Ω]	-0.045 [Ω]
R_{10}	0.0 [Ω]	0.1 [Ω]	0.033 [Ω]
R_{1I}	0.1 [Ω]	0.0 [Ω]	-0.17 [Ω]
R_{20}	0.005 [Ω]	0.005 [Ω]	0.005 [Ω]
C_1	120 [F]	120 [F]	120 [F]
C_2	6000 [F]	6000 [F]	6000 [F]

Table 5.3.1 – Linearly approximated battery model parameter constants

One interesting point to note was the inclusion of a much larger capacitance in the second RC branch. This was included to account for the drift of the terminal voltage during constant current discharges that was at a rate much higher than that expected from normal discharge. This capacitance is nearly identical to half that of the battery capacity itself, which hints at a correlation between a chemical process at one terminal of the battery.

5.5 Battery conclusion

This chapter presented the assumed equivalent circuit model applied for a single 12V battery from the battery bank used in the laboratory test stand. The battery was subjected to a series of charge and discharge profiles in order to observe the transient response characteristics. Equivalent circuit parameters were extracted from the response characteristic that proved to be functions of both SOC and battery current. Parameters were developed from the initial extractions and manually modified to best fit the transient characteristic. The model was verified via simulation in MATLAB by comparisons to measured data, acting as a battery observer that developed a SOC estimate. Finally, the battery observer was implemented in the hardware setup to estimate the SOC of the battery pack.

6. State-Of-Charge management

6.1 Automatic SOC limit algorithm

One of the most important components to the operation of an energy storage element in a Microgrid using the CERTS concept is the on-board management of state of charge. As the CERTS concept employs a great deal of self-sufficiency in the individual microsources, bereft of high speed communication from a master controller, maintaining a nominal state of charge is a task appointed to the on-board controller alone.

6.1.1 Power limitations of charge and discharge cycles

The control methodology used in this document is employed to ensure that the state of charge of the battery has both the power capability available to absorb transients in the system and the energy reserve to support the auxiliary power needs in the system for a pre-determined amount of time. This requires assessing both the power capabilities and energy reserve as a function of the state of charge.

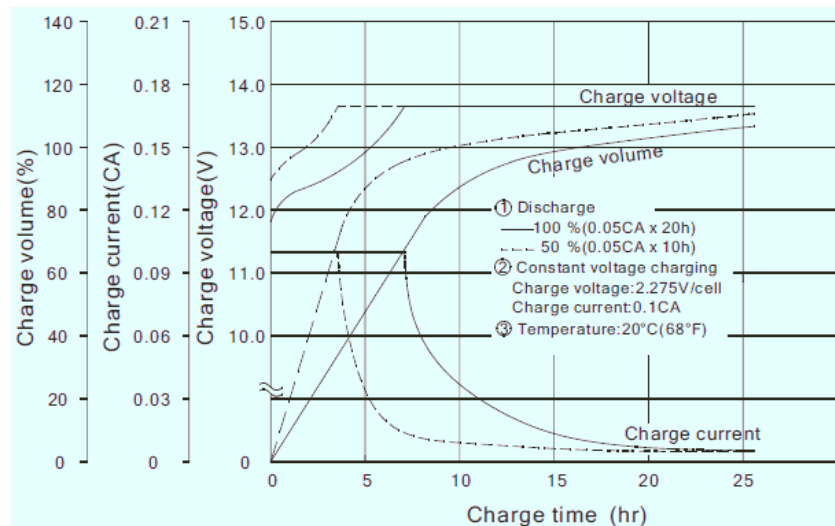


Figure 6.1.1 – Charging characteristic of 5Ah VRLA battery

From the charge current characteristic shown in figure 6.1.1, it is clear that there are two regions of charging operation: a region where the charge impedance of the battery is low and the safe charging region is defined by the limitation of charge current and the following region where the charging voltage becomes the predominant limitation. The boundary between the two determines the maximum charging power, or the maximum power that the battery can safely absorb on a continuous basis. As previously mentioned in the battery handling section, the charge current limitation comes from the generation of dissolved oxygen in the electrolyte from inefficiencies in the charge process. Therefore, the charge current limitation can be exceeded if the dissolved oxygen is kept low enough to not discharge oxygen through the sealing valves. If the oxygen recombination rate can be assumed to be directly proportional to the oxygen concentration, a simple linear model can be used to approximate and control the oxygen concentration. If the charge efficiency is known, and the proportion of disassociation that accounts for the charge inefficiency, the rate of oxygen generation can be calculated and compared to the rate of natural oxygen recombination. The overall rate can be taken into account considering the volume of electrolyte that the oxygen could diffuse into, which ultimately defines the energy absorbed in the short-term overcharge process. Though this analysis is not within the scope of this work, the results would be useful for determining the envelope of reasonable charge practices for extended battery lifetime.

One of the keys to ensuring that there are proper power capabilities from the battery pack is ensuring some allowance for over-current on charging. The dissolved oxygen characteristic suggest that charge current limitation can be exceeded on a short time basis, but the charge current must be de-rated after an over-charge event to ensure that transient power requirements do not exceed the hard oxygen concentration limit.

During discharging, the current is limited by the internal impedance which affects the terminal voltage. Secondly, the overall efficiency of the discharge is diminished with increased discharge rate.

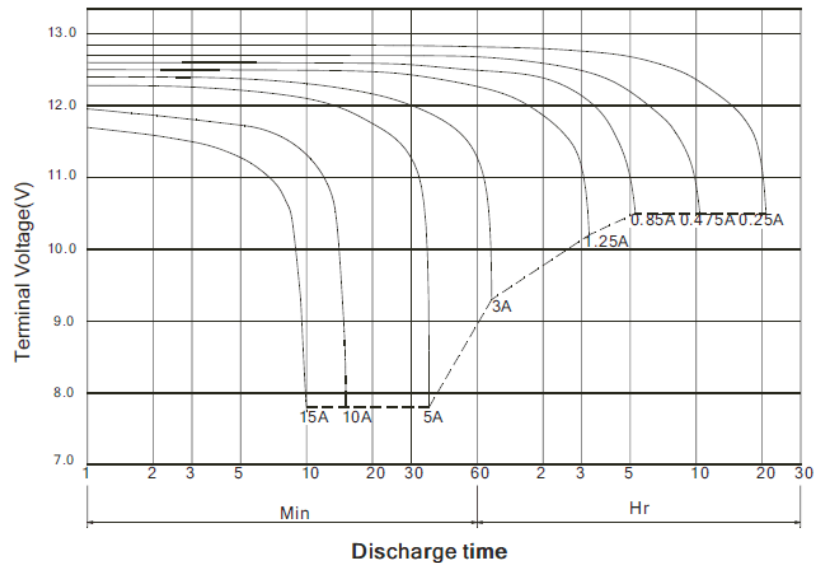


Figure 6.1.2 Discharge voltage characteristics under various discharge rates

VRLA batteries are typically rated for discharges that are at a 20 hour rate. From figure 6.1.2, it can be discerned that the available energy from the battery diminishes significantly, lasting only 37 minutes at the 1-hour discharge rate. This requires that a state of charge algorithm would take into account the increased depletion of capacity for increased rates of energy usage.

It can also be seen in figure 6.1.2 that the terminal voltage of the battery reduces drastically where the discharge voltage nears the end of usable capacity. This end of usable capacity defines a minimum power at end of life for each discharge rate. This characteristic helps define the minimum allowable power specified for the system.

6.1.2 Definable limits on state of charge

With the minimum requirement of bi-directional power flow, the upper and lower SOC limits can be defined. Secondly, by defining the amount of reserve energy required for backup purposes in the event of islanding, the nominal operating space is limited further by an amount proportional to the duration and power rating of the specified backup requirement, defined as the energy reserve limit. Furthermore, a point above the energy reserve limit, named the lower marginal limit is specified as some value marginally greater than the energy reserve limit. The marginal limit defines a hysteretic point where the control of the energy storage element will return to nominal operation, as opposed to the at-limit control strategy.

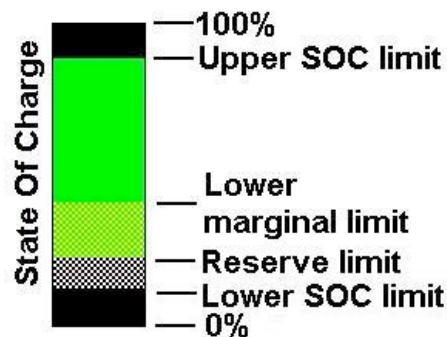


Figure 6.1.3 – Classification of the charge-state limits

6.1.3 At-limit control strategy

The strategy employed here to maintain an adequate charge state to satisfy the previously stated requirements is relatively simple in implementation. While the SOC is within the nominal region, the unit is able to output or absorb power as defined by the user set-point and system loading (frequency). Beyond the upper SOC and lower reserve

limits, a proportional with integrated (PI) controller is implemented to modify the output power of the system. In the case of the upper SOC limit, the PI controller will use a SOC command of the upper limit. Once the state of charge is reduced below the upper limit and the integrator has gained a positive value, then the unit will return to normal operation. The lower limit can utilize a variety of strategies to maintain the SOC on the lower end; two of which are presented here. One strategy would define a commanded charge rate until the SOC reaches the lower marginal limit. The other would implement a PI controller on the SOC similar to the upper limit control which could use either the reserve limit or the lower marginal limit as the commanded charge levels. In the case where a PI control was used to bring the SOC from the reserve limit to the lower marginal limit, a charge-rate limit would have to be imposed at the preferred rate of charge to protect the battery and/or achieve a certain level of efficiency while charging.

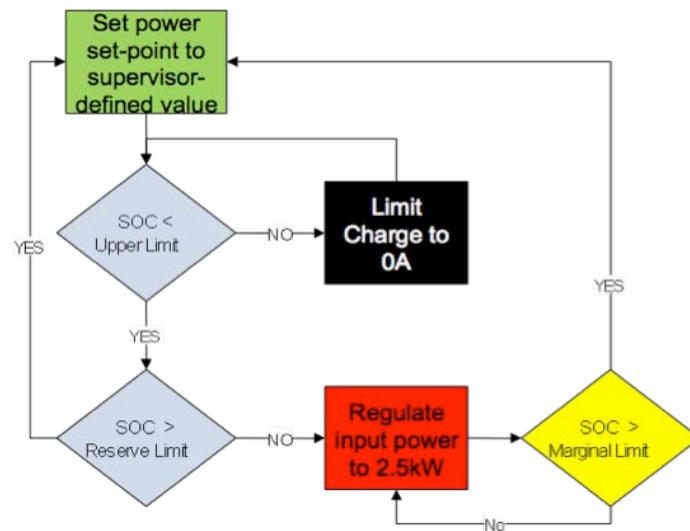


Figure 6.1.4 – SOC top-level limit control strategy

6.2 Automated SOC limit controller

As previously described in the previous section the SOC limit controller will only act when the state of charge is outside the defined range. For the purposes of this section, the upper and lower SOC limits will be defined at 0.8pu and 0.3pu respectively. The marginal limit will be defined at 0.4pu which is designated to be the limit at which the battery has charged up enough to regain the normal droop characteristic defined by the supervisor-specified power or flow set-point.

6.2.1 EMTP model of SOC limit controller

The EMTP implementation of this controller utilizes only one signal from the state of charge and has one output that defines a power-modifier. The power modifier, or P_{mod} , is a per-unitized value that offsets the normal control law acting off the measured and reference power to control the output frequency.

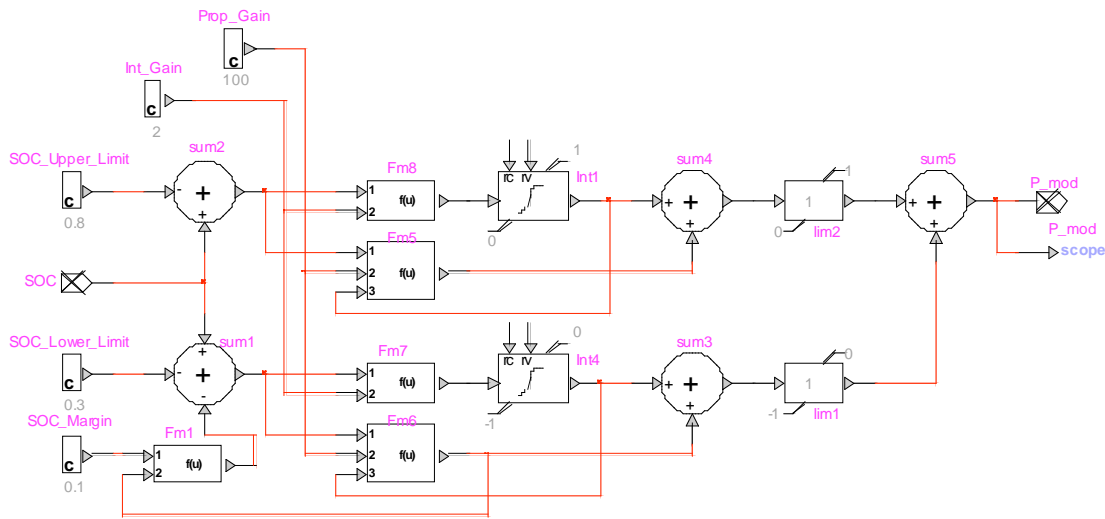


Figure 6.2.1 – EMTP Implementation of the automated SOC limiting controller

The controller is configured such that once a non-zero error is accumulated between the reference SOC boundaries and the measured SOC. The integrators are

limited on one side to a value of zero which occurs when the SOC is within the normal operating range. When the measured SOC is greater than that of the upper limit, the integrator begins climbing at a rate determined by the integrated error gain. In figure 6.2.1, this gain has a value of 2. The accumulated non-zero value then modifies the power error signal. This modification at the upper limit could be considered an increase in the power set-point or a decrease in the measured power output. The net effect is an increase in power output until the SOC is no longer increasing.

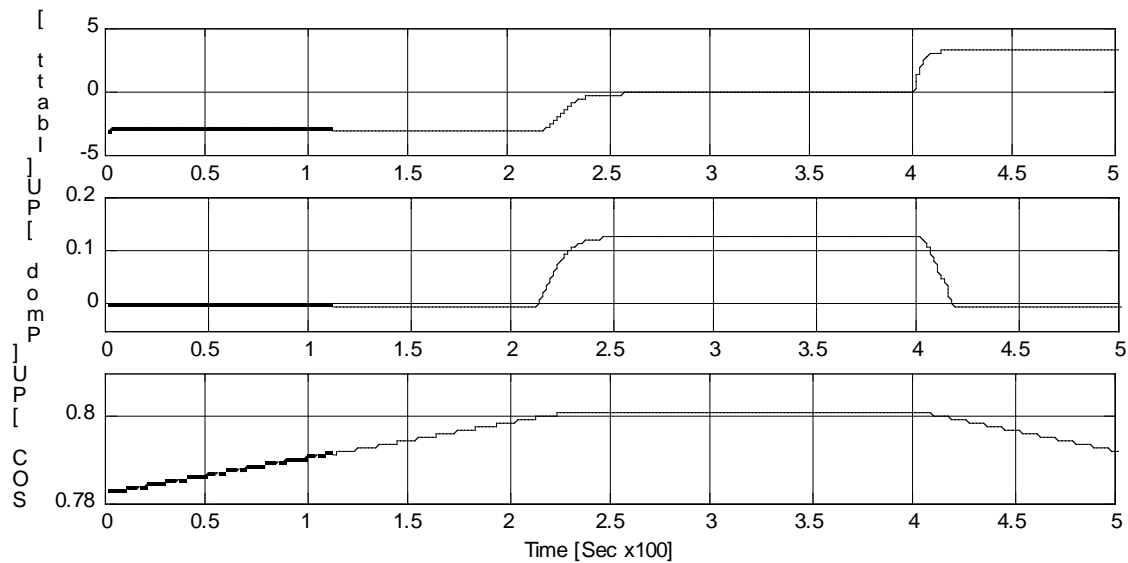


Figure 6.2.2 – Operation of the automated SOC limiting controller at the upper limit

From the characteristic in figure 6.2.2, it can be seen that once the upper SOC limit is reached, that the PI controller begins to act and regulates the charging current to nearly zero in approximately 30 seconds. At 400 seconds in figure 6.2.2 the operating point of the load changes and the system frequency droops, changing the specified output power to a different point according to the power frequency droop characteristic. At this point the SOC falls below the upper limit, causing the integrator to unwind. Eventually, the integrated output specifying an increase in power output from the integrated portion

of the limit controller will be less than the proportional controls error signal specifying less power output. However, the controller will be restricted from specifying a decreased output power at the upper limit, because of the output limiter. The limiter also provides a seamless transition from limited to unaffected operation.

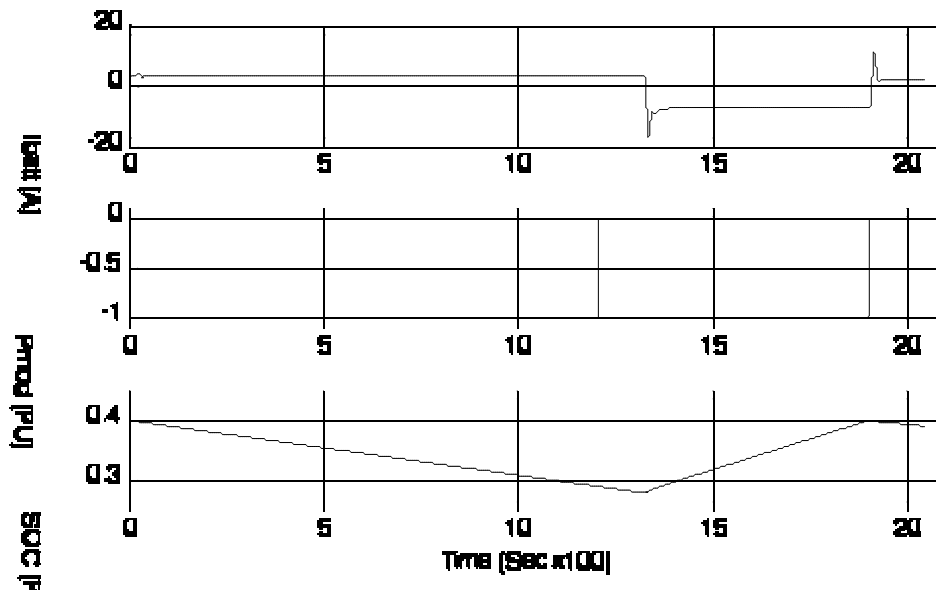


Figure 6.2.3 - Operation of the automated SOC limiting controller at the lower marginal limit

At the lower marginal limit, there is a slightly different characteristic specified as compared to the behavior of the upper limit. In an attempt at quickly regaining normal operation of the energy storage unit, the limit controller places a SOC command marginally greater than that of the reserve limit, consistent with figures 6.1.3 and 6.1.4. The result is a modification of the power command up to 1pu so that the battery will charge, taking power from other sources to do so. In the case illustrated in figure 6.2.3, the source is grid-connected, so the extra power required to charge the battery as well as supply local loads is simply pulled from the grid connection. Figure 6.2.4 illustrates the operation of the lower SOC limiter when in island operation without any other microsources connected

7. System test results

To confirm results from simulation and examine the effects of external perturbations on the operational and transient response characteristics of the system were investigated under SOC-limiting conditions. The operation of the system under nominal SOC is unchanged from that of previous work regarding microsources [35]. Therefore, the analysis in this section is restricted to SOC-limit operation only.

This section investigates the SOC-limit operation of the energy storage element through load transients and SOC paths across specified limits. The two types of events are demonstrating two separate characteristics of the system. While the step-changes of load demonstrate transient stability, their response is dictated by the natural response of the system, in whatever mode it happens to be in, limited or nominal operation. The events that occur when SOC limits are encountered are intentionally slower in response than the load-changing transients to avoid imparting resonant dynamics on the system. The time constant of each system is between two and four seconds, which is intentionally gauged against the time constant of a slow-reacting source such as a diesel genset. This ensures that even though the SOC limit controller will dictate the power output of the energy storage element in steady state, the transient power-sharing characteristic will still exist for conditions when slow-reacting sources suffer an output capability deficit during load transients. The accumulated SOC error during these transients is not significant in this case as it is assumed that the capacity of the energy storage element is much greater than that of the temporary accumulated error. Secondly, although the exact time-based characteristic of the charge current limitations is not known, the average recommended charge current may be exceeded in transient conditions but should not pose any significant battery damage. This conclusion comes from the relatively small response

time to system transients on the order of seconds compared to the battery handling recommendations from the battery manufacturers which were reported to be on the order of fractional minutes.

7.1 Power mode stability under load changing & islanding

Power mode utilizes output power, compared to the commanded output power, as the feedback error used in the proportional frequency droop characteristic. Since the unit output power requires no outside information, the unit only operates off unit-output information and is not sensitive to system variables such as line loading. Therefore, the relative placement of the unit is arbitrary, lending the applications of power-mode devices to more installation locations than units designed to regulate line flow. Also, the characteristics of devices in power mode are more easily understood as they operate off local output and are not affected by system loading. In this section, results from various configurations will be presented that demonstrate transient stability even while the SOC-limit controller is engaged.

7.1.1 SOC lower-limit-control response while grid connected

The most fundamental investigation into the operation of the limit controller at the lower SOC limit in a grid connected state. Since it is assumed that the grid is stiff enough to not vary its frequency based on the power demanded at microgrid levels, the frequency-based droop characteristics are effectively decoupled.

In this test, the SOC of the battery is set to an epsilon above the lower limit. At $t=7$ seconds, the power set-point of the energy storage element is set to 1kW, causing the almost immediate violation of the lower SOC limit and engaging the lower limit mode. In the lower limit mode, input power becomes the controlled variable, which explains the immediate step-decrease in power output as a function of the proportional gain on the PI controller. After $t=8$ seconds, the power output steadily decreases to -2kW, as specified by the lower-limit controller.

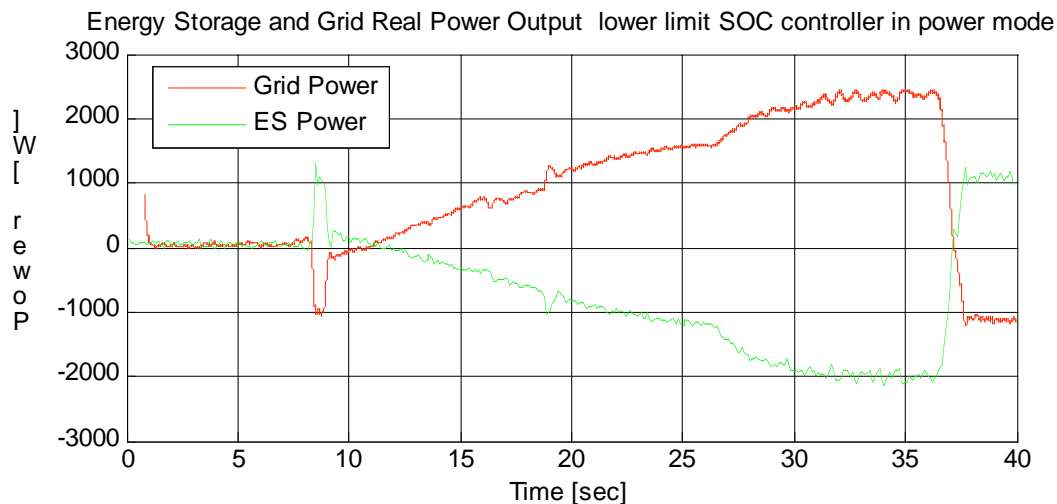


Figure 7.1.1.1 – Grid and Energy Storage power contribution

The characteristic of the reactive power are relatively decoupled from the real power trends except for the small cross-coupling that exists from the portion of resistance in the transmission lines and filter elements. It should be noted that some voltage sags and peaks in the grid voltage can affect the reactive power in a microgrid significantly,

which is another reason for the implementation of the reactive power vs. output voltage characteristic to limit the sensitivity to grid voltage variations.

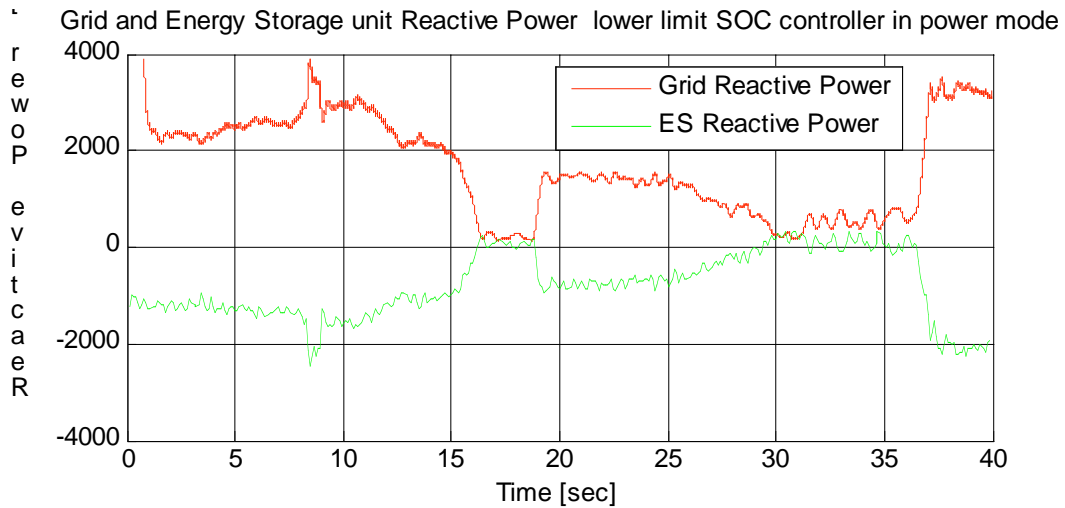


Figure 7.1.1.2 – Grid and Energy Storage reactive power contribution

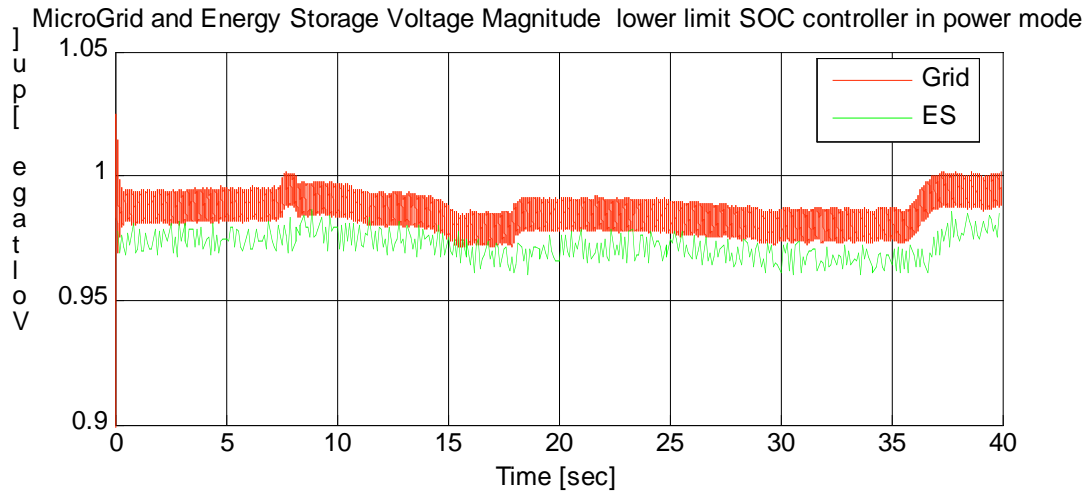


Figure 7.1.1.3 – Grid and Energy Storage per-unit voltage magnitudes

The voltage remains relatively constant, varying between 0.97pu and 0.99pu. The variation shows some pliability of the grid supply which can generally be attributed to the aforementioned resistances in the network.

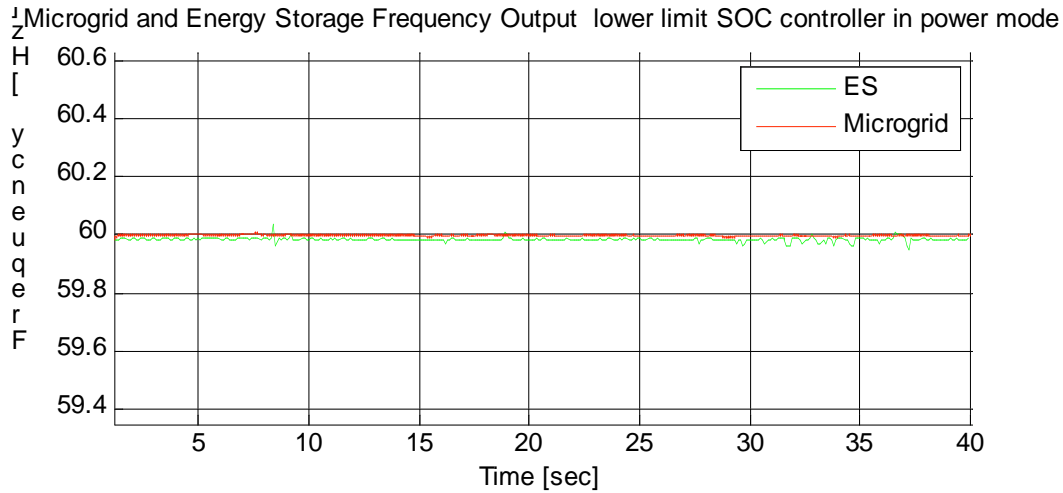


Figure 7.1.1.4 – Grid and Energy Storage operational frequencies

Figure 7.1.1.4 shows the relative frequency invariance of the grid-connected microsource. It is because of this invariance due to grid dominance that the amount of tests involving grid connection alone is small compared to the islanding and islanded dynamics of a microgrid.

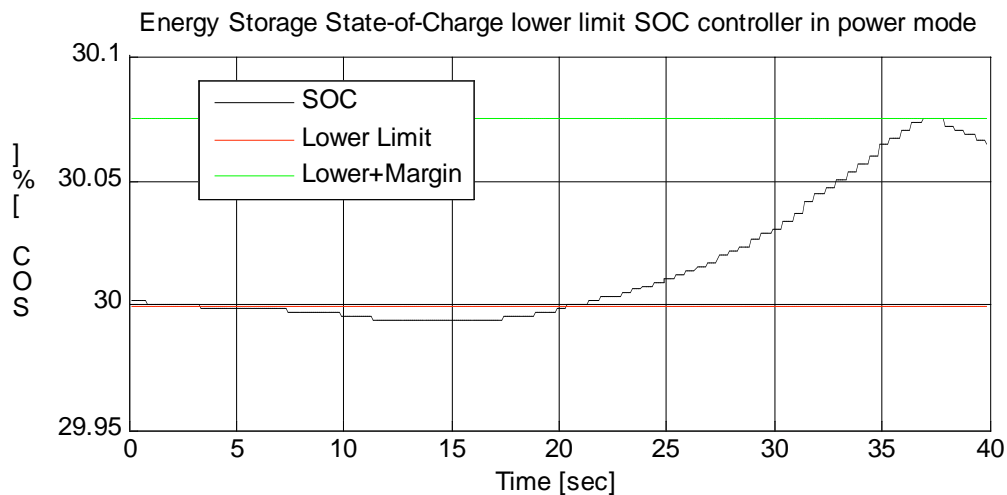


Figure 7.1.1.5 – Battery State-of-Charge through lower-limit event

Figure 7.1.1.5 shows the characteristic of the SOC through the entire lower-limit event. The margin was set significantly small in this case in order to capture the entire cycle in a reasonable amount of time, but it can be seen that the system reaches the steady-state set-point of -2kW well before the lower+margin limit is reached. In the beginning of the event, it can be seen that the SOC falls below the specified lower limit

and as previously mentioned, this error is considered insignificant in regard to the size of the battery element itself. This error is actually an artifact of the limitations on the role of the SOC limit controller. From the initial transient at t=7seconds, it can be seen that the proportional error causes a change in power output of approximately 800W, which results from the proportional gain being approximately 1/3 that of the droop characteristic.

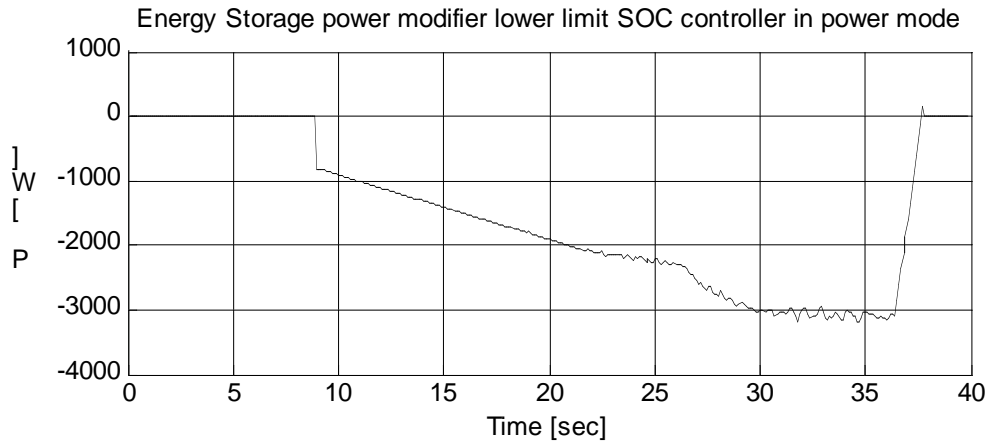


Figure 7.1.1.6 – Power Modifier command through lower-limit event

If the proportional gain was tuned higher, the embedded droop characteristic would be increased in slope, reducing the transient power-sharing characteristics.

As a proof of the effect of the power modifier (P_mod) on the droop characteristic, the modified equation describing power-versus-frequency droop is presented in equation 7.1:

$$freqchg = (P_reference - Pdq_filt + P_mod)*p_droop/10000 \quad (7.1)$$

The P_mod value for the lower limit is developed by the following equations:

$$P_mod_int += (P_err*Ki_LL_soc)/10 \quad (7.2)$$

$$P_mod = P_mod_int/10+(P_err*Kp_LL_soc)/100; \quad (7.3)$$

As previously described, the error signal is generated from a comparison between the specified charge power and the real power output by the system. The resulting equation is presented in equation 7.4.

$$P_err = P_charge-Pdq_filt \quad (7.4)$$

Considering only the proportional term of the power modifier, the simplified form of the frequency droop can be calculated as follows:

$$\text{freqchg} = [\text{P_reference} - \text{Pdq_filt} + ((\text{P_charge} - \text{Pdq_filt}) * \text{Kp_LL_soc}) / 100] * \text{p_droop} / 10000 \quad (7.5)$$

Assuming that Kp_LL_soc is 50, as used in the tests, the equation reduces further to:

$$\text{freqchg} = [(\text{P_reference} - \text{Pdq_filt}) + (\text{P_charge} - \text{Pdq_filt}) / 2] * \text{p_droop} / 10000 \quad (7.6)$$

From equation 7.6, it becomes clear that even though the charge controller has half the proportional control as that of the power reference controller, that the overall droop that occurs as a function of power output errors is increased by 50% on an instantaneous basis. The net result is a reduction in transient power sharing by 33% for the same change in frequency, but contrarily should still provide similar power compensation at a 50% greater change in frequency.

7.1.2 SOC upper-limit-control response while grid connected

The upper SOC limit response is different than the lower limit behavior as the goal for the upper limit controller is simply to limit the SOC to an upper value so that on a transient basis the system is still capable of sinking enough power to stabilize the system. This requires using SOC and not power as in the lower limit case as the controlled state variable.

In the upper-limit test here, the energy storage element is in a grid-connected configuration and begins at a state of charge very close to the upper limit while charging at approximately 1kW ($P_{\text{reference}} = -1000$). At $t=6$ seconds, the upper limit is reached, engaging the upper-limit controller.

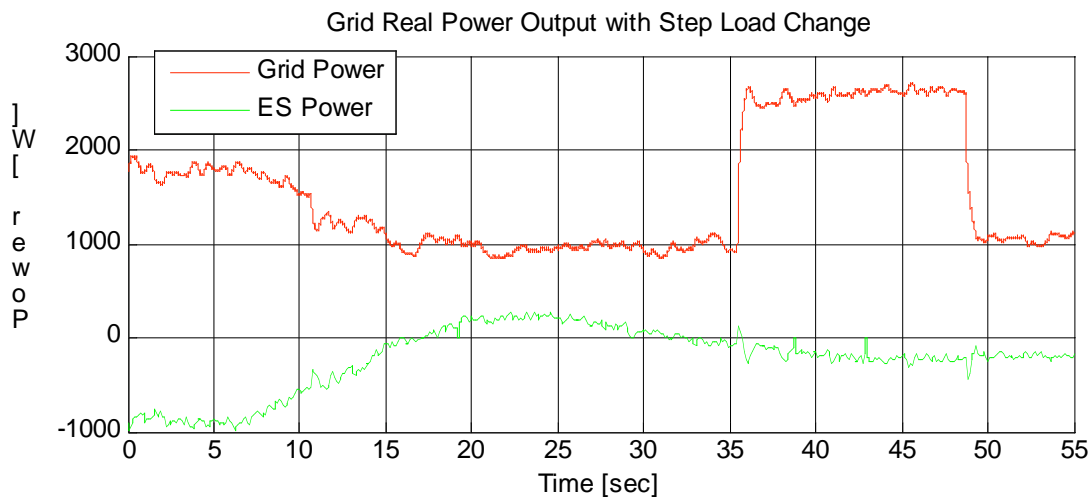


Figure 7.1.2.1 – Grid and Energy Storage power contribution

Figure 7.1.2.1 shows the gradual increase in output power from $t=6$ to $t=23$ seconds, exhibiting the typical PI controller overshoot as a function of accumulated error. At $t=35$ and $t=48$ seconds respectively, a 2.4kW load was added to and removed from the system to show the stiffness of the additional controller under step-changes in system loading.

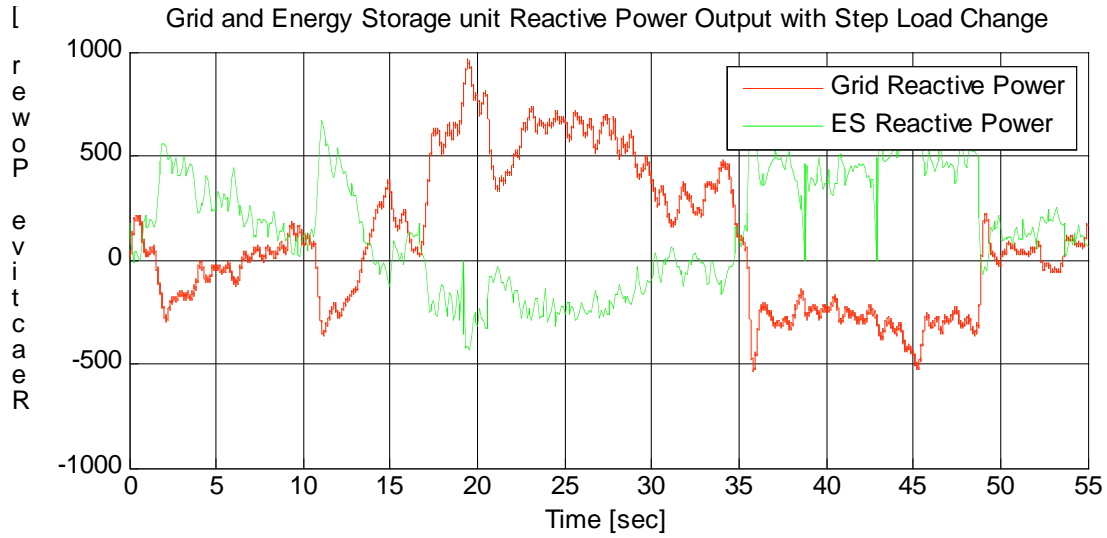


Figure 7.1.2.2 – Grid and Energy Storage reactive power contribution

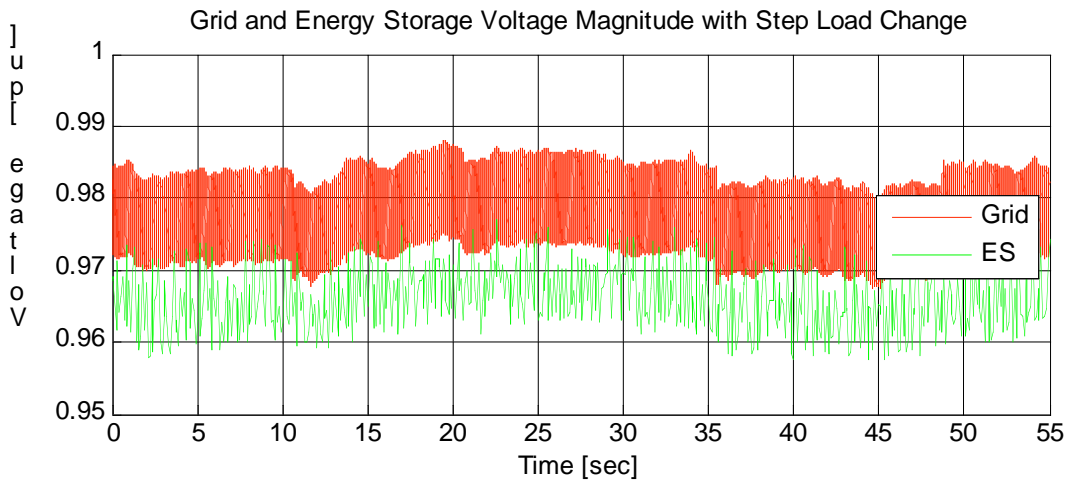


Figure 7.1.2.3 – Grid and Energy Storage per-unit voltage magnitudes

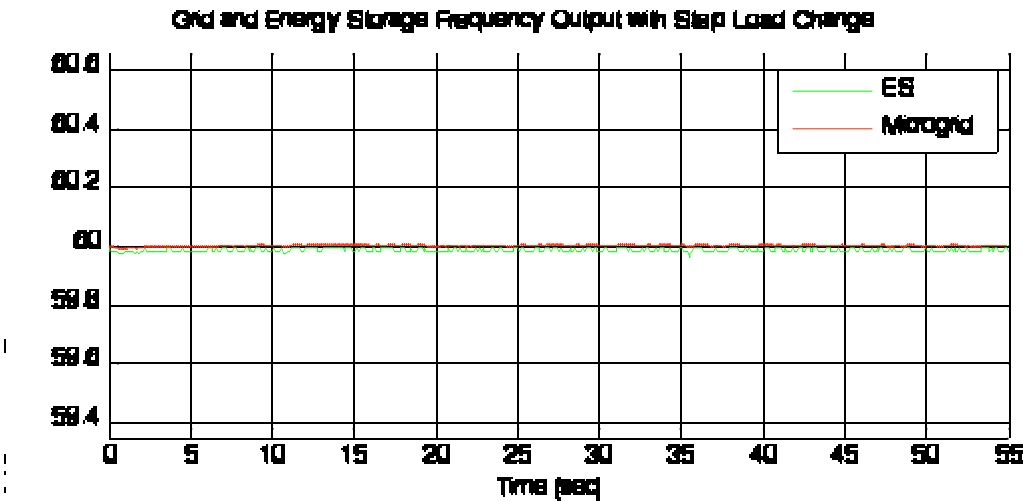


Figure 7.1.2.4 – Grid and Energy Storage operational frequencies

Figures 7.1.2.2-4 indicate that, barring minor changes in reactive power signs, that relatively little happens from a system voltage and frequency standpoint, indicating that other sources on the microgrid would be relatively unaffected by the occurrence of an upper limit event.

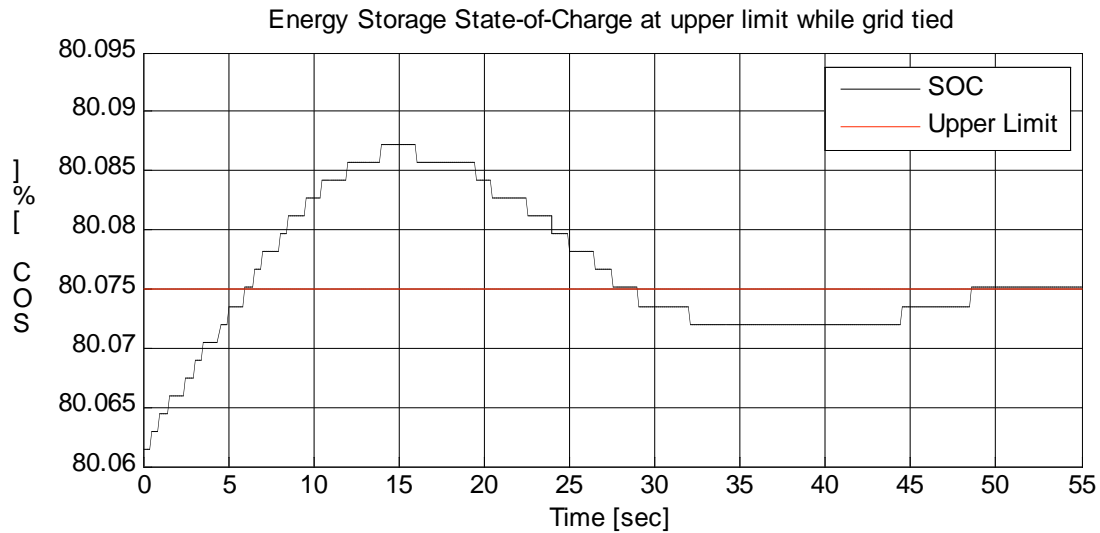


Figure 7.1.2.5 – Battery State-of-Charge through upper-limit event

The SOC characteristic in figure 7.1.2.5 shows an under-damped response, but the steady state error is, as expected, zero. The quantum of the SOC is also quite apparent which is as a result of the 16-bit value used to describe the SOC. It is also apparent that the overshoot error is approximately 0.01% of the battery capacity, a negligible amount in this case.

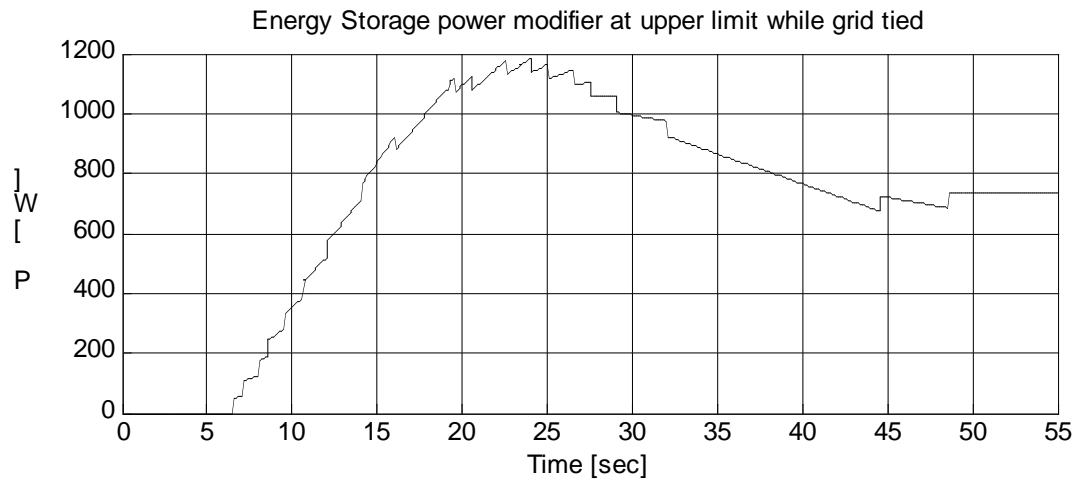


Figure 7.1.2.6 – Power Modifier command through upper-limit event

The power modifier for the upper limit case presented in figure 7.1.2.6 shows a general trend mimicked in the power characteristic in figure 7.1.2.1, which effectively controlled the SOC to an upper limit value in the time scale of this test. One readily apparent characteristic of the power modifier is the jagged characteristic that comes as a result of the quantum of the SOC that lead to proportional changes in the power modifier value. In this case, the quantum equate to approximately 50W, causing a negligible effect at the system level.

7.1.3 Islanding event under SOC lower-limit-control mode, no other sources connected

Island events are particularly important in a Microgrid as they can sometimes mean a significant step-change in power output, requiring immediate response to support on-site loads. In the world of energy storage systems, the ability to island even when in a limit-controlled mode is necessary to ensure that the local loads will be supplied, assuming there is some energy reserve available.

In this test, the energy storage unit was commanded to have a positive power output and discharged to the lower preferable charge state to engage the lower-limit controller. This initial transition occurs at t=1 second, visible from figures 7.1.3.1, 5 & 6.

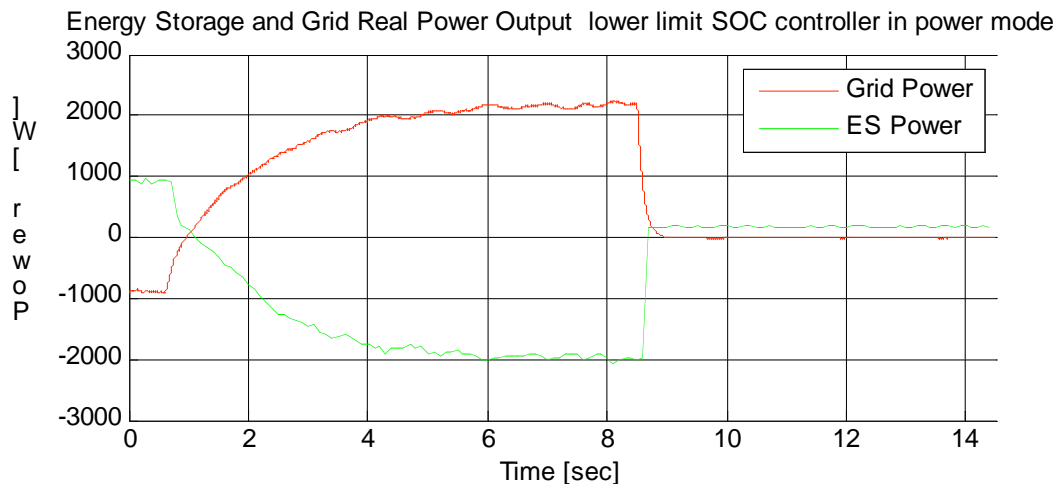


Figure 7.1.3.1 – Grid and Energy Storage power contribution

It can be seen that once the lower-limit controller engages, the power changes with the typical natural-response as presented in section 7.1.1, but changes dramatically at t=8.5 seconds when the island event occurs. Because of the very small on-site load, the energy storage element becomes very lightly loaded, but still outputs around 250W for system power losses.

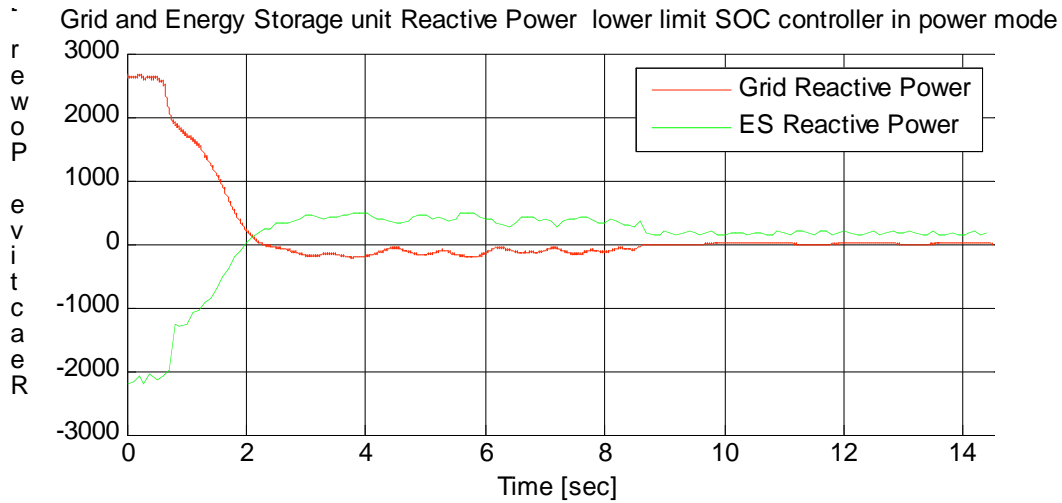


Figure 7.1.3.2 – Grid and Energy Storage reactive power contribution

The reactive power characteristic through this event indicates that the grid voltage was slightly higher than that of the Microgrid, causing a lower magnitude of reactive power to circulate during the controlled charge state caused by the lower-limit SOC controller.

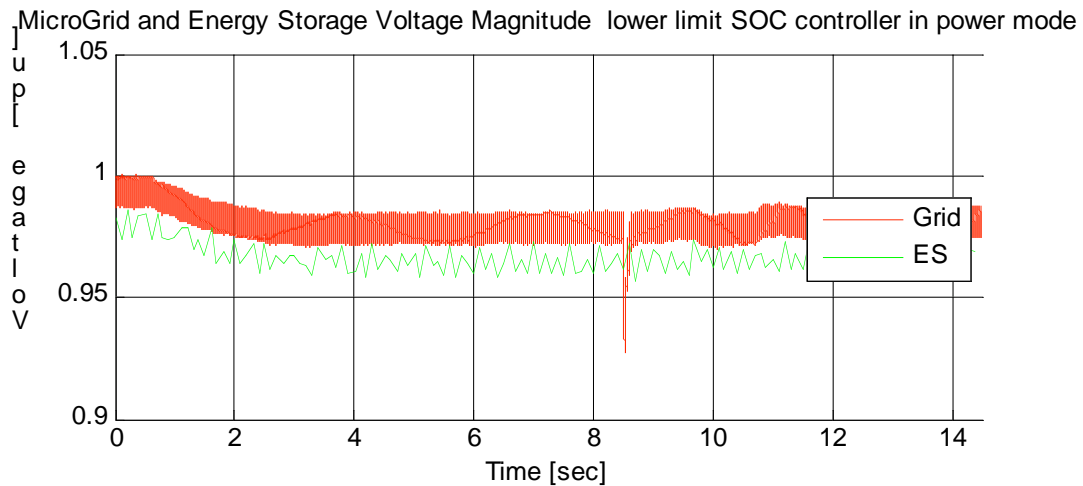


Figure 7.1.3.3 – Grid and Energy Storage per-unit voltage magnitudes

Figure 7.1.3.3 concurs with this result, again indicating a R/X ratio of the system that is not insignificant.

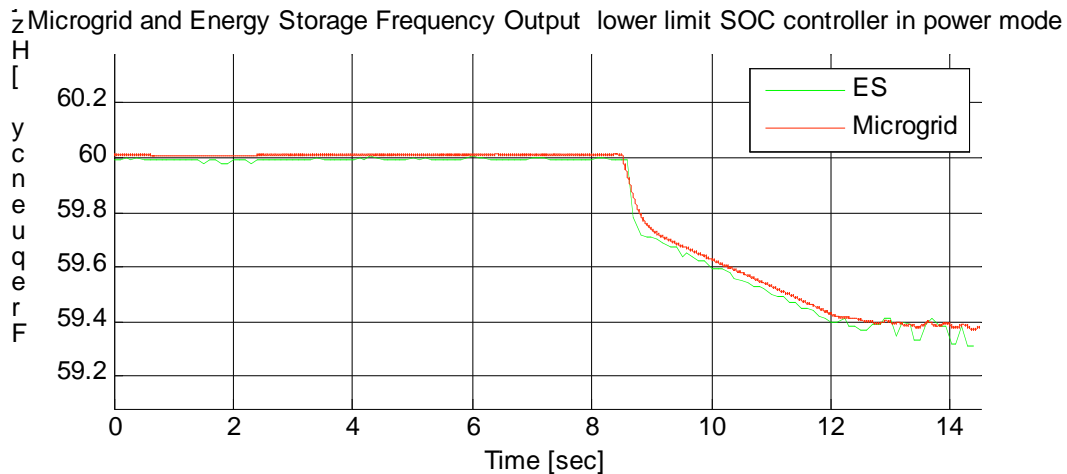


Figure 7.1.3.4 – Grid and Energy Storage operational frequencies

The most interesting characteristic as a result of the island condition is the frequency characteristic driven by the lower-limit controller. Initially, at $t=8.5$ seconds, the frequency drops proportionally to the measured error in the power set-point, with the power modifier, and measured power output. It is then noticeable that the frequency drops linearly until 59.4Hz, indicating two separate phenomena. The linear rate is due to the slew-rate limitation on the power command, which is enacted if the power error is greater than 1kW. The specified slew rate limits the integration rate of the integrator to 1kW/sec, which is enacted to further ensure stability in the system during large power transients. Within the 1kW error limit, the proportional contribution varies linearly, providing adequate damping in the system to ensure proper settling time. However, in this case, since the energy storage element is the only source on the microgrid, varying the frequency does not change the power output. It is for this reason that the SOC limit controller has a frequency domain restriction of ± 0.6 Hz. This domain was determined to be marginally larger than the normal operating range of the Microgrid frequency, which should load all of the sources to maximum power output at 59.5Hz, ensuring that the SOC limit controller will only change the operational frequency to marginally less than

the lower and marginally greater than the upper in efforts to control the SOC. Beyond the 0.5Hz limit, it is then assumed that the system will not cause any more power changes. Secondly, the frequency range trigger of 59.5-59.4Hz could also be used as an S.O.S. flag to signal a condition on the microgrid will only remain stable for a short period of time.

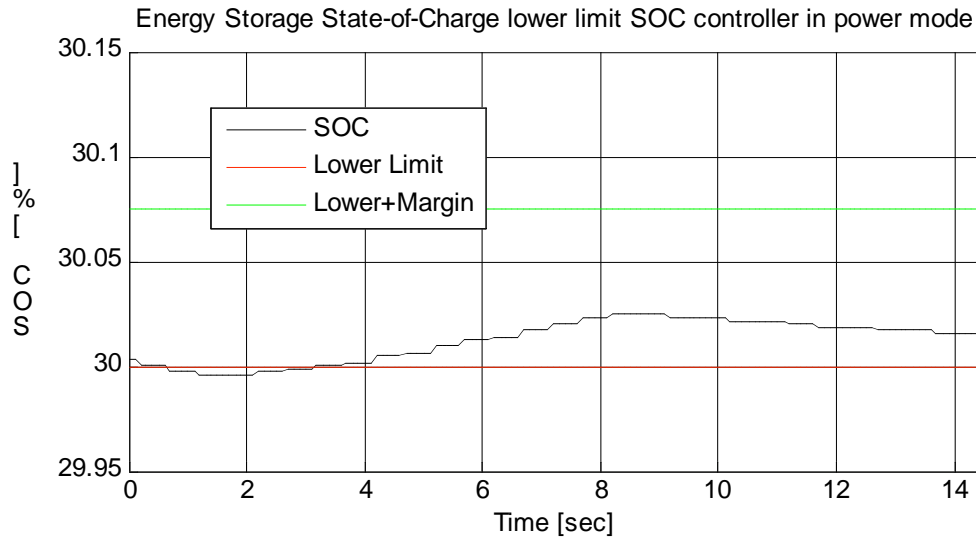


Figure 7.1.3.5 – Battery State-of-Charge through upper-limit event

The state of charge characteristic presented in figure 7.1.3.5 displays a characteristic that reaches the lower limit but is not effectively controlled to reach the marginal buffer as it is not supported by any other variable-output source. It is also important to note that this characteristic would occur similarly with the addition of constant-power loads and constant-power sources such as fuel-cells or intermittent renewable sources.

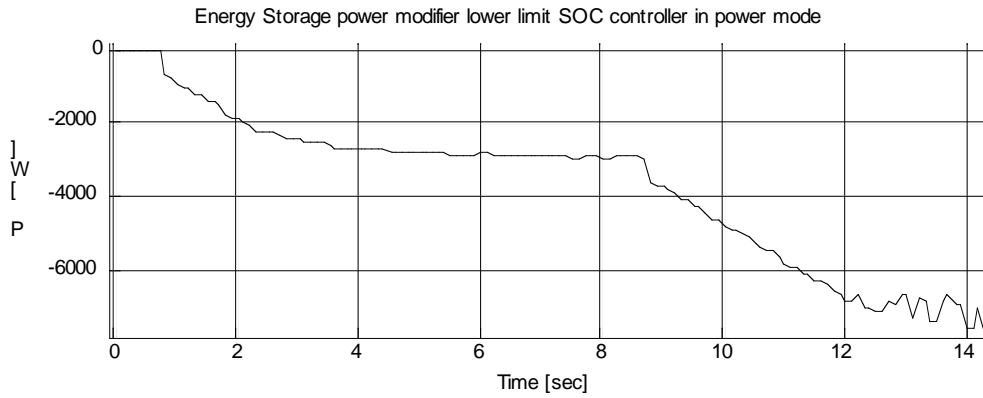


Figure 7.1.2.6 – Power Modifier command through lower-limit event

At the lower frequency limit of 59.4Hz, the power modifier command appears noisy as the command is balanced to a value that is both within the frequency limits and appropriately attempting to increase the power input to the system. The magnitude of these fluctuations could be reduced by tuning the dead-band between the frequency domain controller main control equations. Secondly, the oscillations could be eliminated completely by an account of the power versus frequency droop equation, but was not implemented for this test.

7.1.4 SOC lower-limit-control mode response characteristic while islanded with microsource

When in an islanded configuration, the power vs. frequency characteristic balances the relative loading between the sources as a function of system frequency. Investigating the lower-limit SOC controller response characteristic in this configuration becomes interesting because the controller now has to deal with variations in system frequency while attempting to control the relative load-angle that determines the power output. First, this test illustrates a nominal operating point different than 60Hz, where the power set-points are modified by the same per-unit value.



Figure 7.1.4.1 - Energy Storage and Microsource power contribution

The power characteristic above shows the paired power contributions from each source with approximately 2.4kW of load on the system. From inspection of figure 7.1.4.1, it is clear that the controller response characteristic is seemingly unaffected by the loss of a constant frequency reference. In this case, since the loading on the system does not change, the controller simply applies an offset to the power set point to cause battery charging. The figure itself indicates a SOC limit encountered at t=3sec and

recovering at 14.7 seconds due to the attainment of the marginal SOC above the lower nominal limit..

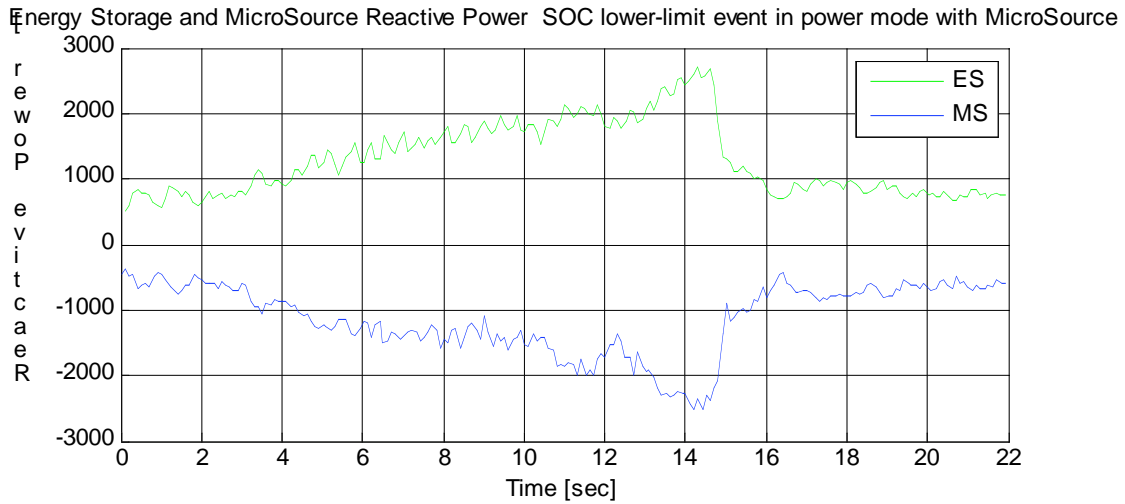


Figure 7.1.4.2 - Energy Storage and Microsource reactive power contribution

The reactive power characteristic in this test also shows the R/X ratio of the microgrid through cross-coupling in the control algorithm. It is interesting to note the 1:1 ratio of the reactive power circulation to real power delivered. This should result in an effective de-rating of the power of the converter to 70.7% of the VA capacity of the power devices.

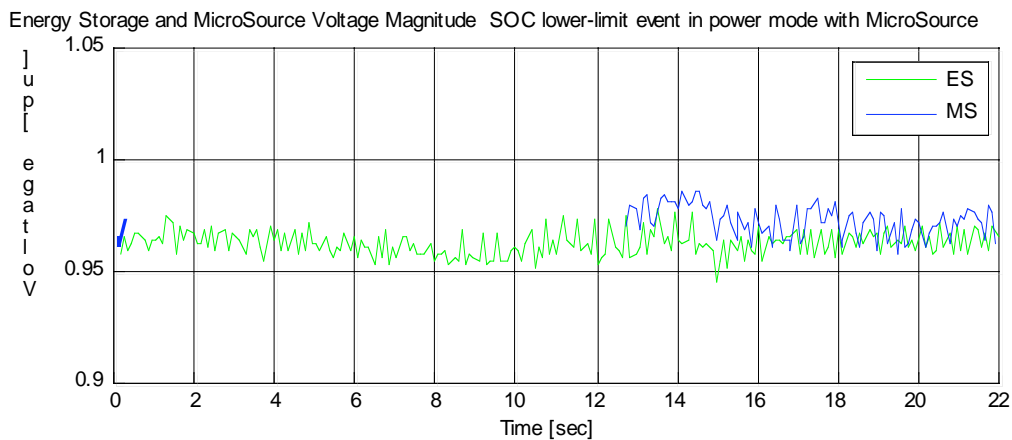


Figure 7.1.4.3 - Energy Storage and Microsource voltage magnitude

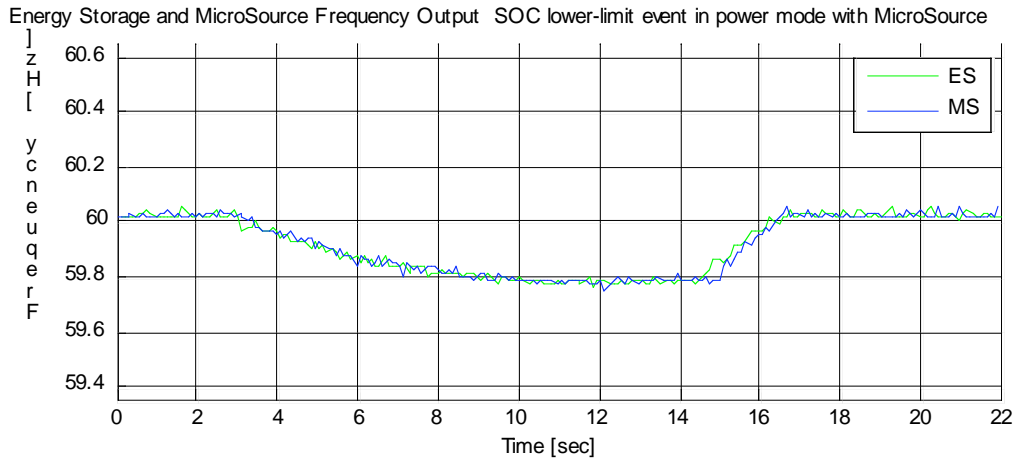


Figure 7.1.4.4 - Energy Storage and Microsource output frequency

The output frequency characteristic clearly shows the entry into the lower limit mode as well as the slew-rate-limited exit from the limited mode. Slew-rate limiting is used so that the power set-point does not change too quickly, saving the system from having to adjust its power output too quickly and not exciting natural frequencies in the system.

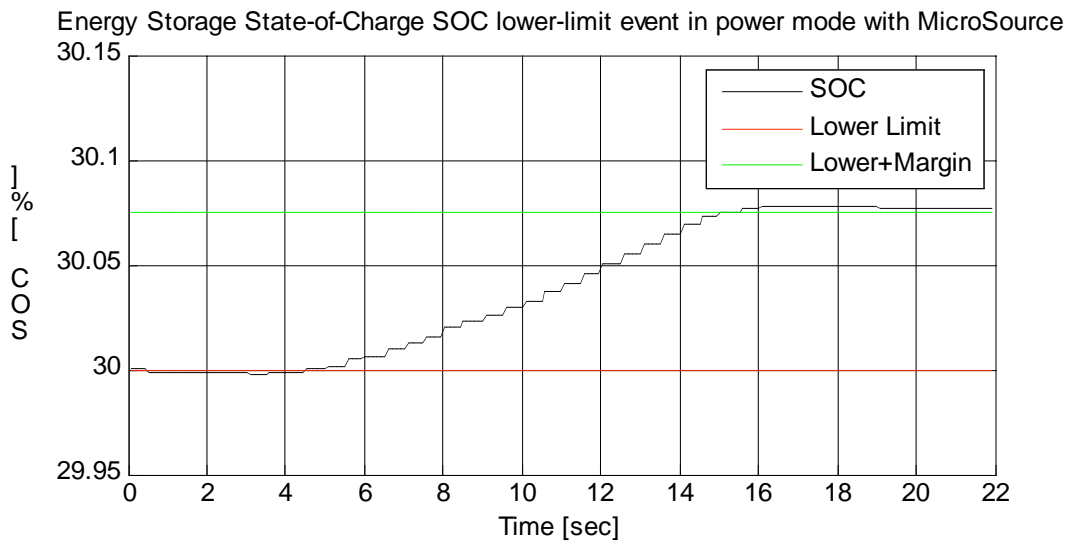


Figure 7.1.4.5 – Energy Storage State of Charge through lower-limit event

The characteristic in figure 7.1.4.5 clearly shows the control of the SOC to be effective, charging once below the lower limit and reinstating the initial power set-point after the SOC has reached the proper value.

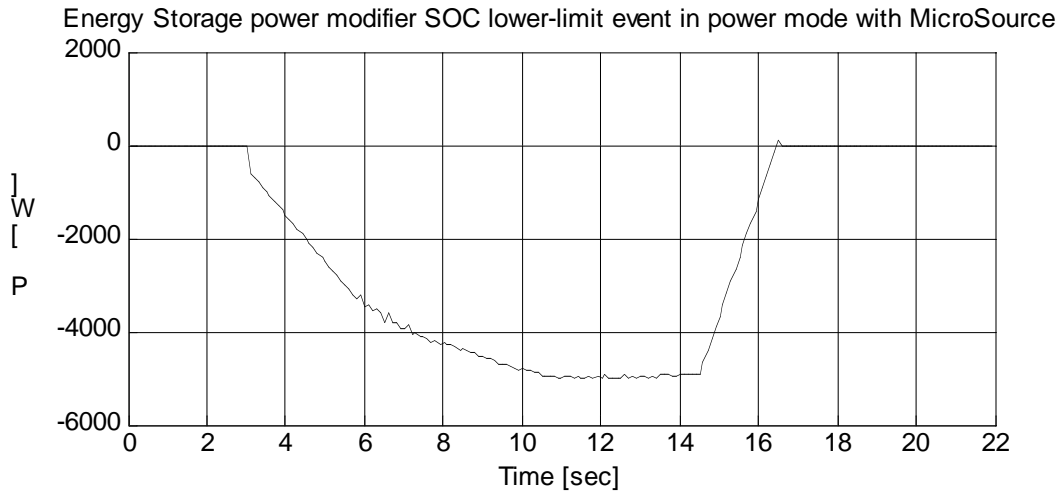


Figure 7.1.4.6 – Power Modifier command through lower-limit event

The power modifier command, which is very similar in shape to the frequency characteristic through the lower-limit event, achieves a greater value than that shown in section 7.1.1. A greater value is necessary because the droop-characteristic of the microsource requires a droop in frequency to change the power output. This droop in frequency requires a constant error in the power error calculation, previously presented in equation 7.6. In short, because the two systems have droop-based power characteristics, the power modifier command must reach approximately twice the value as compared to the grid-connected case.

7.1.5 SOC upper-limit-control mode response characteristic while islanded with microsource

While in an islanded configuration, the upper limit can easily be encountered with a negative power set-point or a lighter-than-expected system loading. In any case, the power modifier command will still avoid over-charging by increasing the output to approximately zero. The system will remain in this controlled state until either the system loading or power set-point increase enough to cause positive power output from the unit itself. However, it is important to note that the system will still respond on a transient basis to assist in frequency regulation and voltage regulation. In this case, similarly to the previous case where the lower limit was encountered, the power modifier command will be approximately twice as large to affect the frequency of the system as well as increase the power output of the energy storage element.

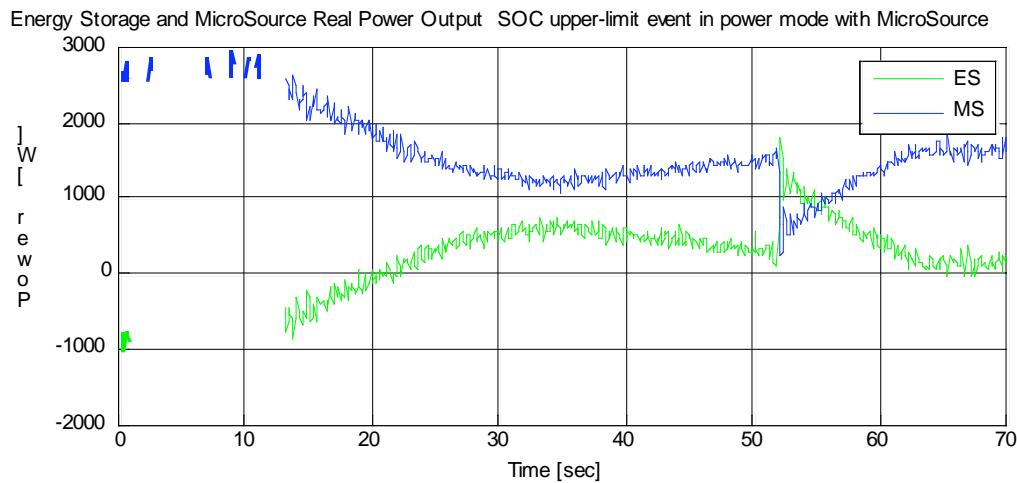
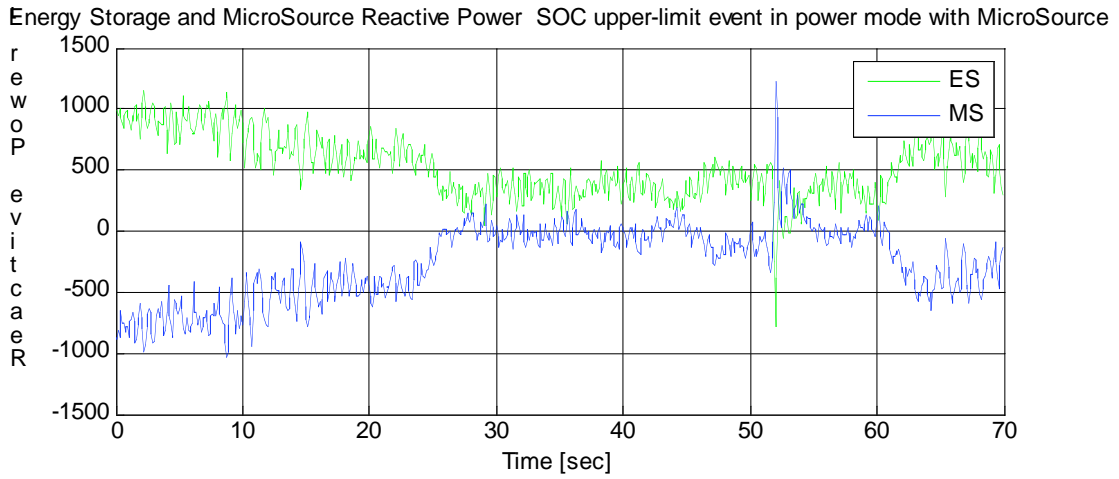


Figure 7.1.5.1 - Energy Storage and Microsource power contribution

The power characteristic in figure 7.1.5.1 shows how for the first 40 seconds, that there is the expected under-damped response from the PI controller, and reacting to an increase in power set-point at $t=52\text{sec}$, initiating a recoil from the controlled state. Though the output power of the energy storage element overshoots the steady-state command of zero output at the upper limit, the overshoot is somewhat desirable to ensure

that the SOC is actually the controlled variable and that SOC drift does not occur as a function of near-zero power measurement error.



7.1.5.2 - Energy Storage and Microsource reactive power contribution

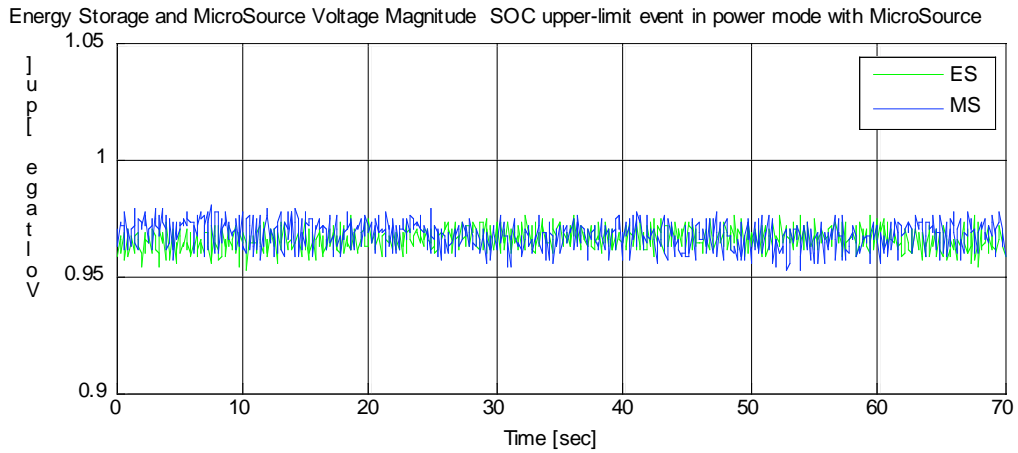


Figure 7.1.5.3 - Energy Storage and Microsource voltage magnitude

The reactive power and system voltage characteristics are relatively inconsequential here, but they are included for completeness in describing the characteristics of the event.

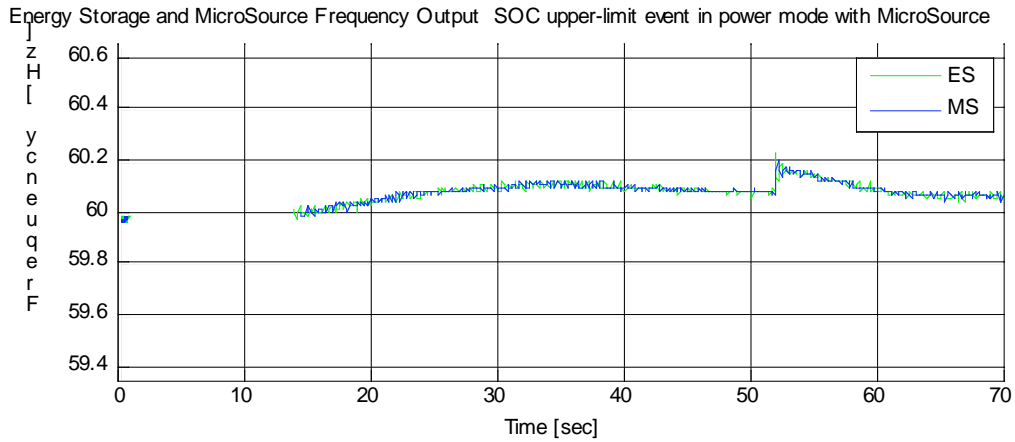


Figure 7.1.4.4 - Energy Storage and Microsource output frequency

The system frequency characteristic shows a slight increase which is expected from the increase in power command given to energy storage element. At $t=52\text{sec}$ the system frequency increases dramatically as the power set-point is increased from -1000W to 200W . With the power modifier value added on top of the power command, the microsource output drops to nearly zero for a moment, but quickly resets as the power modifier value diminishes due to the SOC falling below the upper limit.

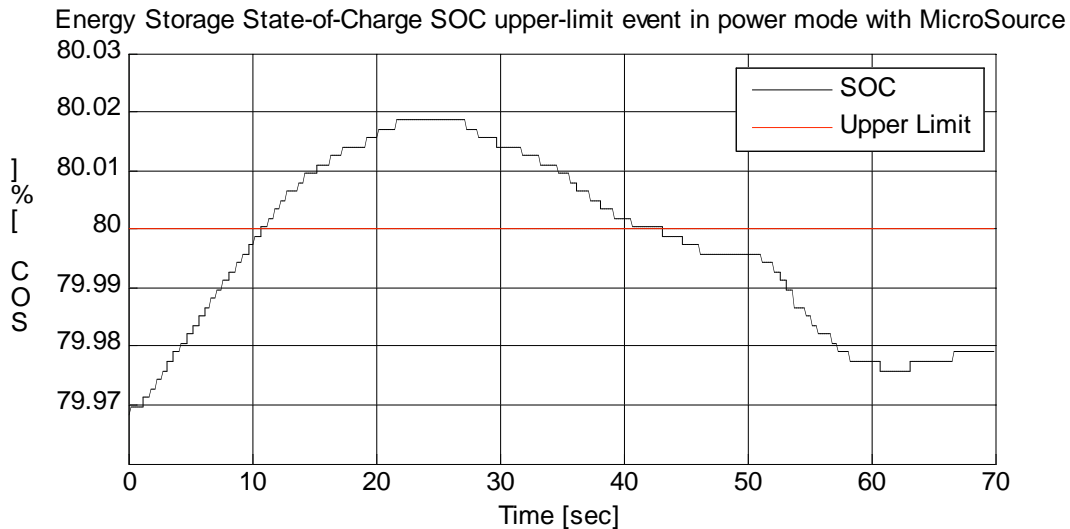


Figure 7.1.5.5 – Energy Storage State of Charge through upper-limit event

Upon comparison between figures 7.1.5.5 and 7.1.5.6 that the upper limit controller engages at approximately $t=10\text{sec}$ when the SOC exceeds the lower limit. The

increase in power set-point is also visible on these figures, shown as steep decreases in both SOC and the power modifier command.

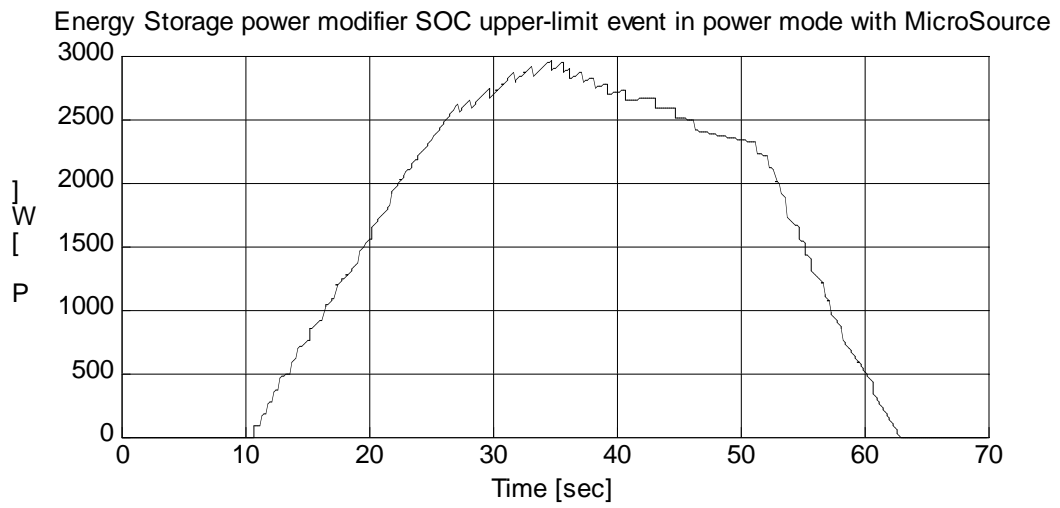


Figure 7.1.5.6 – Power Modifier command through upper-limit event

7.1.6 Islanding event under SOC upper-limit-control mode, no other sources connected

This test simulates the reaction of the energy storage element after an island event with no other sources to contribute to supporting the on-site load. While in upper-limit control mode, the power modifier has attained a value of 1kW to counteract the -1kW power set-point, as can be seen in figure 7.1.6.6. However, once the island event occurs at t=25sec, the energy storage element is forced to supply the on-site load of 1kw. The addition and removal of 1kw of additional load occurs at t=44sec and t=49sec respectively, causing the energy storage element to temporarily supply an increased load power demand.

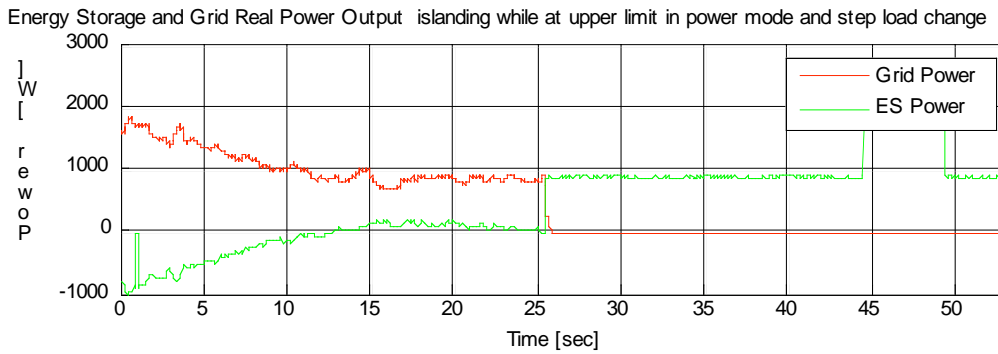


Figure 7.1.6.1 - Energy Storage and grid power contribution

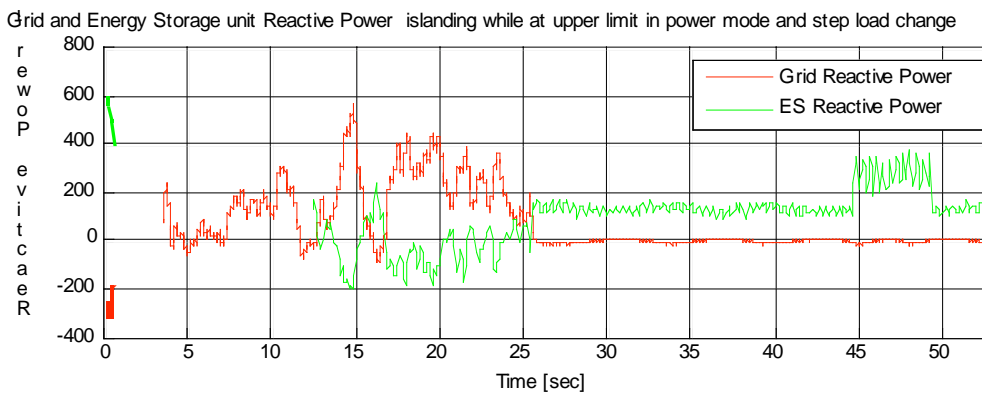


Figure 7.1.6.2 - Energy Storage and grid reactive power contribution

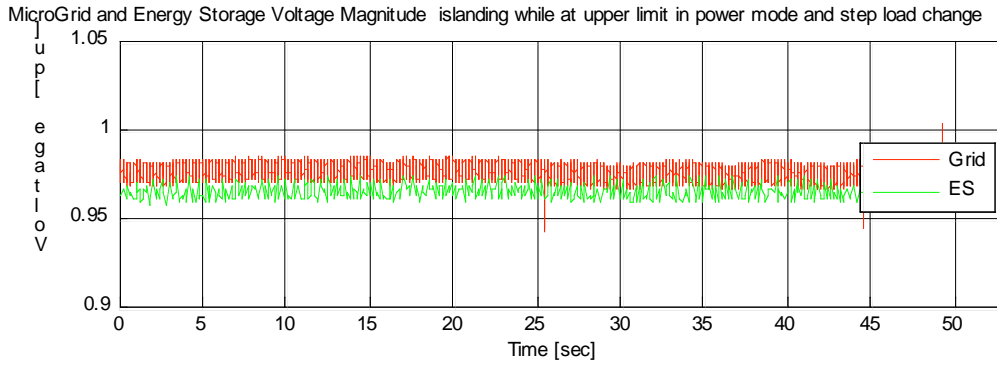


Figure 7.1.6.3 - Energy Storage and grid voltage magnitude

The reactive power and voltage magnitudes are again included for completeness, showing no consequential results.

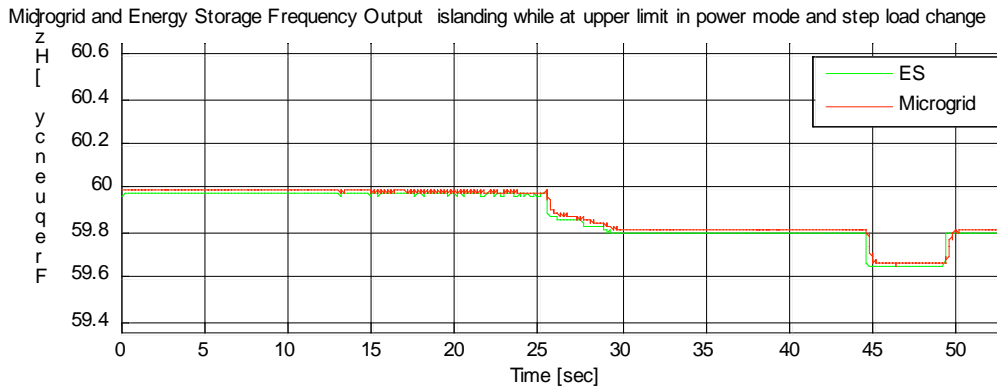


Figure 7.1.6.4 – System frequency through island event

The system frequency characteristic is interesting in that the immediate droop following the island event is caused by the error between the modified power command and the actual power output which is the entirety of the system loading due to the limit controller’s involvement. Once the SOC begins falling and the power modifier command reduces to zero, the power imbalance increases by another 1kW, doubling the droop by t=30sec. Finally, the temporary step-load of 1kW causes further decreases in system frequency, as expected.

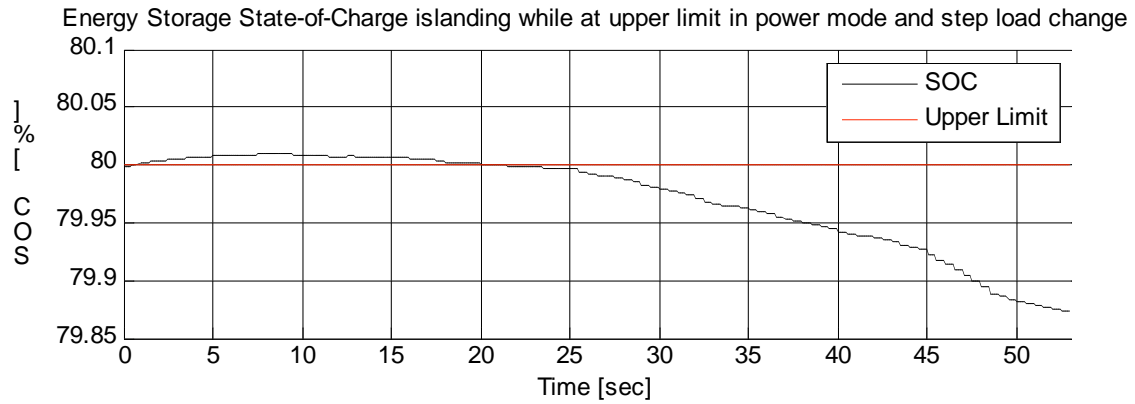


Figure 7.1.6.5 – Energy Storage SOC through island event

As it can be seen from figure 7.1.6.5, the SOC quickly falls below the upper limit following the island event. Without any other sources connected and load power to supply, the SOC has no means of increasing as the reduction in output frequency has no effect on power generation or load usage.

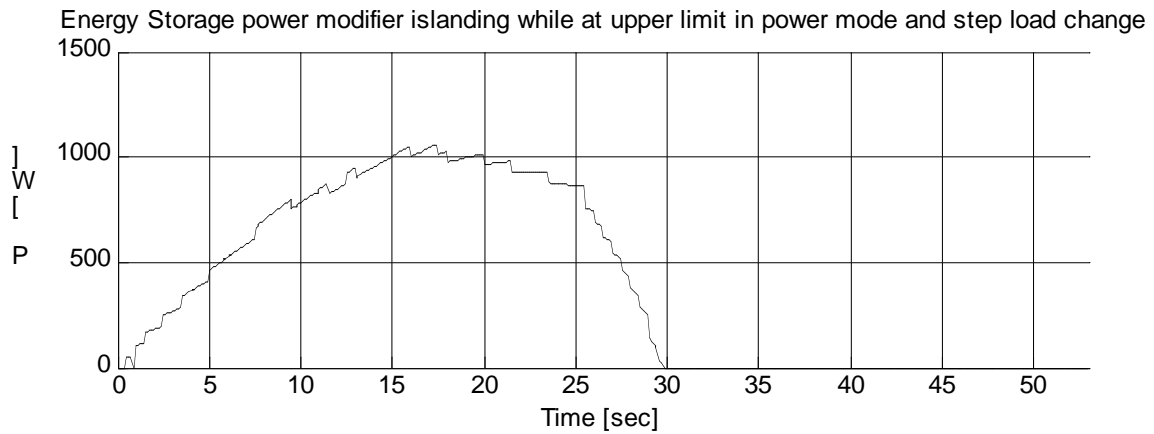


Figure 7.1.6.6 – Power Modifier command through island event

7.1.7 Islanding event under SOC lower-limit-control mode with microsource connected

An island event in a SOC lower-limit control mode with another source attached is the foremost issue to confront when considering the addition of an energy storage element to a CERTS microgrid. During operation at a nominal state of charge, the energy storage element would behave exactly as a microsource, whose characteristics have been thoroughly investigated previously in [35]. It should be noted that the energy reserve in all cases is finite and the eventual discharge of the energy storage element will always cause a lower-limit-controlled state. However, in this experiment, the island event occurs while in a limited mode to simulate a worst-case scenario and testing whether the characteristics of the response still remain favorable and within the specified frequency limits of the microgrid.

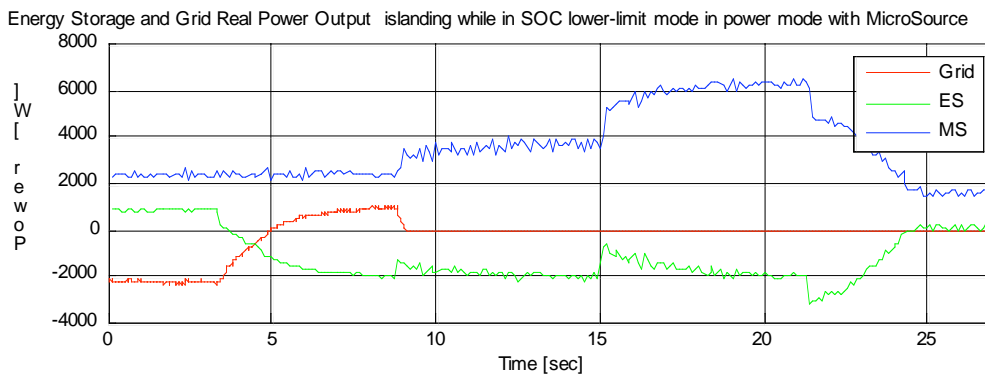


Figure 7.1.7.1 - Energy Storage, Microsource, and grid power contribution

This test explored not only an island event in a limited state, but also investigated the power sharing characteristic during step-load changes in the system. As can be seen from figure 7.1.7.5, the SOC reaches the lower limit at t=4sec, causing an increase in grid flow, as can be seen in figure 7.1.7.1, to supply the charge current to the energy storage element. At t=9sec, before the energy storage element was given enough time to bring the SOC up to the marginal limit, an island event was triggered, removing the grid

contribution to the load demand. At $t=15\text{sec}$ and $t=21\text{sec}$, a 2.4kW load was added to and removed from the system respectively. At 22 seconds, the SOC reaches the marginal limit causing the slew-rate-limited recoil of the power modifier.

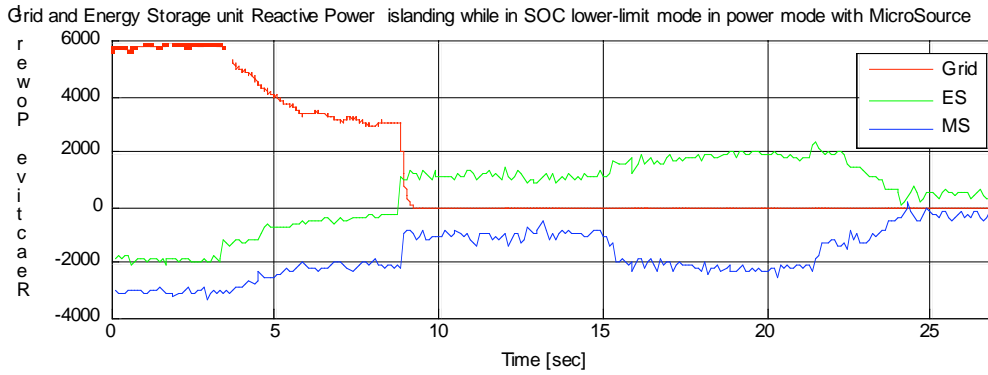


Figure 7.1.7.2 - Energy Storage, Microsource, and grid reactive power contribution

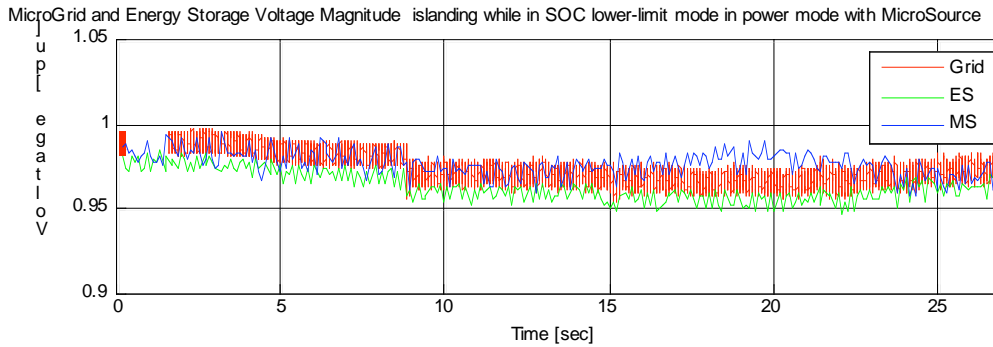


Figure 7.1.7.3 - Energy Storage, Microsource, and grid voltage magnitude

The reactive power and voltage magnitude characteristics shown in figures 7.1.7.2&3 show that the grid-supply voltage was set at a slightly higher value than that of the microgrid, causing a non-negligible amount of reactive VARs to be absorbed by the energy storage element and microsource prior to islanding. However, this should not affect the power characteristics that will be discussed further below.

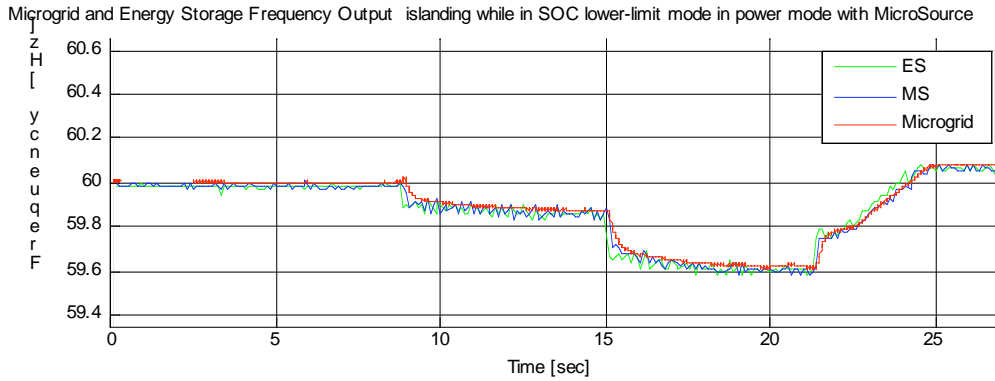


Figure 7.1.7.4 – System frequency through island event w/ Microsource

The system frequency characteristic is largely driven initially by the grid and then by the microsource. At the end of this test when the energy storage element exits the controlled state, the system frequency is one developed between the power set-points of the two sources and the system loading. The droop in frequency at 9 seconds and 15 seconds can be explained by increased loading to the microsource due to islanding and step-load increase respectively. Increase in frequency occurs at 21 and 22 seconds due to step-load decrease and the SOC limit controller respectively. At the end of the test, the frequency increases above that of the grid, indicating that the power set-points are greater than that of the system loading.

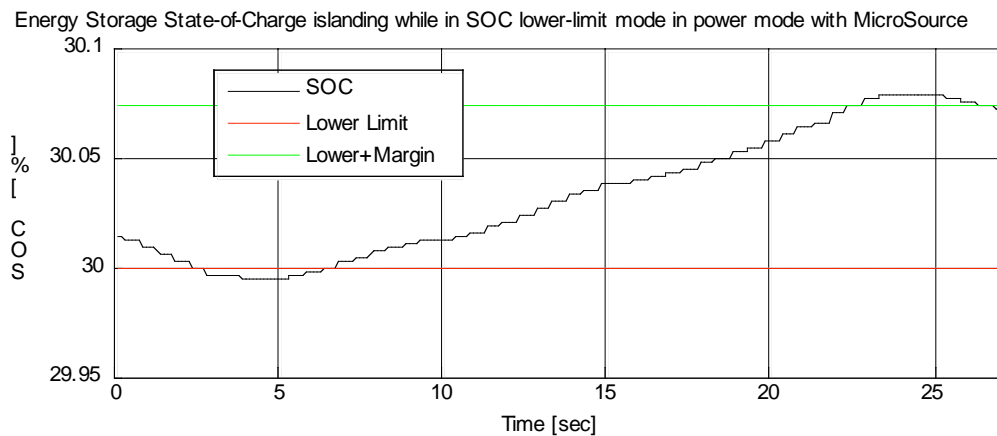


Figure 7.1.7.5 – Energy Storage SOC through island event w/ Microsource

Figure 7.1.7.5 shows the characteristic of the SOC throughout the island and step-load events. It is quite interesting to note the relatively unaffected charging trend even

through the various events. Looking back again upon figure 7.1.7.1, the charging power on the energy storage element is largely unaffected on a continuous basis, obviously yielding to transient conditions as designed to assist in transient suppression.

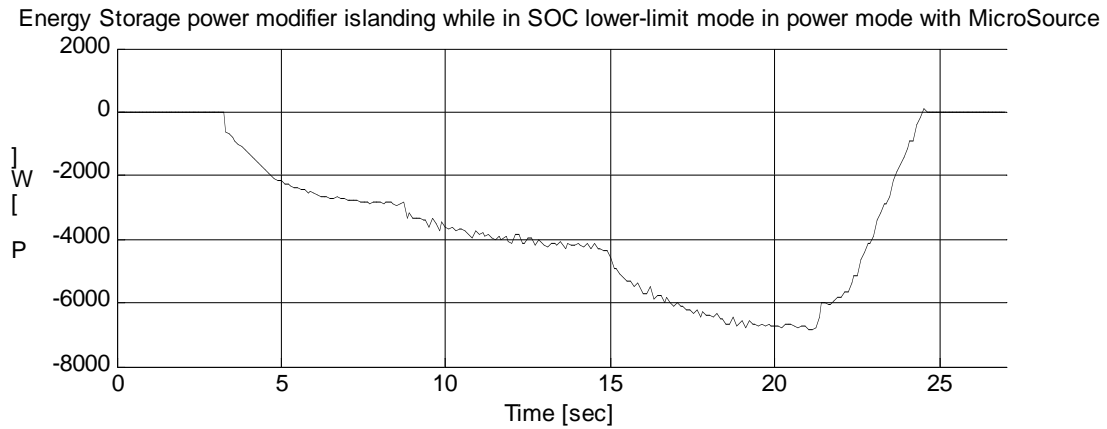


Figure 7.1.7.6 – Power Modifier command through island event w/ Microsource

The response shown here illustrates the effectiveness of the lower-limit controller to accomplish the dual tasks of providing transient stability and load supply even while in a limited condition. Secondly, this response demonstrates the seamless nature with which the SOC can be managed while grid connected or islanded.

7.1.8 Islanding event under SOC lower-limit-control mode with diesel genset connected

An islanding event with a diesel genset is quite similar to islanding with a microsource with the exception of the time constant of the response from the rotating machine as compared to the inertia-less microsource. In this test, the energy storage element is placed in a controlled charge or ‘lower limit’ mode by setting a 1kW positive power set-point while grid connected at t=9.5sec. Once the steady-state charging condition is established, a load is added and removed at t=17sec and t=18.5sec to show that the output of the synchronous machine and the energy storage element are unaffected while grid connected. The islanding event occurs at t=22sec, causing a large increase in power output from the energy storage element initially.

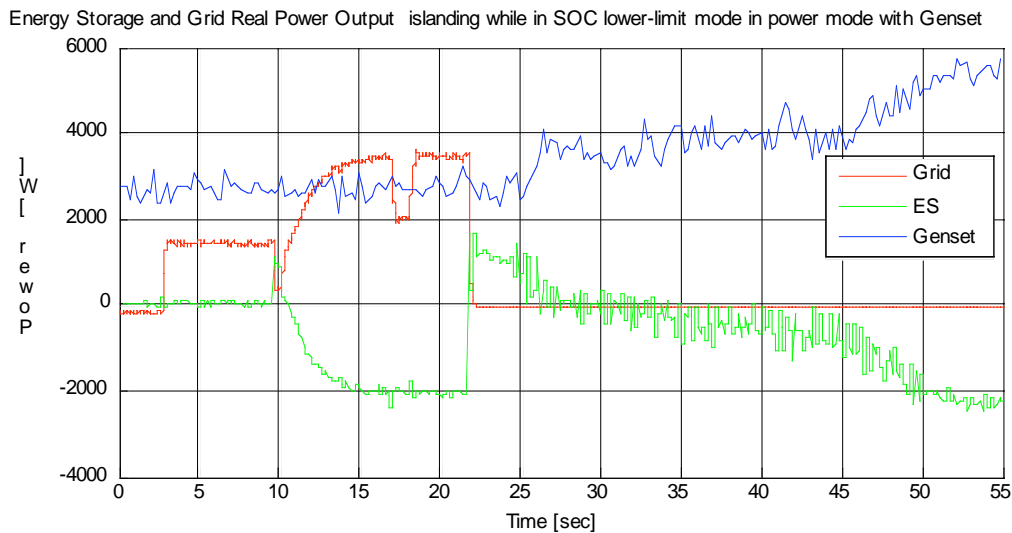


Figure 7.1.8.1 - Energy Storage, Genset, and grid power contribution

The power from the genset does not change initially, but after 25 seconds steadily increases its power output to a level specified by the droop characteristic. During this time, the controller reduces the output frequency of the energy storage element down to 59.4Hz where it saturates. Similar to the test in section 7.1.3, the saturated operation of the controller sacrifices charge current to support the load demand. This response time is

uncharacteristically slow for a small genset but the response can be attributed to a de-tuned fuel controller. Therefore, in this case, the small diesel genset mimics a larger genset or turbine with a substantially longer transient response time. Regardless of the response time, the resulting steady state operating point establishes itself at t=50sec, charging the battery per the controller's command.

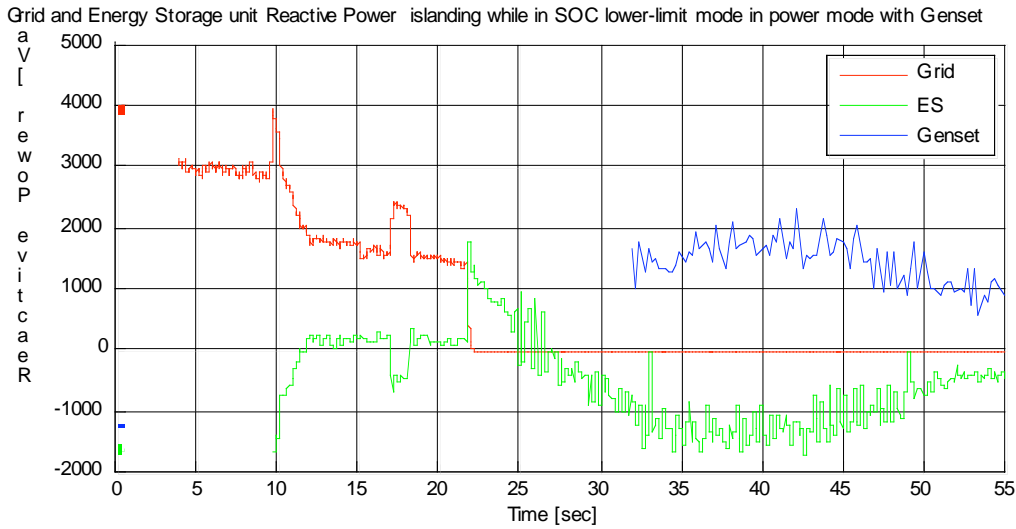


Figure 7.1.8.2 - Energy Storage, Genset, and grid reactive power contribution

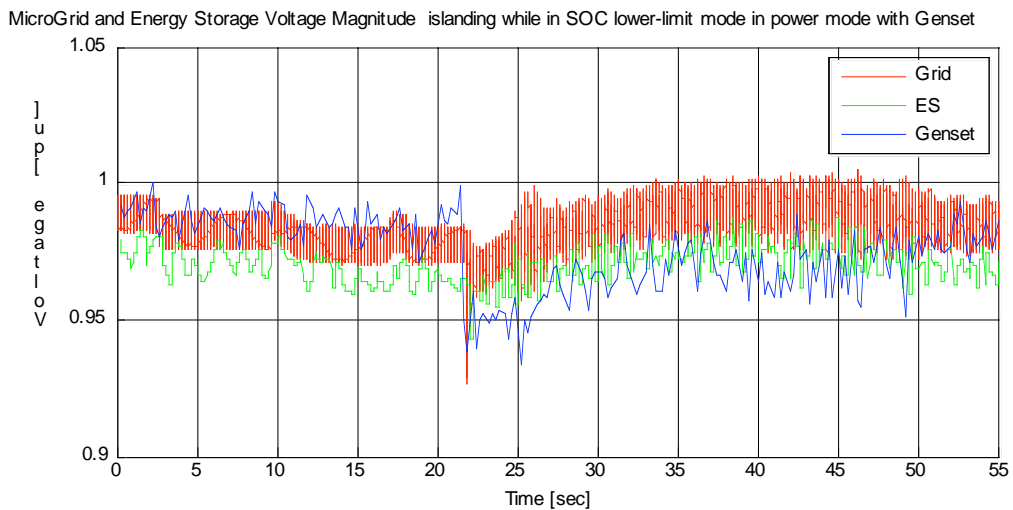


Figure 7.1.8.3 - Energy Storage, Genset, and grid voltage magnitude

The reactive power and voltage characteristics for this event are relatively plain except for a small change in voltage magnitude during the time just immediately after the

island event where it is presumed that the increase in output from the energy storage element reduces the system voltage magnitude because of inverter-side resistances.

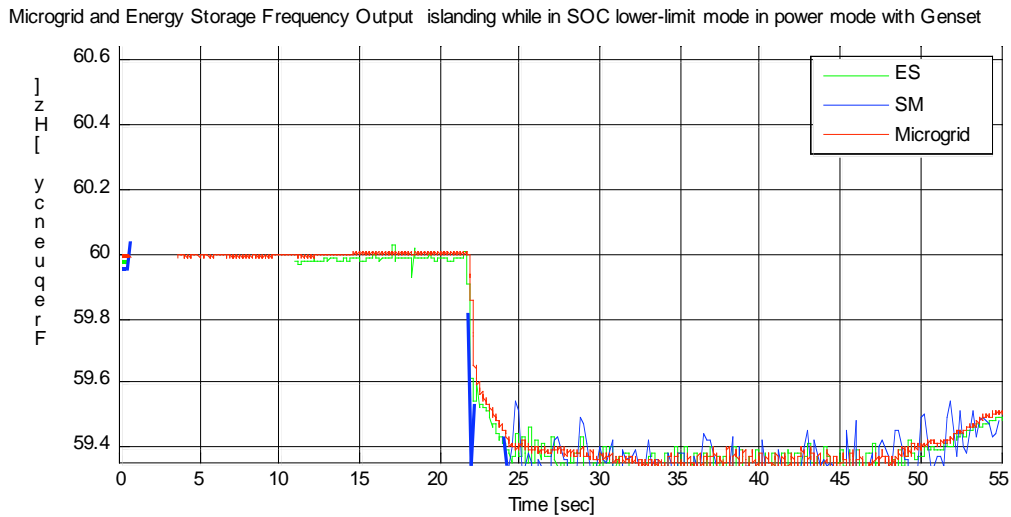


Figure 7.1.8.4 – System frequency through island event w/ diesel genset

The operating point of the system becomes quite clear from inspection of figure 7.1.8.4, the system frequency characteristic. The operation at 59.4Hz shows that the energy storage element has reduced its output frequency to the specified limit without receiving enough power from other sources to support the charging commanded by the lower limit controller. At approximately $t=48\text{sec}$ the genset is producing enough power for the Pmod value to begin to reduce. This characteristic can be seen upon inspection of figure 7.1.8.5&6.

The SOC characteristic clearly shows the regions where the charging condition is satisfied. Through the majority of the second half of the test, the SOC goes relatively unchanged as the genset produces just enough power to support the on-site load.

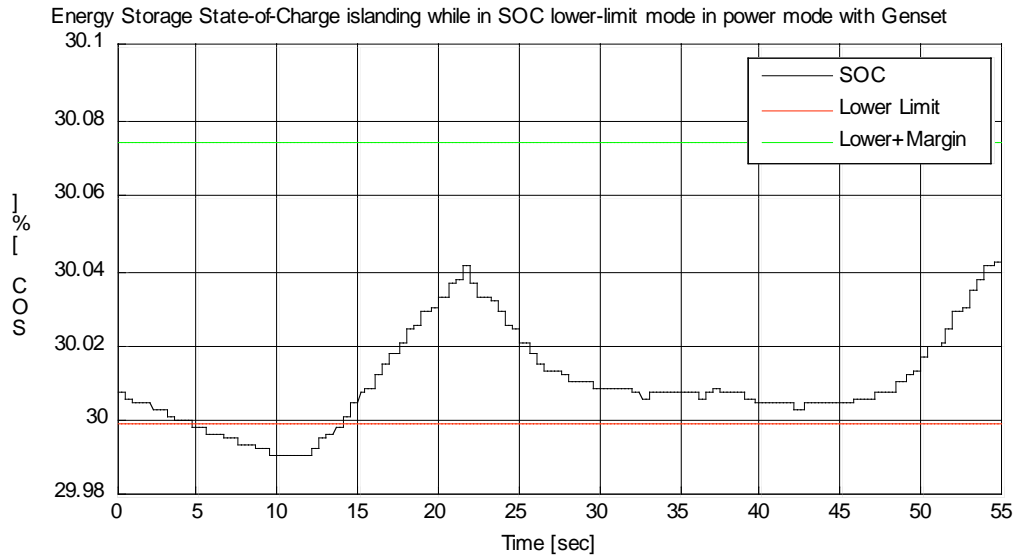


Figure 7.1.8.5 – Energy Storage SOC through island event w/ diesel genset

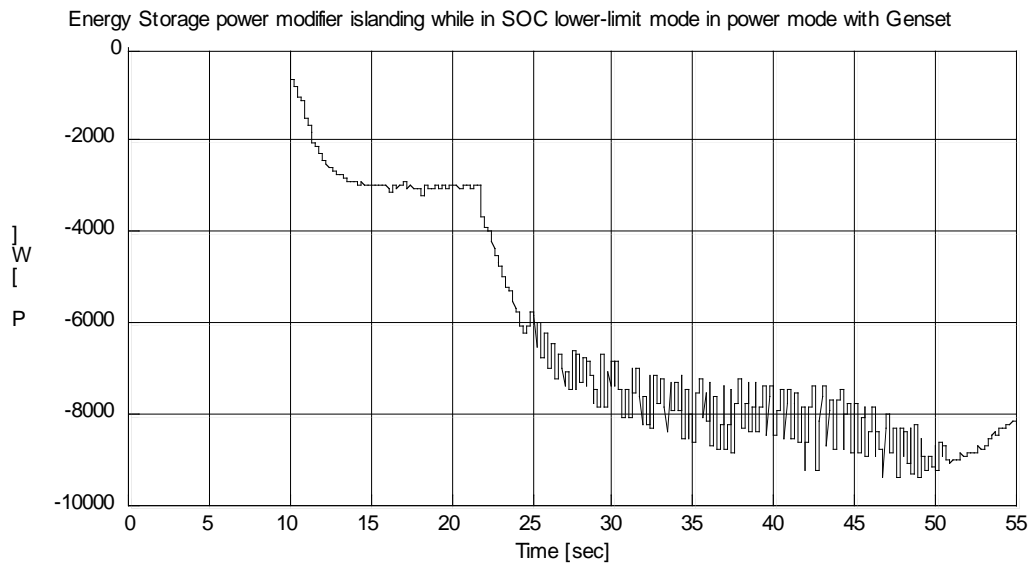


Figure 7.1.8.6 – Power Modifier command through island event w/ diesel genset

The power modifier characteristic in figure 7.1.8.6 shows a characteristic typical of a grid-tied controlled charge from $t=10\text{sec}$ to $t=22\text{sec}$ where the island event occurs. The characteristic becomes rather noisy as the lower frequency limit is exceeded and the controller reduces the value of Pmod.

7.2 Flow mode stability under load changing & islanding

Flow control is a variation on the power control as presented previously except that the power controlled is the power from the feeder to the source. The droop curve changes sign to cause an increase in unit power output for a negative error in flow power, which would reduce the flow power in turn, assuming the connection to other sources is maintained.

7.2.1 Island event under SOC lower-limit-control mode, with microsource connected

The test result presented in this section is very similar to that of section 7.1.7 except that once the grid connection is removed, so too is the feedback to the flow control equation. Therefore, neglecting the effect of the power modifier, the microgrid frequency then gets set to the zero-flow intersect point of the energy storage unit.

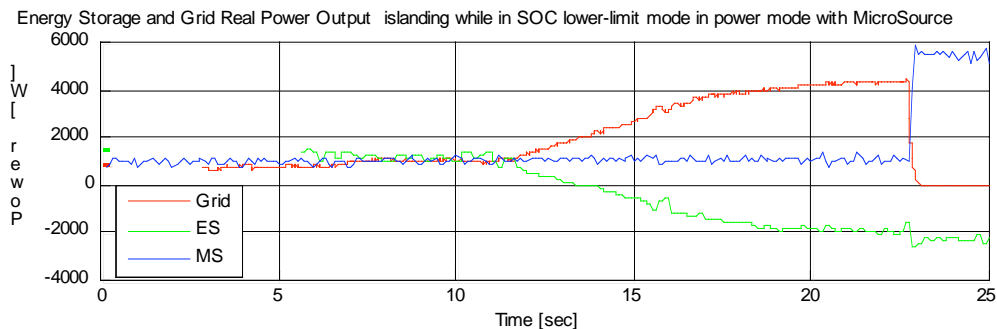


Figure 7.2.1.1 - Energy Storage, Microsource, and grid power contribution

In this test, there appears no contribution from the energy storage element during the island transient at $t=23\text{sec}$ because of the open-loop nature of the unit in flow control when islanded. Since the flow feedback is zero, the reaction of the energy storage element at island is to drop frequency in hopes of absorbing more power to increase the grid flow. This reaction in combination with the power modifier command resulted in a system frequency dip to the limit of 59.5Hz, where the power from the microsource is

approximately 5.8kW as defined by its own power vs. frequency droop. Without any assistance, the microsource picks up the entire additional load. However, it is important to note that if the system loading was greater and caused the microsource to saturate, that the energy storage element would begin accepting less power and may even put out power depending on the demand. This characteristic was presented in section 7.1.3 and 7.1.8.

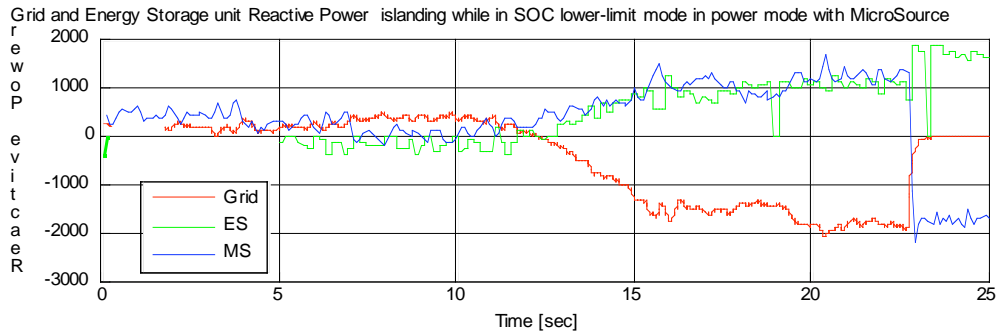


Figure 7.2.1.2 - Energy Storage, Microsource, and grid reactive power contribution

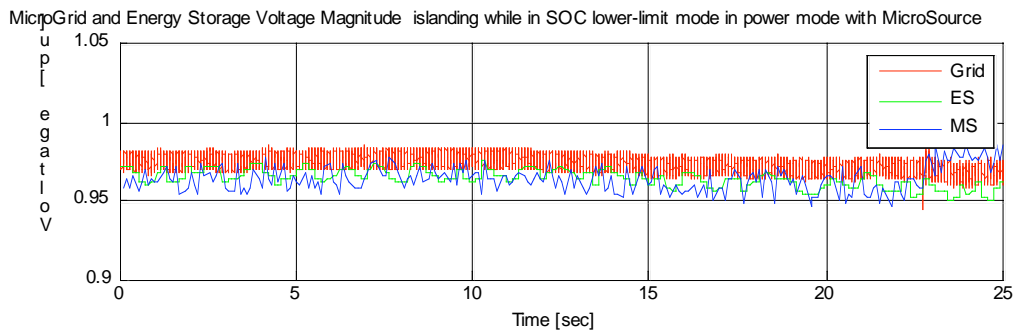


Figure 7.2.1.3 - Energy Storage, Microsource, and grid voltage magnitude

The reactive power and voltage magnitude characteristics are presented for completeness here, but present no significant results of note.

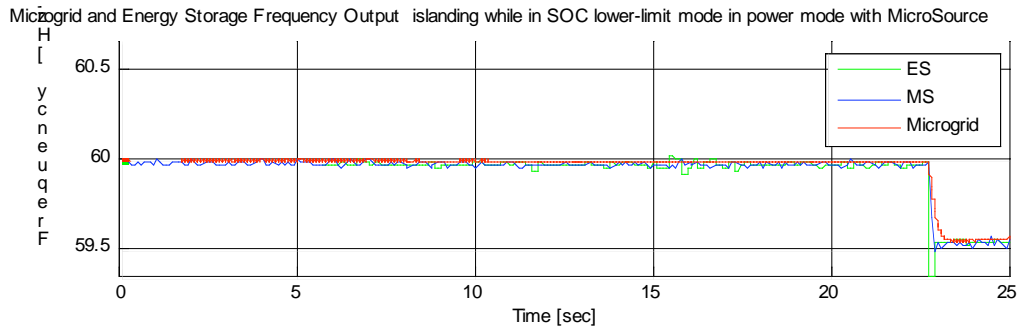


Figure 7.2.1.4 – System frequency through lower-limit event w/ microsource

The frequency characteristic presented here is quite interesting just past the island event at t=23sec. It shows how the energy storage element frequency decreases more than that of the microsource, effectively increasing the phase angle between the two sources, and increasing the relative loading on the microsource with respect to the energy storage element. This characteristic can be seen in figure 7.2.1.1 where the microsource increases and the energy storage element does not.

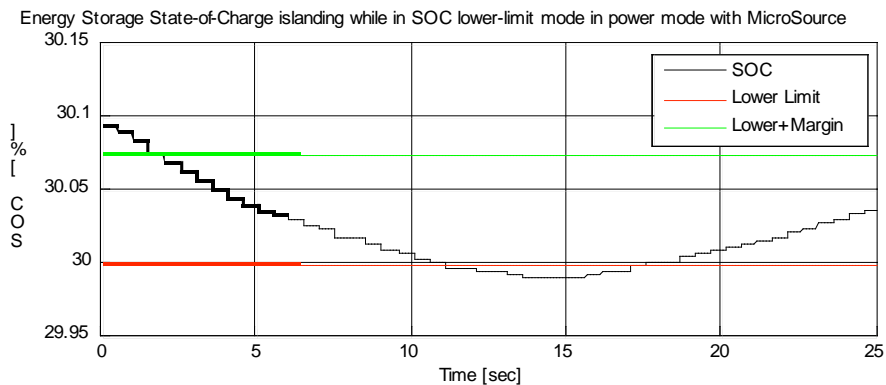


Figure 7.2.1.5 – State of Charge through lower-limit event w/ microsource

The characteristic of the state of charge through the lower limit event appears to be completely unaffected by the island event, which is somewhat expected from the power characteristic presented in figure 7.2.1.1. It should be noted, however, that this apparent continuity is purely coincidence, matching the frequency of the zero-feedback flow mode to the 59.5Hz system frequency.

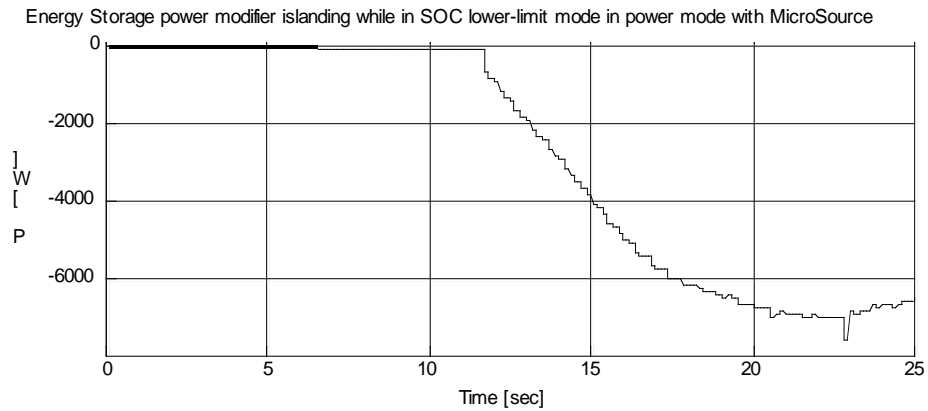


Figure 7.2.1.6 Power modifier through lower-limit event w/ microsource

The power modifier shows a similarly unaffected behavior as the power characteristic presented previously, except for the two data points that are offset by approximately 800W. Overall, the results of this test indicate that the system frequency will be determined by the unit in flow control as well as the power modifier, if it is engaged. This should indicate that the use of flow mode at the entry point of a microgrid is useful while grid-connected, but operates in an open loop manner when islanded, negating the droop characteristics of the system within the power capabilities of the unit itself.

7.2.2 Island event under SOC upper-limit-control mode, with microsource connected

The test result presented in this section is very similar to that of section 7.1.5 except that once the grid connection is removed, so too is the feedback to the flow control equation. Therefore, neglecting the effect of the power modifier, the microgrid frequency then gets set to the zero-flow intersect point of the energy storage unit.

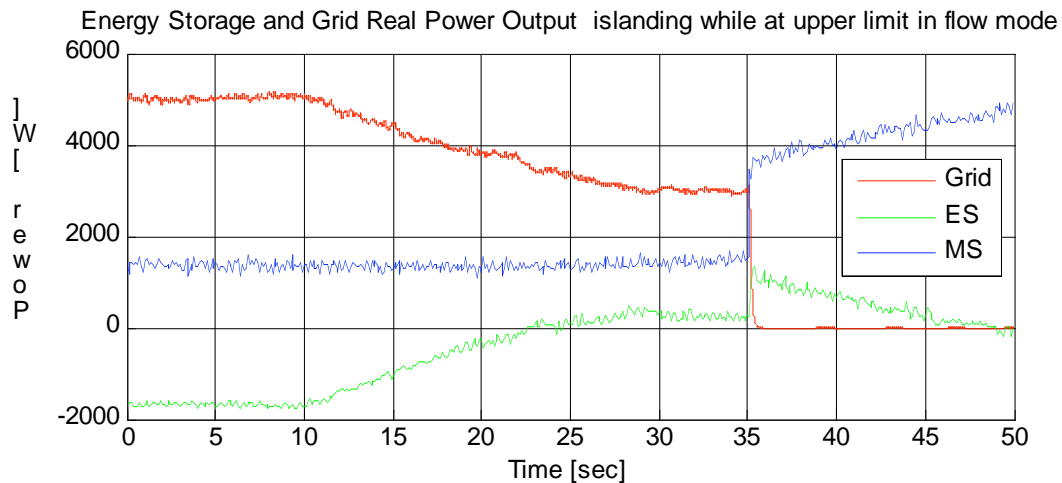


Figure 7.2.2.1 - Energy Storage, Microsource, and grid power contribution

The upper limit characteristic is similar in many ways to the lower limit event presented in section 7.2.1: the limit controller modifies the flow command via the power modifier value, and the island event causes a significant drop in frequency as the system was previously importing power prior to the island event. One interesting point here is that the energy storage element appears to assist in the initial support of the on-site load immediately after the transient, and it does, but only because the amount of flow commanded just prior to the island event was around 3kW, defining a zero-feedback frequency of 59.8Hz, as can be seen in figure 7.2.2.4. At this frequency, the microsource has not drooped enough to support the entire on-site load and causes a power deficit that must be supplied from the energy storage element. Since the energy storage unit is in

flow mode, there is no direct feedback from the output power of the unit except for power-limitations, and therefore there is no droop-curve interaction that will change the system frequency. Interestingly enough, the only frequency change that does occur comes from the power modifiers addition as a function of the SOC error above the upper limit.

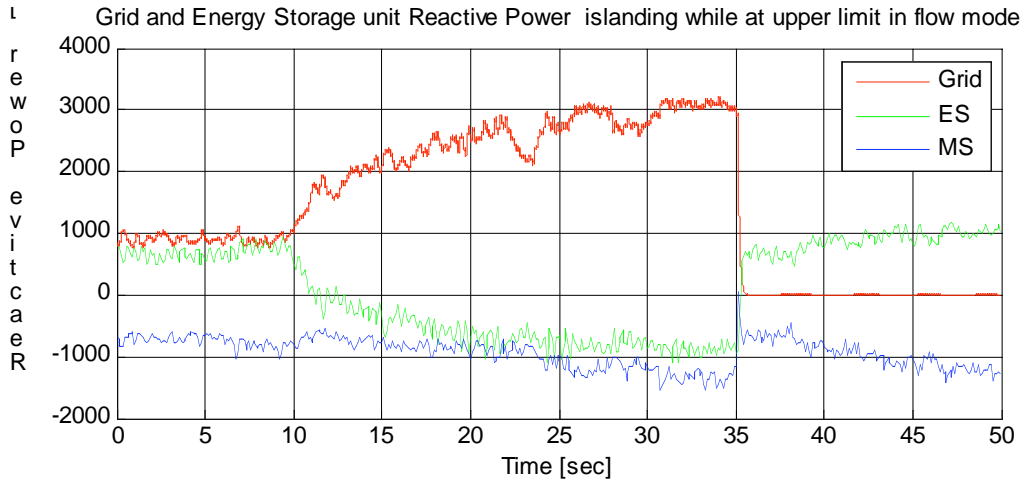


Figure 7.2.1.2 - Energy Storage, Microsource, and grid reactive power contribution

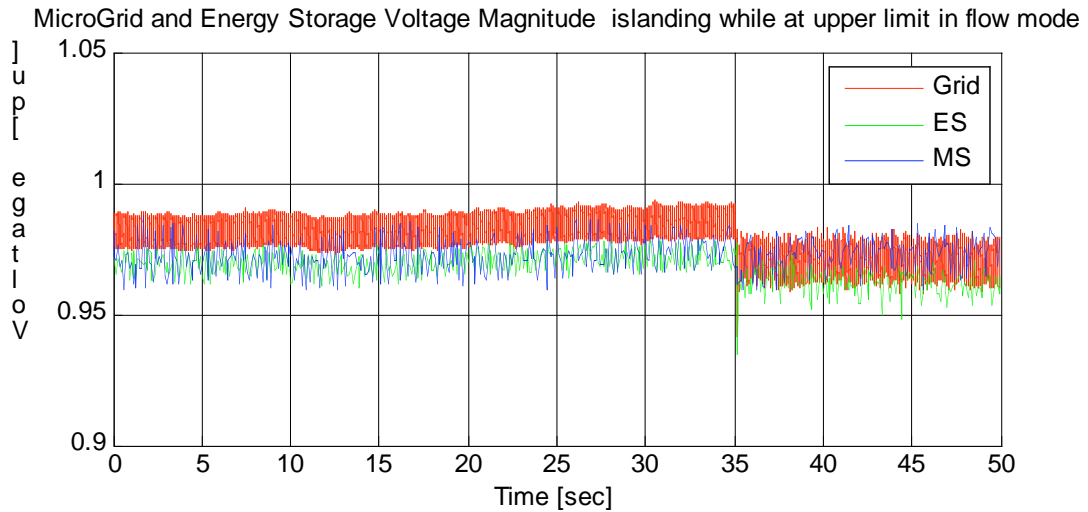


Figure 7.2.1.3 - Energy Storage, Microsource, and grid voltage magnitude

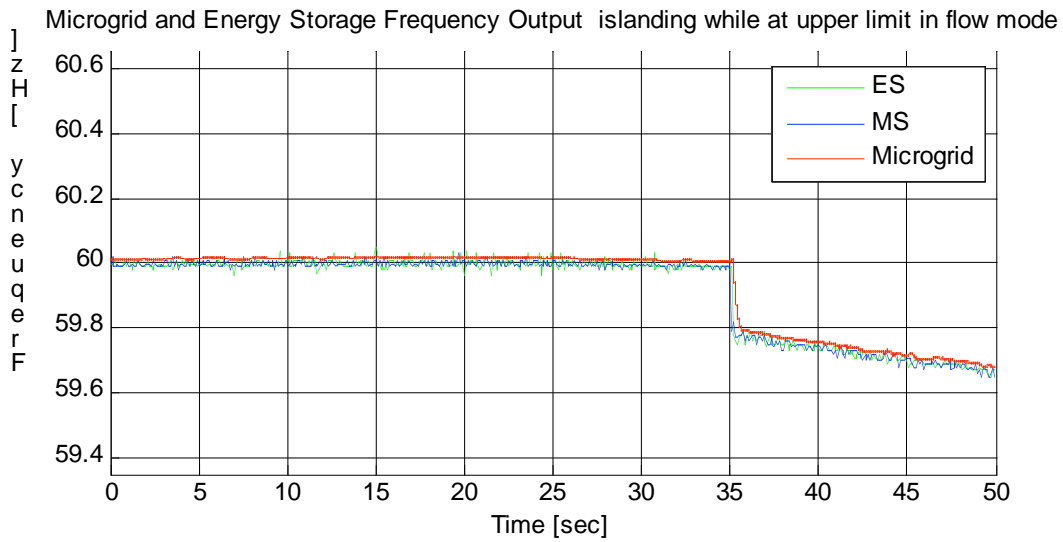


Figure 7.2.2.4 - System frequency through upper-limit island event w/ microsource

The system frequency appears to change linearly post-transient, but in actuality, it is simply a proportional response to the reduction in the power modifier, which is presented in figure 7.2.2.6.

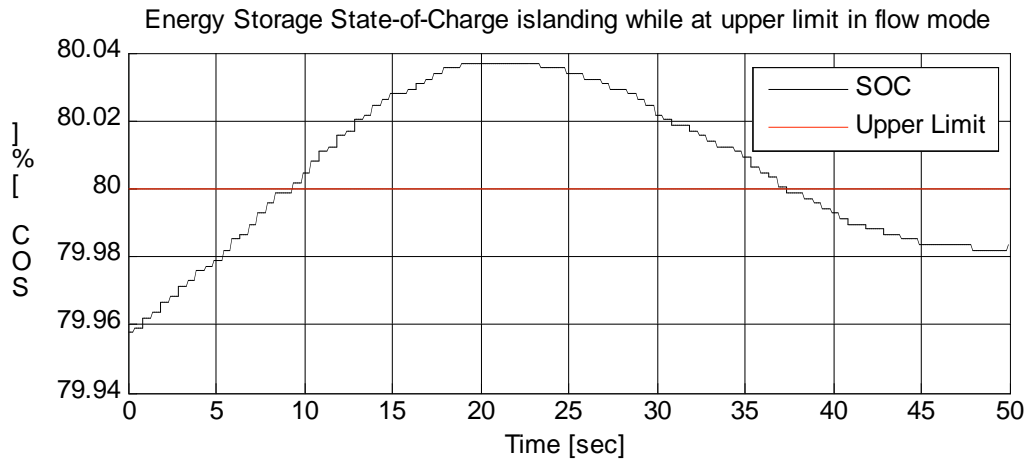


Figure 7.2.2.5 State of Charge through upper-limit island event w/ microsource

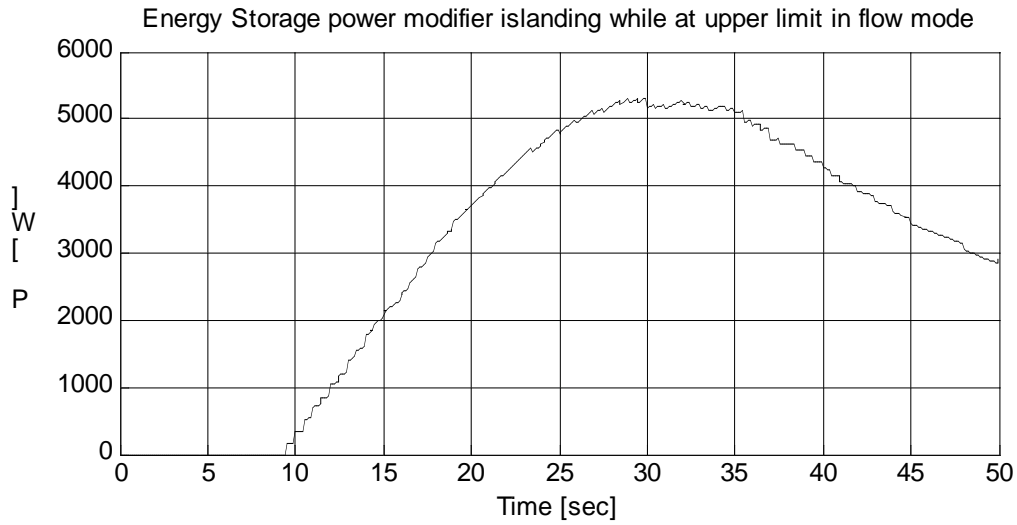


Figure 7.2.2.6 Power modifier through upper-limit island event w/ microsource

7.2.3 Flow control notes:

The characteristics presented here in regard to island events highlight the relative impracticality of operating an energy storage element in flow mode at the entry-point of the microgrid. As presented in sections 7.2.1&2, the loss of a feedback to the frequency of the source restricts the frequency of the system and removes all of the power-sharing characteristics that exist with power mode while islanded.

8. Conclusions

8.1 Summary of contributions:

This investigation has shown that energy storage systems add an extra degree of flexibility to a microgrid by allowing the temporal separation between generation and consumption of power. Regardless of what other purposes the energy storage unit is used, it was investigated here primarily for its backup power capabilities, ensuring that when an islanding event occurs that there will be a master frequency source on the system that can sink or source power depending on the disparity between fixed-power sources such as wind, solar, and geothermal plants and the current system power demand. This investigation utilized batteries as the energy storage medium for both its power capabilities as well as the energy reserve capacity considering cost. Though it has been noted that some other microgrid projects have chosen flywheels for their energy storage medium, it has been shown that long periods of power sinking or sourcing make batteries the obvious choice currently.

It was determined that the placement of an energy storage element near the entry-point of the microgrid allowed for feeder-flow regulation without communication lines to provide necessary information to operate. However, it was demonstrated in the hardware results section, the loss of flow-feedback that occurs as a result of islanding, will fix the microgrid frequency and negate the droop characteristics within the power capabilities of the energy storage unit.

A battery model was developed in this document and it was shown that a dual time-constant model could be matched to the battery response characteristics well enough

to not exhibit noticeable disparities between the model and measured data. Data was presented on the manner in which the batteries were cycled in order to produce the measured data used for the battery modeling process. The modeling processes, as well as the raw extracted parameters, were presented. Next, two separate battery models were developed for two separate purposes: in one case, accuracy and not processing time was paramount, whereas in the second case, processing time was limited and certain sacrifices had to be made on accuracy to develop a linear model that could be utilized efficiently in a time-sensitive manner. Lastly, the battery model was implemented in simulation as well as in a microcontroller; both were part of a battery state of charge observer that utilized terminal voltage error as the feedback to adjust for drift in the coulombic summation.

To effectively control the state of charge of the energy storage element, upper and lower limit-controllers were developed to keep the SOC within specified preferable limits. The controller utilized a power modifier variable (P_{mod}) to modify the power set-point. The upper SOC controller controlled the SOC directly, developing an error signal from the upper limit and the current SOC, engaging only when the error was positive and disengaging when the output goes negative. The lower limit controller controls the SOC indirectly by closing a loop on the input power, commanding the system to charge at a specified rate until a marginal value above the lower limit is reached. Both controllers represent different approaches to SOC management and they are equally as effective. From a system standpoint, there is no specific reason for using two types of control for different limits, but including both types illustrates the operation of each.

Extensive testing of hardware revealed that the system is inherently stable under a variety of operating conditions, including upper and lower controlled states. The algorithm was demonstrated to operate autonomously, providing an added feature to the plug-and-play topology of the CERTS microgrid. Various additions to the control laws included a saturation that limited the role of the limit controllers beyond 0.6Hz in either direction, slew rate limitations on the power modifier command, and limit-triggered controller engagement. The 0.6Hz limitation provides a nominal operating point just beyond the specified operating frequency range of the microgrid which is 0.5Hz. This allows for operation at a region beyond the 0.5Hz limit, but within the 1Hz limit, to signal a non-preferential situation such as a critically low battery state of charge. Since the controller will not act beyond 0.6Hz, the impact to frequency-sensitive loads set to 59Hz is minimized. At frequencies just beyond the normal operation range, the frequency itself is useful as a communication signal in engaging the startup sequence for back-up diesel generators. One issue with extending the frequency range of the system includes increased difficulty re-synchronizing with a larger difference frequency after a fault has cleared, but considering the microgrid is largely inertia-free, the effect of hard-closing the static switch should be minimal.

Overall, the limit controller has well behaved characteristics. It provides autonomous management of the state of charge of the battery, retains some of the transient suppression abilities even in a controlled state, and operates seamlessly regardless of system frequency. Regardless of the power set-point specified by the supervisory controller, this control methodology will ensure plug-and-play functionality of the energy storage unit.

8.2 Future Work

A great deal of work has gone into the UW-Microgrid as well as microgrid research around the world to bring the state of the art to where it is today. This work contributed mainly towards the autonomous management of a lead-acid battery bank in a microgrid environment. Opportunities for future work are on-line state of charge and state of health algorithms to report back in more detail the capability and reliability of the battery to increase robustness of the power system. Much work has been going on in the field of battery SOC estimation, but a more complete solution would assist in the work done here to increase reliability if implemented in a power system.

Secondly, the transient characteristics and handling considerations for different battery chemistries should be investigated, specifically high-energy batteries such as flow batteries that would increase the energy capabilities of an installed unit. Flow batteries utilize separate tanks for positive and negative electrode reactions which represents a significant shift in the battery modeling effort. However, the existence of separate electrolyte tanks may provide opportunities for the use of pilot sensors for directly determining state of charge. Lastly, hybrid battery-capacitor systems should be investigated to quantify the additional benefit of higher peak-power capabilities.

References

- [1] Kiehne, Heinz. Battery Technology Handbook. CRC Press, 2003.
- [2] BP5-12. 2009. B.B. Battery. 12 May. 2009 <<http://www.bb-battery.com/productpages/BP/BP5-12.pdf>>.
- [3] Laman, F. C., Bose, C. S. C., & Dasgupta, S. R. (1998). *Accelerated failure testing of valve regulated lead-acid batteries using gas studies*, IEEE Telecommunications Energy Conference
- [4] Ciobotaru, M., Teodorescu, R., & Agelidis, V. G. (2008). *Offset rejection for PLL based synchronization in grid-connected converters*, IEEE Applied Power Electronics Conference and Exposition
- [5] Akhil, A., Swaminathan, S., Sen, R. (2007). *Cost Analysis of Energy Storage Systems for Electric Utility Applications*. Sandia National laboratories.
- [6] Bath County Pumped Storage Station. 2009. Dominion . 12 May. 2009 <<http://www.dom.com/about/stations/hydro/bath.jsp>>.
- [7] American Superconductor. 2009. American Superconductor. 12 May. 2009 <<http://www.amsc.com/>>.
- [8] Whittingham, M. Stanley. "Electrical Energy Storage Using Flywheels." Materials Research Society Volume 33, April 2008: 419-420.
- [9] Energy Density. 2009. Transwiki. 12 May. 2009 <http://wiki.xtronics.com/index.php/Energy_density>.

- [10] Energy Storage. 2008. Wikipedia. 12 May. 2009
<http://en.wikipedia.org/wiki/Energy_storage>.
- [11] SCE – Self Generation (Distributed Generation). 2009. Southern California Edison.
12 May. 2009 <<http://www.sce.com/customergeneration>>.
- [12] Baba, J., Suzuki, S., Numata, S., Yonezu, T., Kusagawa, S., Denda, A., et al. (2005).
Combined power supply method for micro grid by use of several types of distributed power generation systems, IEEE Power Electronics and Applications
- [13] Barnes, M., Kondoh, J., Asano, H., Oyarzabal, J., Ventakaramanan, G., Lasseter, R., et al. (2007). *Real-world MicroGrids An overview*, IEEE System of Systems Engineering.
- [14] Barton, J. P., & Infield, D. G. (2004). *Energy storage and its use with intermittent renewable energy*, IEEE Transactions on Energy Conversion.
- [15] Binduhewa, P. J., Renfrew, A. C., & Barnes, M. (2008). *Ultracapacitor energy storage for MicroGrid micro-generation*, IEEE Power Electronics, Machines and Drives Conference.
- [16] Codeca, F., Savaresi, S. M., & Rizzoni, G. (2008). *On battery state of charge estimation: A new mixed algorithm*, IEEE International Conference on Control Applications.
- [17] El-Fouly, T. H. M., El-Saadany, E. F., & Salama, M. M. A. (2006). *One day ahead prediction of wind speed using annual trends*, IEEE Power Engineering Society General Meeting.

- [18] El-Fouly, T. H. M., El-Saadany, E. F., & Salama, M. M. A. (2008). *One day ahead prediction of wind speed and direction*, IEEE Transactions on Energy Conversion.
- [19] Georgakis, D., Papathanassiou, S., Hatziargyriou, N., Engler, A., & Hardt, C. (2004). *Operation of a prototype microgrid system based on micro-sources quipped with fast-acting power electronics interfaces*, IEEE Power Electronics Specialists Conference.
- [20] Gu, W. B., Wang, G. Q., & Wang, C. Y. (2001). *Modeling the overcharge process of VRLA batteries*, Battery Conference on Applications and Advances.
- [21] Gyuk, I., Kulkarni, P., Sayer, J. H., Boyes, J. D., Corey, G. P., & Peek, G. H. (2005). *The united states of storage [electric energy storage]*, IEEE Power and Energy Magazine.
- [22] Jayawarna, N., Barnes, M., Jones, C., & Jenkins, N. (2007). *Operating MicroGrid energy storage control during network faults*, IEEE International Conference on System of Systems Engineering.
- [23] Jenkins, D. P., Fletcher, J., & Kane, D. (2008). *Lifetime prediction and sizing of lead-acid batteries for microgeneration storage applications*, IEEE Renewable Power Generation.
- [24] Jones, C. E., Fitzer, C., & Barnes, M. (2006). *Investigation of microgrids*, IET International Conference on Power Electronics, Machines and Drives.

- [25] Jossen, A., Spath, V., Doring, H., & Garche, J. (1999). *Battery management systems (BMS) for increasing battery life time*, IEEE International Telecommunications Energy Conference.
- [26] Krishnamurthy, S., Jahns, T. M., & Lasseter, R. H. (2008). *The operation of diesel gensets in a CERTS microgrid*, PhD thesis, University of Wisconsin – Madison.
- [27] Kutluay, K., Cadirci, Y., Ozkazanc, Y. S., & Cadirci, I. (2005). *A new online state-of-charge estimation and monitoring system for sealed lead-acid batteries in telecommunication power supplies*, IEEE Transactions on Industrial Electronics.
- [28] Lasseter, R. H. (2007). *Certs microgrid* , White Paper, University of Wisconsin - Madison
- [29] Lasseter, R. H., & Paigi, P. (2004). *Microgrid: A conceptual solution*, IEEE Power Electronics Specialists Conference.
- [30] Lasseter, R. H. (2008). *Extended CERTS microgrid* , White Paper, University of Wisconsin - Madison
- [31] Mao Meiqin, Ding Ming, Su Jianhui, Liuchen Chang, Sun Min, & Zhang Guorong. (2008). *Testbed for microgrid with multi-energy generators*, Canadian Conference on Electrical and Computer Engineering.
- [32] McClay, C., & Litchev, P. (2002). *Risk management issues for distributed generation*, IEEE Power Engineering Society Winter Meeting.

- [33] Misra, S. S., & Noveske, T. M. (1997). *Some design aspects and the role of AGM separator in VRLA batteries*, IEEE International Telecommunications Energy Conference.
- [34] Nichols, D. K., Stevens, J., Lasseter, R. H., Eto, J. H., & Vollkommer, H. T. (2006). *Validation of the CERTS microgrid concept the CEC/CERTS microgrid testbed*, IEEE Power Engineering Society General Meeting.
- [35] Piagi, P., & Lasseter, R. H. (2006). *Autonomous control of microgrids*, IEEE Power Engineering Society General Meeting.
- [36] Stevens, J., & Klapp, D. (2007). *CERTS microgrid system tests*, IEEE Power Engineering Society General Meeting.
- [37] Szymborski, J., Hunt, G., & Jungst, R. (2001). *Examination of VRLA battery cells sampled from the metlakatla battery energy storage system*, Battery Conference on Applications and Advances.
- [38] Venkataramanan, G., & Illindala, M. (2002). *Microgrids and sensitive loads*, IEEE Power Engineering Society Winter Meeting.
- [39] Wang, X., Sideratos, G., Hatziargyriou, N., & Tsoukalas, L. H. (2004). *Wind speed forecasting for power system operational planning*, IEEE International Conference on Probabilistic Methods Applied to Power Systems.
- [40] Zoka, Y., Koeda, K., Sugimoto, A., Yorino, N., & Kawahara, K. (2005). *An economic evaluation for an autonomous independent network of distributed generators*, International Power Engineering Conference.

Appendix A: Control System Block Diagrams

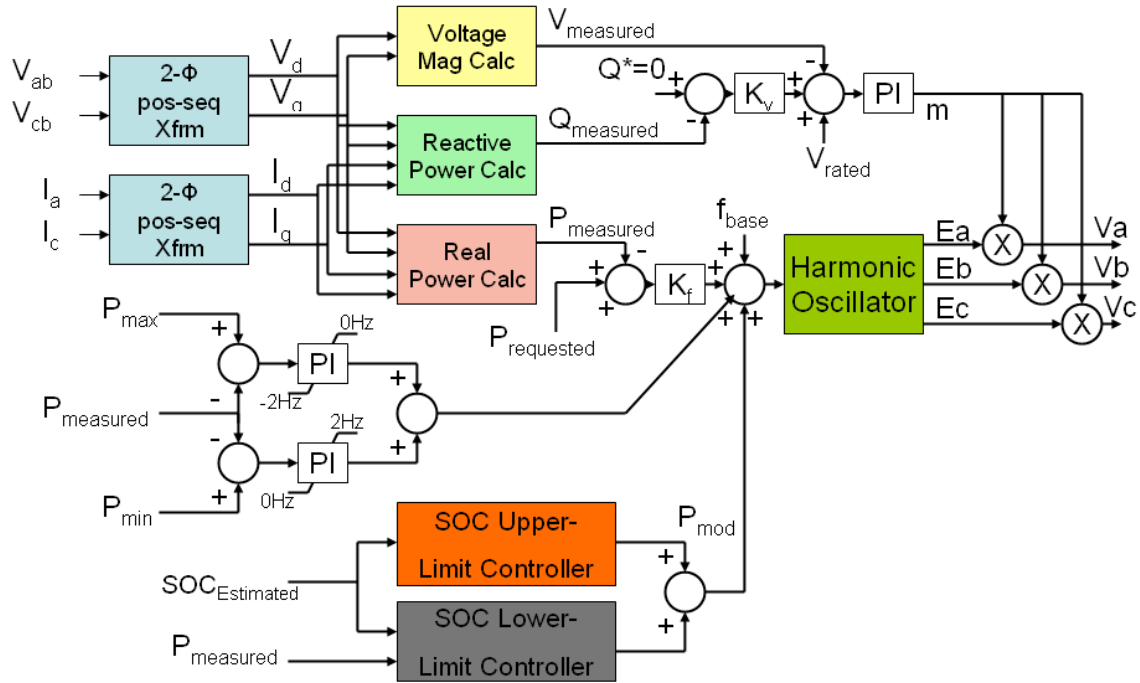


Figure A-1 Inverter Controller Software Block Diagram

Presented above is the overall block diagram of the control system implemented in software for the hardware testing presented in chapter 7. On the input to the controller are four measured values which get transformed into respective q-axis and q-axis quantities in the stationary frame, aligning the q-axis with phase ‘a’ of the output filter capacitor voltage and output reactor phase ‘a’ line current for the voltage and current vectors respectively. The voltage magnitude is calculated from the orthogonal summation of the quantities V_d and V_q . Real power is calculated from the in-phase components of the current with respect to the voltage:

$$P_{\text{measured}} = V_d \cdot I_d + V_q \cdot I_q \quad (\text{A.1})$$

Reactive power is calculated from the orthogonal current with respect to the phase voltage, resulting in a positive value for capacitive VARs (currents leading voltages):

$$Q_{\text{measured}} = V_d \cdot I_q - V_q \cdot I_d \quad (\text{A.2})$$

A.1 Power vs. Frequency droop gain selection

The error between the requested power and the measured power is multiplied by the droop factor ($k_f = 0.1 \text{ Hz/kW}$) that defines the nominal operational frequency. The droop factor used here corresponds to a full 1Hz droop for a 1pu power of 10kW. The ideal case would specify a 0.5Hz droop for a power error corresponding to 1pu power output in the worst case where the 60Hz power set-point was set to the minimum power. For a normal prime mover, this gain should be set to a value corresponding to 0.5Hz for 1pu of power output (eg. 0.05Hz/kW for a system rated at 10kW). However, because of the bi-directional capabilities of the energy storage element, the operational range within 0.5Hz can be accomplished by reducing the droop-rate further. For example, if we assume that the energy storage element has a P_{\min} of -0.5pu (-5kW) and a P_{\max} at the full 1pu rating, the appropriate droop should be 0.033Hz/kW. This reduction in droop gain would ensure operation within then +/-0.5Hz window so long as both the power set point, as well as the power output, remain within the bounds of the specified power limits.

One caveat to the previously presented droop gain guideline is in a situation where the P_{\min} and P_{\max} values are expected to change significantly through the allowable state of charge values (see figure 1.2.1). If the range of P_{\max} - P_{\min} could change drastically and the 0.5Hz range is a hard design constraint, the maximum range between P_{\max} and P_{\min} should be used as the design range. As a final exception, the range can be varied to suit the operating point capabilities of the energy storage element, but the resulting dynamics of on-the-fly droop gain adjustments have not been evaluated in the work contained herein.

A.2 Power limit controller explanation and gain selection

The power balance is the primary means of adjusting the output frequency of the voltage waveform, but can be further modified by the power and SOC limit controllers if the respective system parameters are out of limits. Limiting the maximum and minimum average power the system outputs is critical to managing the health of the batteries and the power converter itself. Though the upper and lower limits can be ultimately defined by a variety of parameters (see battery handling considerations in section 4), the result is a single maximum and/or minimum power that the system can sink/source safely that is then enforced by the power limiting controller. The power limit controller is a proportional-integral controller that operates when a value of measured power is outside of the specified safe-operation range. The topology of the power-limit controllers are identical to the SOC-upper-limit controller presented in figure A-2, in that both the integrator and the output is limited to the same value, removing wind-up effects at the engagement and disengagement of the limit controller. The gains for the power-limit controllers used here are 0.05Hz/kW for the proportional gain and 0.5Hz/(kW-sec) for the integral gain, resulting in per-unitized gains of 0.5 and 5 for the proportional and integral gains respectively.

The limitation imposed on the output is significant as well. The 0Hz lower limit for the Pmax limiter and the 0Hz upper limit for the Pmin limiter act to keep the controllers dormant during conditions when the specified power output is within the Pmax-Pmin range. As previously mentioned, limiters are enforced on the integral value and the output, avoiding output delay as a result of integrator offset. The opposing limits of 2Hz and -2Hz for the Pmin and Pmax limiters, respectively, serve a less critical function. The maximum 2Hz deviation allows for the system to retain a reasonable frequency even when under drastic loading conditions. This limit is definable by the system manager but

should adhere to two design points: 1) the limit should be set to a magnitude large enough to trip frequency triggers on non-essential loads (usually about 1Hz) and 2) should be set to a limit small enough to avoid stalling and over-speeding of generators.

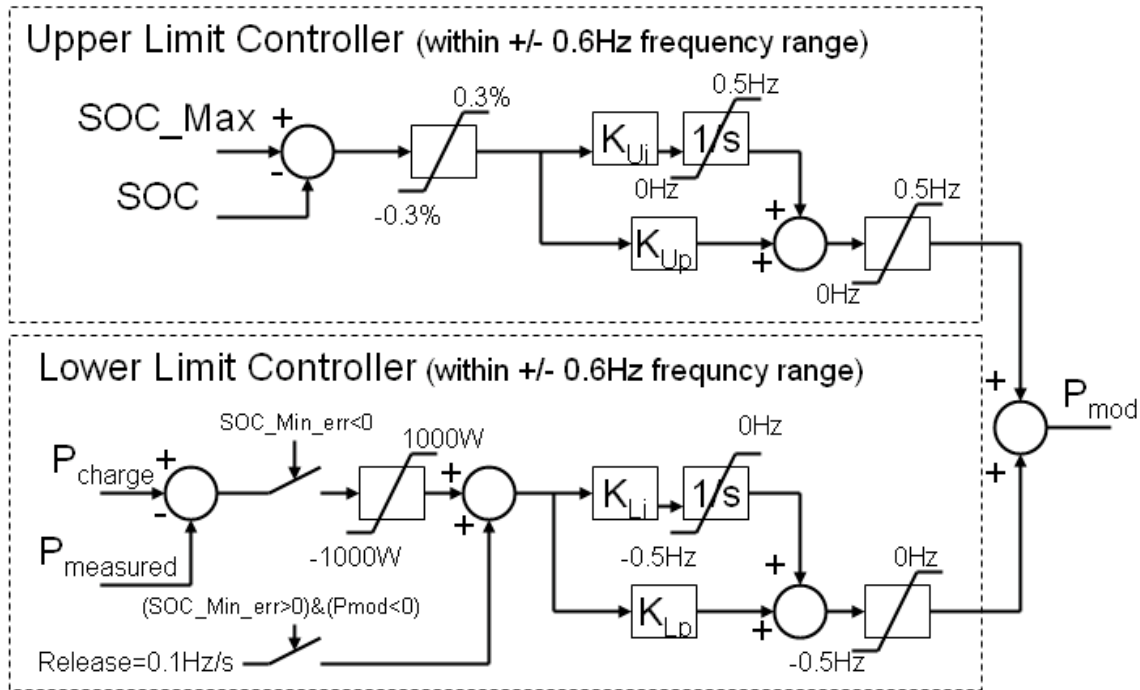


Figure A-2 SOC upper and lower limit controller block diagram detail

A.3 SOC limit controller explanation and gain selection

As previously mentioned, the SOC limit controllers can also affect the system frequency. However, one of their main attributes is a maximum variation of 0.5Hz (the full range of power for the source). This limit allows the SOC limit controller to provide any frequency variation up to a full counteraction to a set point anywhere within the P_{max} or P_{min} limits. More importantly, the 0.5Hz limitation allows the action of the P_{max} and P_{min} power-limit controller to overtake the action of the SOC limit controller in the event that both the SOC and the power limits are exceeded, giving priority to system protection over SOC management.

A.3.1 SOC Upper Limit Controller

The upper limit controller operates on an error signal originating from any SOC above the maximum SOC. It utilizes a PI controller acting on an initial error which results in a small but acceptable amount of overshoot, exhibiting a damped response. In the work here, the maximum SOC is specified as 0.8pu as this provided an adequate ability to accept charge. Upon inspection of figure 6.1.1, it becomes apparent that the battery charge characteristic is voltage limited versus current limited around 80% of charge volume. For this analysis, it was determined that the diminishing capacity for charge current became the defining characteristic for the upper limit. Beyond this point, the steady-state charge power acceptance falls below the specified threshold value of 0.33pu. For different chemistries and different battery system and load requirements this upper limit will vary.

Tuning the upper limit controller was a matter of balancing the quick response time of a high gain controller with the unimpeded transient suppression abilities of a system without tight charge state regulation. The integral gain was set to 0.33Hz/(%SOC-sec) and the proportional gain was chosen to provide adequate damping at 2.6Hz/%SOC. These values were defined by experimental adjustment upon the criteria of settling times that exceeded the transient response times but were limited to significantly less than a minute to limit the magnitude of accumulated SOC error. A closed-loop analysis of the system while grid connected reveals a well damped system with a bandwidth of 0.025Hz. It is important to mention, however, that the droop-controller provides damping in the operation of this limit controller as it operates off the SOC which is an integrated state.

A.3.2 SOC Lower Limit Controller

The lower SOC limit controller acts in a notably different fashion than the upper limit controller as it actuates in a hysteretic fashion. It utilizes a conditional trigger to operate in different configurations which comes from a conditional statement that checks whether the SOC is above a preferential point. This preferential point changes to operate the controller in a hysteretic fashion in that the lower preferential point is set to the lower SOC limit while in normal operation. When the lower SOC limit is reached, the preferential point is increased to the marginal limit. The resulting SOC_Min_err, which originates from the comparison between the preferential SOC and the estimated SOC, is used as a mode trigger. It is important to note that the value of SOC used for control is a signal developed from the battery observer covered in section 5 and presented in figure A-3.

The normal mode of the lower limit controller in a non-dormant state affects the system frequency when the SOC is below the preferential SOC point, triggered when the SOC_Min_err is less than zero. Once this condition occurs, the power is regulated through a uni-directional PI controller similar to the upper limit controller. The resulting effect of this controller is the regulation of charge power into the battery. The specified magnitude assigned to P_{charge} is a user preference which should be assigned anywhere between the minimum and maximum recommended charge power. Assigning a lower value may be preferential when considering system efficiency, but will take a longer time to reach the marginal SOC above the reserve limit. As described in section 6.1.4, the charge power is done to eventually attain a SOC that is above the reserve limit, but ultimately restore normal operation, even if only for a short time until the lower limit is reached again.

The lower limit controller incorporates a slew-rate limiter which acts to limit the change in the frequency command that the controller receives. This is an optional addition to the system controller, but it was included to take advantage of the fact that internally generated commands do not have to be step commands. By limiting the rate at which the command changes serves to limit the time rate of change of output that the other sources on the network will encounter. Again, this is an option and does slow the reaction time of the SOC limit controller but given that the SOC is a relatively slowly changing variable, the response time of the controller is significantly faster than the battery requires.

The gains choices of the lower limit controller were chosen to satisfy not only the charge-power requirement, but were also chosen to enable the delay in the response time to provide some transient suppression through quick changes in power output. In essence, the lack of high frequency command tracking allows for high frequency transient suppression activity from the standard power vs. frequency controller. For example, the lower limit gain was chosen to $0.1\text{Hz}/(\text{kW}\cdot\text{sec})$ and the proportional gain was chosen to provide adequate damping at $0.05\text{Hz}/\text{kW}$. If the loop gain is analyzed in parallel with the standard droop controller, two complex poles result describing a damping ratio of 0.5 and a natural frequency of 0.5Hz. This response characteristic could be tuned to real poles for less overshoot in power command, but it is important to realize that the root locus analysis changes based on frequency-droop effects from other sources. With a compliant system frequency, the system becomes more well damped but since the system can be configured with any range of power rating per unit change in frequency, there are many possible solutions other than the grid-connected case. The general trend, however, is the lower the kw-per-Hz ratio, the more well damped the power controller response becomes.

Once the state of charge increases to the new preferential SOC which is defined as the marginal limit above the lower reserve limit, the controller releases the system through a ramp-rate of 0.1Hz/sec until the controller output has increased to 0Hz at which point the preferential SOC is returned to the lower reserve limit. Without the release rate, the controller would continually impose a power command offset on the system. The value of 0.1Hz/sec was chosen to exhibit slew-rate limiting characteristics, changing the power command by 2kw/sec. This value is determined by the transient response characteristics of other sources on the microgrid which will have to reduce power output to compensate for the reduction in charge power entering the energy storage element. Higher slew rate offer faster release times, but may cause increased emissions from generators and unnecessary frequency and voltage magnitude fluctuations.

A.3.3 Frequency Domain of SOC Limit Controllers

One important feature of the SOC limit controller is its ability to output power even in low SOC charge states. This feature is essential to the stable system operation while islanded, providing essential backup power to support local loads while energy is available in the battery even though it has exceeded the reserve limit. Essentially, the operation of the SOC limit controller is limited to a range of $\pm 0.6\text{Hz}$, which is slightly outside the $\pm 0.5\text{Hz}$ window of normal operation. Secondly, the frequency range of 59.4-59.5Hz can be then used to transmit somewhat of an SOS signal to supplementary generation to come online.

If it is determined that the operation of the SOC limit controller causes a controller frequency that is outside the $\pm 0.6\text{Hz}$ range, the current output of the SOC limit

controller is retained, freezing the controller operation, and the previous output is decremented by 0.03Hz which corresponds to approximately 300W when grid connected. The decrementing occurs each iteration of the controller loop (10/second in the work presented here) until the system frequency returns to within the acceptable ± 0.6 Hz range at which time the controller is re-enabled using the previous decremented amount. Code blocks that describe this implementation can be found in Appendix B.

A.3.4 Selection of SOC limit points

The designed SOC limit points are determined from a number of criteria which originate from a comparison between battery capability and specified system requirements such as peak power output, peak power absorption, and specifications of power level and duration of back-up reserve. Also, the estimation accuracy of the SOC must be considered to ensure operation within the safe operating region of actual SOC. Finally, the system manager must determine the marginal buffer between the marginal limit and the reserve limit.

With the framework for limit selection outlined, the selection criteria will be explained further utilizing the verbiage presented in figure 6.1.3. As briefly touched upon in section A.3.1, the upper and lower SOC limits can be defined with respect to the charge and discharge characteristics of the batteries that are usually provided with the datasheet themselves. Charge power decreases within the safe operating range (SOR) as the SOC increases. The discharge power also decreases with SOC assuming a minimum pack voltage, which allows the designer of the energy storage element to find the point correlating the upper and lower charge volumes or SOC points that still maintain a reasonable power capability. As previously mentioned, the end ranges must be buffered

with the known operational error of the SOC estimation algorithm. SOC estimation accuracy is explained further in section A.4, but the net effect is a reduction in the operating space proportional to the sum of estimation errors at each end.

The reserve limit is selected based off of the perceived energy necessary to support back-up power to the microgrid in the event of island while at a low SOC. For example, if:

- energy storage is rated at 1pu-hr
- peak expected demand requires 0.7pu from the energy storage element while other sources are outputting their maximum power
- 1 minute of backup time is required to ensure that a diesel generator will be guaranteed to come online

The reserve limit should be placed at least 0.012pu above the lower SOC limit.

Another final consideration is the magnitude of the hysteretic gap between the lower marginal limit and the reserve limit. The hysteretic margin is notably the most subjective design consideration because the benefit of long or short duration between cycles. A large hysteretic region will offer lesser number of transients on the system that occur during the engagement and disengagement of the lower limit controller, but a lower small hysteretic region will cause the lower limit controller to act for a shorter duration. In the experimental work here, the margin was set extremely low to show transient operation at the engagement and disengagement of the lower SOC controller within one test run.

A.4 Battery observer estimation accuracy and conductance gain selection

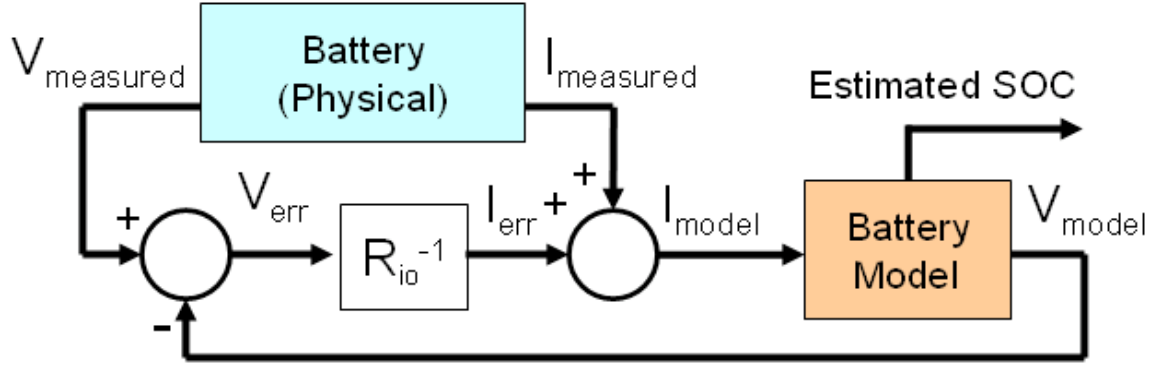


Figure A-3 Battery observer block diagram which develops estimated SOC used for ctrl. In the work presented here, the specific accuracy of the SOC estimation was not measured and left for future work. However, in most cases with an accurate value battery capacity, the battery observer will exhibit a steady state error that correlates to the current offset error in the DC-bus current measurement and the voltage error multiplied by the conductance gain. Satisfying the condition:

$$I_{\text{offset}} = V_{\text{err}}/R_{i_o} \tag{A.3}$$

The choice of the conductance gain $1/R_{i_o}$ (as presented in figure A-3) depends on both the measurement accuracy of the DC-link current as well as the convergence rate upon initialization of the system. In practice, typical values depend entirely on the measurement accuracy of the DC-link voltage and current that feed the battery observer. Higher gains offer faster convergence but are more noise sensitive. Lower gains adjust the SOC less based on input noise offering smoothing effects on input noise but will be more sensitive to current offset errors.

The SOC error is proportional to the voltage error multiplied by the inverse derivative of the open circuit voltage characteristic:

$$\text{SOC}_{\text{err}} = (V_{\text{err}} / \frac{dV}{d\text{Coulomb}}) \tag{A.4}$$

Fortunately in the case of the upper and lower limits, the open circuit voltage change per coulomb is larger at the upper and lower states of charge, reducing the estimation error.

A.5 Voltage magnitude controller explanation and gain selection

The voltage magnitude controller is a PI controller with 90% feedforward value, leaving 10% to be managed by the PI controller. The 90% value was inherited from the previous controller established in the UW microgrid, which should be augmented to 100% for more effectiveness. The PI controller itself has a 95-105% limitation on the command versus the reference voltage specified by the user. Secondly, the integrator on the PI controller is limited to 0.2pu. The proportional gain has been set to approximately 0.9V/V, which should allow slow wind-up of the integrator. The integrator gain has been set to 10V/(V-sec).

Appendix B: Power Modifier SOC Limit Control Code

The following sections of code are executed in sequence to perform SOC limit-control operations.

```
//Define error signals for control
SOC_max_err=SOC-SOC_max;
SOC_min_err=SOC-SOC_min;
```

```
//Trigger upper limit mode
if(SOC_max_err>0)
{
    if(SOC_Upper_Limit_Ctrl==0)
    {
        P_offset=Pdq_filt; //Capture power output at entry into limit mode
    }
    SOC_Upper_Limit_Ctrl=1; //Enable upper limit control
}
```

```
//Trigger marginal addition to SOC_min at lower end (hysteresis)
if(SOC_min_err<0)
{
    SOC_min=SOC_min_nominal+SOC_margin;
    SOC_min_err=SOC-SOC_min;
    if(SOC_Low_Limit_Ctrl==0)
    {
        P_offset=Pdq_filt; //Capture power output at entry into limit mode
    }
    SOC_Low_Limit_Ctrl=1;
}
```

```

//The P_mod code (upper limit)
if(SOC_Upper_Limit_Ctrl==1)//0.6Hz max droop
{
    if((SOC_max_err<0) || (freqchg>(-MaxFrqChg) && freqchg<MaxFrqChg))
    {
        if(SOC_max_err>100)//slew-rate limiting
        {
            P_mod_int += 100*Ki_soc;
            P_mod = P_mod_int+100*Kp_soc;
        }
        else //normal operation
        {
            P_mod_int += (SOC_max_err)*Ki_soc;
            P_mod = P_mod_int+(SOC_max_err)*Kp_soc;
        }
    }
    SOC_Sequence_State = 3;
    if((P_mod<=0) && (SOC_max_err<0))//exit limit control mode
    {
        SOC_Upper_Limit_Ctrl=0; //Disable upper limit control
        P_mod_int=0;
        P_mod=0;
        SOC_Sequence_State = 0;
    }
}

```

```

//The P_mod code (lower limit)
if(SOC_Low_Limit_Ctrl==1)
{
    SOC_Sequence_State = 4;
    if(SOC_min_err<=0 && freqchg>(-MaxFrqChg) && freqchg<MaxFrqChg)
    {
        P_err = P_charge-Pdq_filt;
        if(P_err<-1000)
        {
            P_mod_int -= 100*Ki_LL_soc;
            P_mod = P_mod_int/10-10*Kp_LL_soc;
        }
        else
        {
            P_mod_int += (P_err*Ki_LL_soc)/10;
            P_mod = P_mod_int/10+(P_err*Kp_LL_soc)/100;
        }
    }
    else
    {
        if(P_mod>=0)//exit limit control mode
        {
            SOC_Low_Limit_Ctrl=0;    //Disable lower limit control
            P_mod_int=0;
            P_mod=0;
            SOC_min=SOC_min_nominal;//Remove marginal addition to
SOC_min
            SOC_Sequence_State = 0;
        }
        else
        {
            P_mod += 250;
        }
    }
}

```

```
//Limit the role of SOC Limit controller beyond 0.6Hz
if((freqchg>(MaxFrqChg+5)) && (P_mod>0))
{
    P_mod_int -= 300;
    P_mod -= 300;
}
if((freqchg<(-MaxFrqChg-5)) && (P_mod<0))
{
    P_mod_int += 300;
    P_mod += 300;
}
```

```
//Limit the magnitude of influence of P_mod to 10kW
if (P_mod>10000)
{
    P_mod_int += 10000-P_mod;
    P_mod=10000;
}
if (P_mod<(-10000))
{
    P_mod_int += -10000-P_mod;
    P_mod=-10000;
}
```

Appendix C: Hardware configuration diagram

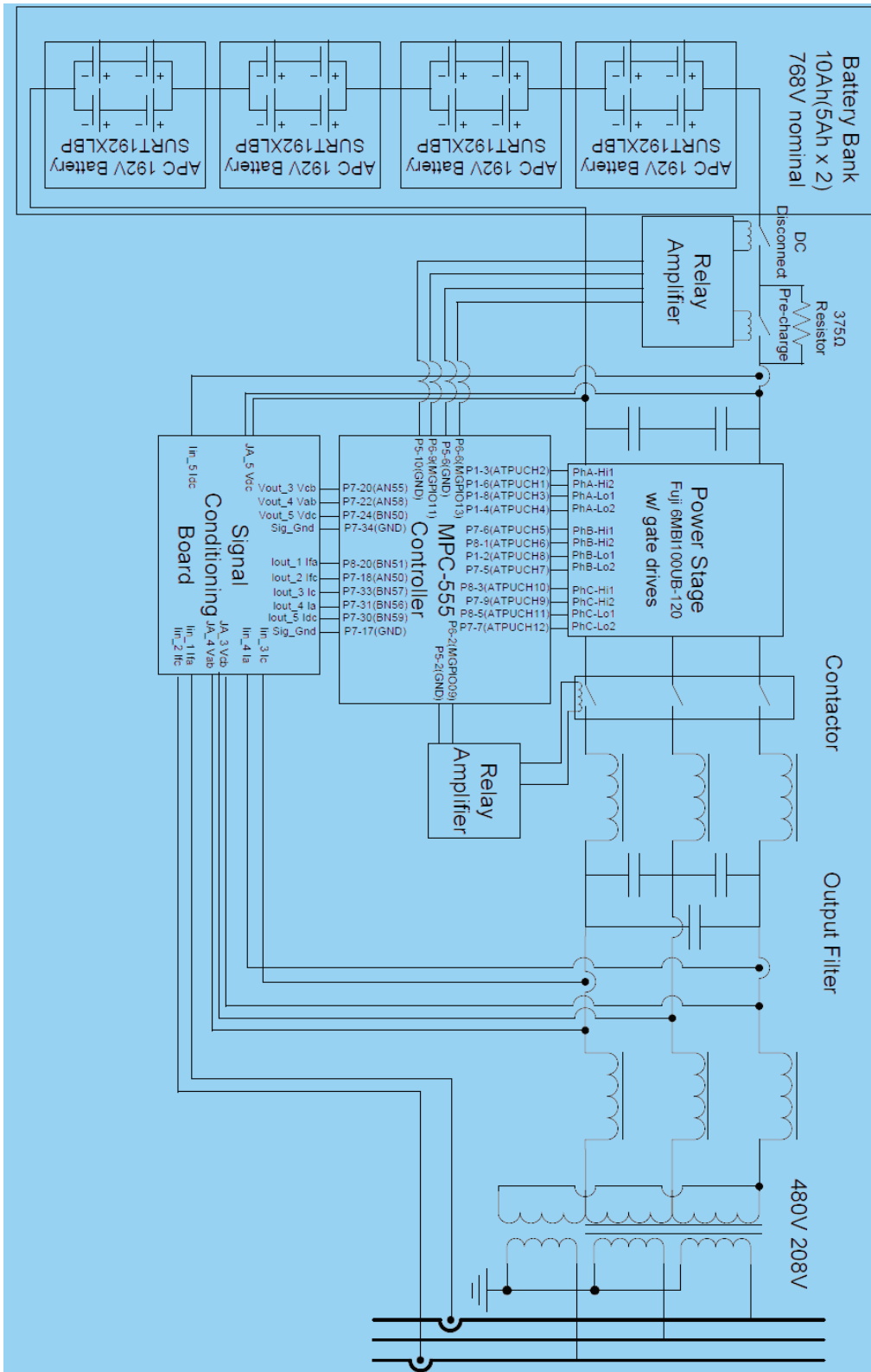


Figure C-1 Hardware Configuration Diagram

Appendix D: Harmonic Oscillator Code

```
phAsinq = phAsinq + ((wdt+freqchg)*phAcosq>>18);  
phAcosq = phAcosq - ((wdt+freqchg)*phAsinq>>18);  
phBcosq = (-phAcosq>>1)+0.86602*phAsinq;  
phCcosq = (-phAcosq>>1)-0.86602*phAsinq;
```

```
vzs=-(vmax+vmin)>>1;  
phAm = (modidx*(phAcosq+vzs))>>14;  
phBm = (modidx*(phBcosq+vzs))>>14;  
phCm = (modidx*(phCcosq+vzs))>>14;
```

Appendix E: Battery Specification Sheet



Valve Regulated Lead-Acid Rechargeable Battery



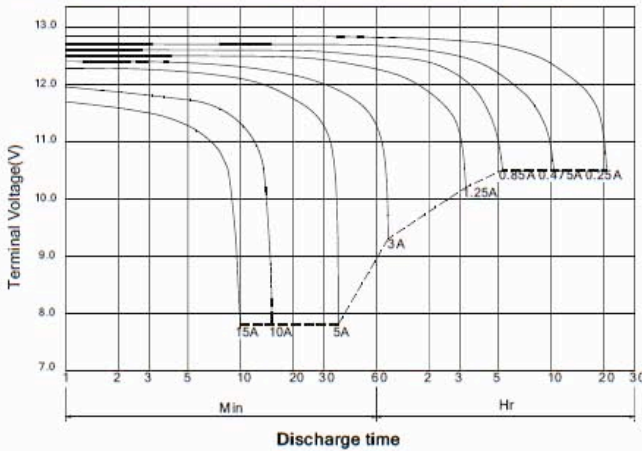
BP5-12

The battery is constructed by plates, separators, safety valves and container. Since the electrolyte is held by a glass-mat separator and plates, the battery can be used in any direction and position (but upside-down should be avoided) without leakage.

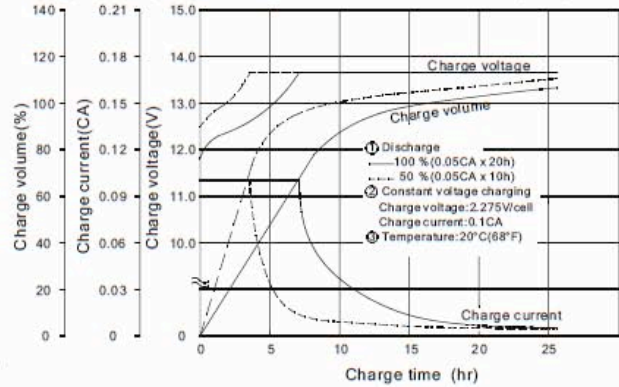
PERFORMANCE SPECIFICATIONS

Nominal Voltage(V).....	12 volts(6cells in series)
Nominal Capacity(Ah)	
20 hour rate F.V.(1.75V/cell) (250mA to 10.50volts)	5.00Ah
10 hour rate F.V.(1.75V/cell) (475mA to 10.50volts)	4.75Ah
5 hour rate F.V.(1.75V/cell) (850mA to 10.50volts)	4.25Ah
1 hour rate F.V.(1.55V/cell) (3000mA to 9.30volts)	3.00Ah
Approximate Weight.....	1800g(3.97lbs.)
Terminal	
Standard.....	Type T1
Optional.....	Type T2
Internal Resistance (Fully Charged Battery).....	≤ 27m Ω
Maximum Discharge Current For 5 sec.(A).....	75 A
Maximum Charge Current(A).....	1.5 A
Ambient Temperature	
Charge.....	0°C(32°F)~40°C(104°F)
Discharge.....	-20°C(-4°F)~50°C(122°F)
Storage.....	-20°C(-4°F)~40°C(104°F)
Vibration test	
Frequency: 16.7Hz	
Amplitude: 4mm	
Vibrate the battery horizontally or vertically for 60 minutes. The battery have no abnormality.	
Case.....	ABS: UL 94-HB
Dimension(mm/inch)	
Length ±1.5mm.....	90/3.54
Width ±1.5mm.....	70/2.76
Container Height ±1.5mm.....	102/4.02
Total Height ±2mm.....	106/4.17
Application.....	Electronic Doorbells, Toy-Cars, Fans, UPS.

BP5-12 Battery discharge characteristics (25°C/77°F)



Battery Charging Characteristics (Typical example of the charge characteristics for the standby use)

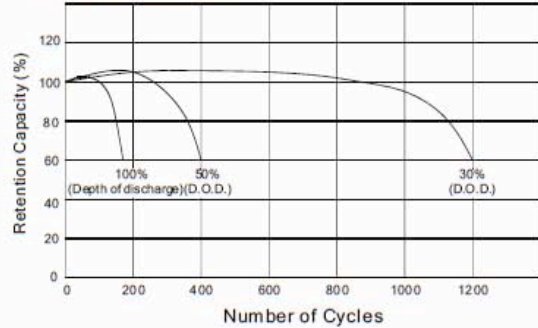


Charging Procedure

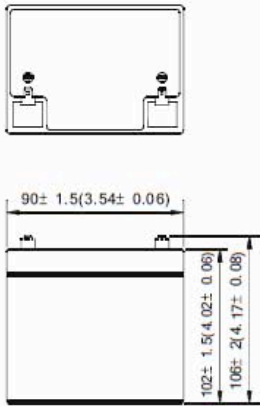
Application	Charging method	Charging Voltage at 20°C (V/cell)	Temperature compensation coefficient of charging voltage (mV/°C/cell)	Max. charging current (CA)	Charging time 0.1CA, 20°C (h)		Temp (°C)
					100% discharge	50% discharge	
For standby power source	Constant voltage & constant current charging (with current restriction)	2.25~2.30	-3	0.3	24	20	0~40 (32~104°F)
For cycle service		2.40~2.50	-4	0.3	16	10	

Battery Life Characteristics of Cyclic Use

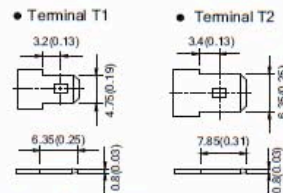
Testing Conditions - Discharge Current : 0.25C Amp (F.V. 1.7V/cell)
 Charging Current : 0.1C Amp
 Charging Volume : 120% OF Discharge Capacity
 Ambient Temperature : 20°C (68°F)



OUTER DIMENSIONS



TERMINAL TYPE mm(inch)



Constant power discharge characteristics at 25°C/77°F

Final Voltage	Discharge time								
	5Min	10Min	15Min	30Min	1Hr	3Hr	5Hr	10Hr	20Hr
10.80V	180.8	133.1	108.6	83.5	36.39	14.57	10.05	5.62	2.96
10.50V	209.2	144.2	111.5	85.9	37.48	14.87	10.20	5.70	3.00
10.20V	222.3	149.4	115.0	87.4	38.16	15.00	10.26	5.73	3.01
9.90V	232.3	152.9	117.6	88.3	38.61	15.10	10.29	5.75	3.02
9.60V	240.0	156.0	120.0	89.0	39.00	15.20	10.32	5.75	3.02

TERMINAL POSITION



B.B. BATTERY CO., LTD.

Web Site: <http://www.bb-battery.com>

USA:
 B&B BATTERY(USA) INC.
 6415 RANDOLPH ST.COMMERCE,
 CA,90040 U.S.A.
 TEL:1-323-278-1900.1-800-278-8599
 FAX:1-323-278-1268
 E-Mail:sales@bb-battery.com

EUROPE:
 B&B BATTERY(EUROPE) B.V.
 3 WIJNGAARDVELD, 9300 AALST,BELGIUM
 TEL:(00)32-53781567
 FAX:(00)32-53781567
 E-Mail:hansdevriese@bb-battery.com

CHINA FACTORY:
 B.B. BATTERY CO., LTD.
 CHENG DONG TRIAL AREA,HUANG GANG,
 RAOPING, GUANG DONG,CHINA,515700
 TEL:86-768-7601001-2
 FAX:86-768-7601469
 E-Mail:maggy@bb-battery.com

HONG KONG:
 NATIONAL TRADING LTD.
 TEL:852-2301-3800
 FAX:852-2739-1182
 E-Mail:bbhk@hkstar.com

JAPAN:
 B&B BATTERY(JAPAN) CO., LTD.
 1375-11 NARAHARA-MACHI,HACHIOJI,
 TOKYO 193-0803,JAPAN.
 TEL:81-426-25-6375
 FAX:81-426-25-6375
 E-Mail:miyata@bb-battery.com

TAIWAN:
 B.B. BATTERY(TAIWAN) CO., LTD.
 TEL:886-6-502-5150
 FAX:886-6-589-8087
 E-Mail:maggy@bb-battery.com



All data shall be changed without prior notice, BB reserves the right to explain and update the information contained herein.

A/3 REV. Jan. 2009